Developments in mean field density functional theory of simple fluids and charged colloidal suspensions

Sascha Khakshouri

Department of Physics and Astronomy
University College London

2007

Thesis submitted for the degree of Doctor of Philosophy

ProQuest LLC
789 East Eisenhower Parkway
P.O. Box 1346
Ann Arbor, MI 48106-1346

I confirm that the work presented in this thesis is my own. Where information has been derived from other sources, I confirm that this has been indicated in the thesis.

Sascha Khakshouri

Abstract

This thesis is concerned with the methods of mean field calculations of the properties of soft matter systems. The first part deals with the application of mean field density functional theory to fluid systems containing small numbers of particles. This is relevant to nucleation studies that can be performed using mean field density functional theory (MFDFT), where the critical clusters that constitute the transition states for phase transitions can be very small. It is also relevant for studies of the behaviour of confined fluids such as fluids in nanopores. The problems in applying MFDFT to small systems are investigated, and modifications to improve the accuracy are identified. These principles are tested on a highly simplified model system of attractive hard rods in one dimension. The second part of the thesis investigates the mean field description of interactions in charged colloidal suspensions within the primitive (PM) model. The phase behaviour of these systems is discussed. In particular, the question of whether experimental observations of coexistence between dense and rarefied phases can be accounted for by mean field theory is discussed. A new approximate method for solving the nonlinear mean field Poisson-Boltzmann equation in the limit of dilute suspensions is proposed. This method is applied to the simple case of charged plates, as well as arrays of spherical colloidal particles. For the latter case, comparisons are made between spherical and cubic Wigner-Seitz cell geometries.

Acknowledgements

I would like to thank my supervisor Dr. Ian J. Ford for his approachability and patience throughout the PhD period. I appreciate the fact that he never objected to discussing, questioning and puzzling over the elementary basics of what we were working on. I would also like to thank him for his readiness to discuss other related issues in statistical mechanics and sharing his research with me. I sincerely appreciate his candidness in letting me know when what I say doesn't make sense, and his way of letting me realise that things I thought at first were simple might be more complicated after all.

In addition to my supervisor I have been fortunate to receive help and input from a number of people. I would like to thank: Dr. Tony Harker who was always prepared to sit down and help with specific questions, Andy Gormanly for keeping the computer systems here up and running and for all of his help on computing related issues, Professor Colin Wilkin for his help with mathematical questions, Dr. Sarah Harris for her inspiration before and at the very beginning of my PhD, Dr. Che Ganarelli who was always available to answer technical questions, Wisdom Beyhum especially for his help with Mathematica and for his proofreading, Dr. Dorothy Duffy and Dr. Matthew Dodgson for their input and suggestions towards the end of the thesis. I would also like to thank other members of the Condensed Matter and Materials Group at UCL not mentioned here.

I would like to express my gratitude to my family for their support throughout my studies, and for enabling me to pursue my interests. Last but by no means least I would like to thank Sukina Natarajan for her help with this work as well as for her moral support and companionship.

Contents

Chapter 1

First-order phase transitions and inhomogeneous fluids

1.1 Introduction

This thesis deals with the application of mean field density functional theory to the calculation of the equilibrium thermodynamic properties of soft condensed matter systems. The technique of mean field density functional theory is applied to two very different types of system. In Chapter 3, the application of this technique to systems containing a small number of particles is investigated. A number of corrections are proposed to increase the accuracy of mean field density functional theory when applied to systems containing a small number of particles. Chapters 4-8 deal with charged colloidal suspensions. In Chapter 6, a new linearisation scheme is proposed for the solution of the nonlinear mean field equations in these systems. The technique is tested in Chapters 7 and 8, through application to well known model systems.

As the underlying motivation of this work is the study of first-order phase transitions, this chapter gives a brief introduction to first-order phase transitions and in particular fluid-fluid phase coexistence. Although the calculations in this thesis are entirely equilibrium calculations, the kinetics of first-order phase transitions is discussed in this chapter, as a motivation for the study of inhomogeneous fluid systems in general.

1.2 Thermodynamics and statistical mechanics of first-order phase transitions

1.2.1 Microscopic approach

Phase transitions are ubiquitous in natural as well as many industrial processes. Examples include rainfall which involves condensation of water vapour, and crystallisation processes that are important in the synthesis of new materials. First-order phase transitions involve transitions between states that have different densities and different entropies. The difference in entropy ΔS has the consequence that these phase transitions involve a latent heat $L = T\Delta S$, such as the heat that must be added to water to make it boil.

Theoretically, the phase diagram of a system can be constructed using the partition function for the system. This is used to obtain a thermodynamic potential which is differentiated to construct equations of state. For a system of identical particles maintained at constant particle number, volume

and temperature (NVT) the classical partition function Z is given by

$$Z = \frac{1}{N!\lambda^{3N}} \int d^N \mathbf{r} \exp(-\beta U(\mathbf{r}^N)) \tag{1.1}$$

where $U(\mathbf{r}^N)$ is the position-dependent part of the system Hamiltonian, $\lambda = h/(2\pi m k_B T)^{1/2}$ is the thermal de Broglie wavelength which comes from integrating over the kinetic degrees of freedom in the system, h is Planck's constant, m is the mass of the particles and $\beta = 1/k_B T$ (k_B is Boltzmann's constant and T is the temperature). The corresponding thermodynamic potential is the Helmholtz free energy defined as

$$F(N, V, T) = -k_B T \ln Z \tag{1.2}$$

First-order phase transitions are characterised by discontinuities in the derivatives of the free energy. The discontinuity of the derivative with respect to temperature reflects the difference in entropy as the system changes from one phase to another.

The partition function represents a weighted sum over all possible states a system can occupy. In most cases this represents an astronomical number of possibilities. For most systems the partition function Z is impossible to evaluate exactly, and approximate methods need to be used. Because the partition function Z is a sum over all possible configurations of the system, the quantities derived from it relate to the equilibrium behaviour of the system in the long-time limit $t \to \infty$. In practical terms this means that such thermodynamic quantities describe the system over timescales that are long compared to all of the microscopic processes through which the system's phase space is sampled.

Kinetics versus equilibrium thermodynamics

Even if the partition function for a system could be evaluated exactly, it would not provide very much information about the kinetics of the phase transitions themselves. This is because the transient unstable states that occur during a phase transition, make an insignificant contribution to the partition function Z. To study the kinetics of a system undergoing a phase transition inevitably requires the introduction of some kind of constraint, that restricts the integral (1.1) to be over regions of the phase space in which the system has properties of the phase that has become unstable. Such constraints are hard to impose in rigorous statistical mechanical treatments that take the microscopic partition function as their starting point [1], however they are naturally built in to more phenomenological theories of phase transitions, and approximate mean field treatments.

1.2.2 Phenomenological approach

At equilibrium, there are typical configurations that make up the dominating contributions to the partition function Z. These configurations represent regions in the system's phase space that it is most likely to occupy. The general theory of phase transitions due to Landau begins by identifying a quantity, the order parameter, that characterises the change undergone by a system during a phase transition. This allows systems to be described on the level of the collective phenomena involved in phase transitions, rather than the full microscopic phase space of the system. In the phenomenological approaches, the free energy of a system is expressed in terms of the order parameter. This introduces an extension of the conventional definition of free energy. Rather than describing a system at equilibrium, this free energy describes a quasi-equilibrium system constrained to have a certain value of the order parameter. The constrained free energy is referred to as the Landau free energy. The equilibrium state of the system is obtained by finding the value of the order parameter for which the Landau free energy is a minimum.

Phenomenological approaches to kinetics

A feature of the phenomenological approach is that it allows the extrapolation of phases beyond the regions in which they represent the stable equilibrium state of the system. This means that the phenomenological approach is also useful in the description of the kinetics of phase transitions.

For systems in which the order parameter is a conserved quantity (such as the density of a fluid ρ) phase transitions are accompanied by spatial variations of the order parameter that leave its total integral over all space unchanged [2]. This is why mean field density functional theory, in which the free energy of a system is expressed as a functional of a spatially varying density, can be useful in the description of kinetics of phase transitions. The technique is also useful for the calculation of equilibrium properties of systems which are spatially inhomogeneous, which is the topic of this thesis.

1.2.3 Phase coexistence in a single-component fluid

The phenomenological approach can be applied to investigate transitions between two fluid states with different densities, such as the liquid-vapour transition. Under conditions of coexistence, the equilibrium state of a system may be such that there are two regions with different values of the order parameter (in this case the fluid density). In each region, the value of the order parameter is assumed to be homogeneous throughout with the exception of the boundary or interface between the two regions. The interface consists of a finite region in which the order parameter is spatially varying. An abrupt change would entail a large free energy cost, but within the Gibbs 'thin wall' approximation, the fraction of particles in the interfacial region is considered to be negligible [2].

The first step is to find the free energy of a fluid constrained to have a homogeneous density throughout. If the constrained free energy per particle $f = F/N$ as a function of the volume per particle $v = V/N$ contains an upward bulge (where $\partial^2 f/\partial v^2$ becomes negative), then the fluid can attain a lower free energy by phase separating into two regions. This is done following the common tangent construction, or lever rule (see Figure 1.1). A hypothetical homogeneous state with specific volume v_0, can reduce its free energy by separating into a mixture of states with specific volumes v_1 and v_2. The proportion of particles that will be in each of these states is

$$\alpha_1 = \frac{v_2 - v_0}{v_2 - v_1}, \qquad \alpha_2 = \frac{v_0 - v_1}{v_2 - v_1} \tag{1.3}$$

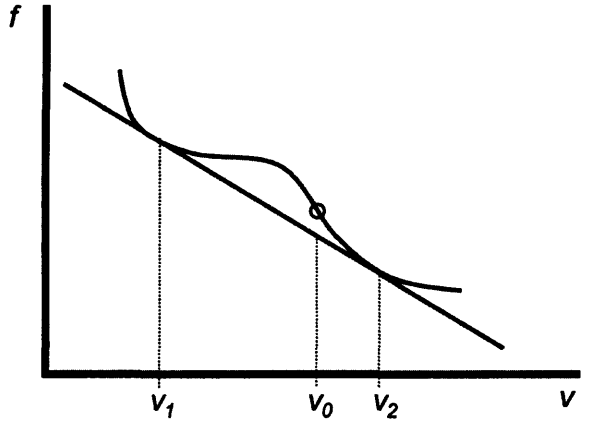

Figure 1.1: Free energy per particle versus volume per particle for a constrained, homogeneous fluid. A system with volume per particle v_0 can lower its free energy by separating into two phases with specific volumes v_1 and v_2.

In the absence of surface effects, the free energy per particle of the inhomogeneous system will be

$$f = \alpha_1 f_1 + \alpha_2 f_2 \tag{1.4}$$

where f_1 and f_2 are the free energies of the two homogeneous states with specific volumes v_1 and v_2 respectively. These two states are called saturated states, and are assumed to be no different from the original constrained homogeneous states with specific volumes v_1 and v_2.

The common tangent construction stems from the requirement that at equilibrium the two co-existing phases must have equal pressures and chemical potentials, that is $P_1 = P_2$ and $\mu_1 = \mu_2$. The pressure is given by $P = -\partial F/\partial V = -\partial f/\partial v$, so equality of pressure implies that tangents to the $f(v)$ curve at v_1 and v_2 must have the same gradient. The chemical potential is defined as $\mu = \partial F/\partial N$, or alternatively as $\mu = G/N$, where G is the Gibbs free energy. The relation between G and F is $G = F + PV$, so that $\mu = f + Pv$. Therefore $\mu_1 = \mu_2$ implies

$$f_1 - v_1 \left(\frac{\partial f}{\partial v}\right)_{v_1} = f_2 - v_2 \left(\frac{\partial f}{\partial v}\right)_{v_2} \tag{1.5}$$

Since the two gradients in (1.5) are the same by the equal pressure condition, this implies that the two tangents also share the same intercept on the f-axis.

1.2.4 Thermodynamic stability

The phase separation from a homogeneous phase illustrated above would not occur if the free energy of the constrained, homogeneous phase did not have the 'bulge' as shown in Figure 1.1, where $\partial^2 f/\partial v^2 < 0$. This allowed the combination of phases at v_1 and v_2 to give rise to a lower free energy than the homogeneous phase at v_0.

This relates to the general concept of thermodynamic stability of a system. A system will be stable with respect to volume or mechanical fluctuations if the free energy is convex with respect to the volume V. This is equivalent to the requirement that the isothermal compressibility κ_T must be positive

$$\frac{\partial^2 F}{\partial V^2} = -\frac{\partial P}{\partial V} = \frac{1}{\kappa_T V} > 0 \tag{1.6}$$

Related to this is the stability with respect to thermal fluctuations. A system will be stable to thermal fluctuations if the free energy F is concave with respect to temperature T. This requires the heat capacity c_V to be positive

$$\frac{\partial^2 F}{\partial T^2} = -\frac{\partial S}{\partial T} = -\frac{c_v}{T} < 0 \tag{1.7}$$

where S is the entropy. When a system becomes unstable both of these conditions are violated simultaneously [1].

1.2.5 Metastability

There are many physical situations in which the kinetic process through which a phase transition takes place is more important in determining what is observed experimentally than the position of equilibrium phase boundaries. Phase boundaries are equilibrium properties of a system calculated in the thermodynamic limit, and represent what occurs over timescales long enough for all microscopic processes to relax. In reality, surface effects lead to situations in which unstable states persist over a long period of time despite the system having traversed an equilibrium phase boundary. These thermodynamically unstable but kinetically stable states are called metastable. If the lifetime of a metastable state is very long compared with the experimental observation time, a phase transition will not be observed, and the thermodynamically unstable state will appear to be stable.

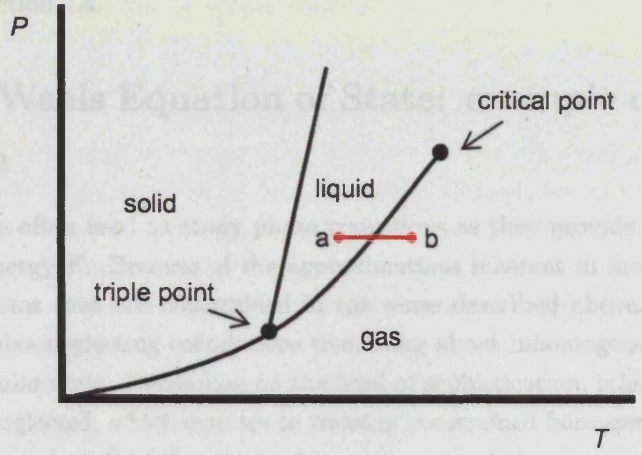

Figure 1.2: P-T phase diagram of a typical single-component substance, showing one path for the liquid-vapour transition by varying the temperature at constant pressure. If the system remains liquid at b or vapour at a it is in a metastable state, and will eventually change to the equilibrium phase.

A well known example of this phenomenon is diamond, which is metastable with respect to graphite at room temperature and atmospheric pressure. Due to the large activation free energy the transformation to graphite is never observed under these conditions. Such effects are characteristic of first-order phase transitions, which are associated with discontinuities in the derivatives of the free energy.

Metastability occurs because when a phase boundary is traversed it takes thermal fluctuations of finite magnitude to nucleate small regions of the new phase out of the unstable phase. These regions then go on to grow and propagate the phase transition through which the system reaches equilibrium. The rate at which the transition progresses is governed by the rate at which these key intermediates can form. The intermediates constitute a transition state which is a bottle-neck for the phase transition.

As an example Figure 1.2 shows the typical phase diagram for a pure, single-component substance. A vapour at point [b] is cooled down to point [a] in the liquid region. Under the right experimental conditions, it may remain in the vapour state even at [a] where the equilibrium phase is liquid. The vapour is then said to be supersaturated. Similarly, a liquid at [a] may be heated up to [b] without boiling. This would be a superheated liquid. These metastable states can be very delicate, and the slightest jarring of the container may bring about the transition to stability.

Experimentally, supercooling or superheating of substance cannot be achieved without the removal of impurities from the system and the avoidance of contact with the walls of a container. For example, studies on metastable liquid water are often done by immersing the water in oil that acts as a medium [1]. These measures aim at suppressing heterogeneous nucleation, which in general occurs faster than homogeneous nucleation. Heterogeneous nucleation occurs when the wall of a container or an impurity in the system facilitate the formation of the new phase by acting as a substrate, reducing the surface free energy cost for the formation of the intermediates to the transition. Homogeneous nucleation requires the intermediates to form in the midst of the system, and is generally a slower process.

The occurrence of metastability has consequences for the experimental determination of phase boundaries. The possibilities of very long timescales for kinetic processes means that experimental data may not necessarily be seen to prove or disprove the existence of thermodynamic phase boundaries under certain experimental conditions. In the study of charged colloidal suspensions for example, phase separation of a homogeneous phase into dense and rarefied phases typically occurs over a timescale of days [3].

While this thesis is concerned exclusively with calculations of equilibrium thermodynamic prop-

erties of systems, some motivation is drawn from the study of kinetics of phase transitions, which is discussed briefly in Section 1.4.

1.3 Van der Waals Equation of State: example of a mean field approach

Mean field theories are often used to study phase transitions as they provide approximate methods to evaluate the free energy F. Because of the approximations inherent in mean field theories, they usually represent systems that are constrained in the sense described above. Mean field approximations generally involve neglecting correlations that bring about inhomogeneities in the system on the microscopic molecular scale. Depending on the level of sophistication, inhomogeneities on longer lengthscales are also neglected, which equates to treating constrained homogeneous systems.

At the heart of most mean field theories is the replacement of the complicated problem of many particles interacting with each other, with one in which every particle interacts with an identical mean field. This allows the partition function (1.1) for N particles to be factored into N identical single-particle partition functions.

$$Z_N = \frac{1}{N!} z_1^N \tag{1.8}$$

In the case of an ideal gas of N non-interacting particles the single particle partition function is $z_1 = \lambda^{-3} V$, where V is the volume of the system.

The Van der Waals treatment of a non-ideal gas can be thought of as an example of a mean field theory. The departures from ideal-gas behaviour arise due to interactions between the molecules in the gas. The effect of the repulsive and attractive interactions are treated separately. This is a feature that carries over into mean field density functional theory discussed in Chapter 2. The effect of the attractive and repulsive interactions on the free energy are calculated without taking into account the effects they induce on a completely homogeneous distribution of particles. The repulsive interactions are approximated to be hard-sphere interactions. These cause a reduction in the volume available to the molecules. To account for this, the volume is altered to be $V - Nb$, where b is roughly the volume taken up by one molecule. The next step is to account for the attractive energy of the particles. If the particles interact through an attractive pair potential $u(r)$, and the correlations brought about by this interaction are assumed not to alter the homogeneous distribution of particles, then the mean interaction between a single pair of molecules is

$$\langle U_1 \rangle = \frac{1}{V} \int 4\pi r^2 u(r) dr = -\frac{2\alpha}{V} \tag{1.9}$$

For a system of N particles, there will be $(N-1)N/2 \simeq N^2/2$ pairs, so the mean attractive energy per particle is $\langle u \rangle = -\alpha(N/V)$, which is proportional to the density. The constant α is positive for an attractive interaction, and characterises the strength of the attractions. The attractive and repulsive effects are combined to construct a mean field partition function. In the mean field approach, each particle is taken to interact independently with a mean field that represents the presence of all the other particles. The mean field single particle partition function is then

$$z_1 = \frac{1}{\lambda^3}(V - Nb)\exp(-\beta\langle u \rangle) = \frac{1}{\lambda^3}(V - Nb)\exp(+\beta\alpha N/V) \tag{1.10}$$

where the exponent is the mean energy of a particle in the system, and the factor $(V - Nb)$ is the volume available to a molecule in the system. It can be seen that all local inhomogeneities brought about by the attractive and repulsive interactions are neglected in this treatment.

Plugging the mean field single particle partition function into (1.8), taking the logarithm and using

Stirling's approximation $\ln N! \simeq N(\ln N - 1)$, results in the free energy per particle f as a function of volume per particle v for the Van der Waals fluid

$$f = -k_B T \ln(v - b)\lambda^{-3} - \frac{\alpha}{v} \tag{1.11}$$

The two terms in the free energy have competing effects with particle density. The first term takes account of the reduction in entropy due to the decrease in the amount of volume available to the particles as the density increases. The second term is the average attractive energy in the system, which lowers the free energy as the density increases.

The free energy is then differentiated to obtain the pressure $P = -\partial f/\partial v$, giving the familiar Van der Waals equation of state

$$(P + \alpha/v^2)(v - b) = k_B T \tag{1.12}$$

Several isotherms in the P-V plane are shown in Figure 1.3. Under certain conditions, the free energy has regions in which $\partial^2 f/\partial v^2$ becomes negative, indicating that the homogeneous phase becomes unstable. The critical temperature T_c is the temperature above which there is no distinction between the two fluid phases. In this region the fluid density changes continuously without a phase transition. Below T_c, the isotherms develop Van der Waals loops, indicating that the homogeneous phases become metastable and then unstable with respect to phase separation into regions of different densities. The boundary between these behaviours is mapped out by the isotherm at the critical temperature $T = T_c$, for which the pressure has an inflection point at the critical point. At $T = T_c$ the liquid-vapour phase transition is a second order phase transition.

Coexistence between phases with different densities can be built into the P-V diagram by use of the Maxwell equal-areas construction. This is equivalent to the common tangent construction in the f-v plane discussed in Section (1.2.3). The requirement for the coexisting phases to have equal chemical potentials means that $f_1 - f_2 = P_{12}(v_2 - v_1)$, where P_{12} is the pressure of the two coexisting phases. Since f is negative of the integral of P with respect to v, this translates to

$$\int_{v_1}^{v_2} P(v)dv = P_{12}(v_2 - v_1) \tag{1.13}$$

This equation describes the straight line (at constant pressure P) that the subcritical isotherms follow in the coexistence region. Graphically the requirement is that the areas above and below a horizontal line cutting through a Van der Waals loop must be equal.

1.3.1 The coexistence region

The equal-areas construction maps out a region of phase coexistence which is demarcated by a boundary called the binodal, labelled b in Figure 1.3. The inner region, demarcated by the spinodal (labelled s), is the region where $\partial^2 f/\partial v^2 < 0$ or equivalently $\partial P/\partial V > 0$. Inside the spinodal region a homogeneous phase is completely unstable, and arbitrarily small fluctuations are sufficient to bring about formation of regions of the new phase. Metastability occurs for a system that is homogeneous inside the coexistence region (where the equilibrium state involves phase separation into two different densities), but outside the spinodal region. The closer to the spinodal, the less stable the system is with respect to density fluctuations. Very close to the phase boundary a homogeneous state consisting of a single phase may persist for a long time. Closer to the spinodal boundary the lifetime of metastable states become shorter, and once the spinodal is reached the system becomes completely unstable. Beyond this point, tiny fluctuations are sufficient to cause the system to separate via spinodal decomposition (discussed in Section 1.4.2). In between the binodal and the spinodal, the phase transition proceeds through nucleation of embryos or clusters of the new phase within the metastable homogeneous phase. Only clusters of a sufficiently large size have a high probability of growing into larger

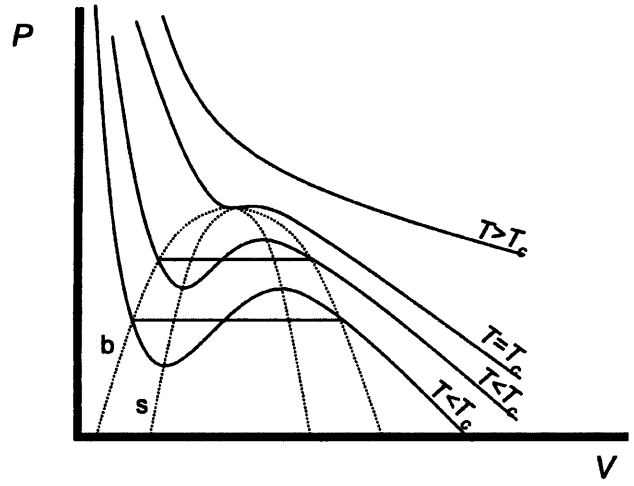

Figure 1.3: Isotherms in the P-V diagram for a Van der Waals fluid. Above the critical temperature T_c isotherms for a homogeneous fluid remain stable. Below T_c the isotherms develop Van der Waals loops indicating that an inhomogeneous system consisting of two different densities becomes more stable. In the coexistence region the equilibrium isotherms follow the straight line obtained from the equal-areas construction. The binodal (labelled b) and spinodal (labelled s) discussed in Section 1.3.1 are also shown.

regions of the new phase. This is because smaller clusters will have a comparatively large surface free energy cost.

The binodal demarcates an equilibrium phase boundary where a homogeneous phase becomes thermodynamically unstable, and the equilibrium state is a combination of states with different densities. A closed system with a uniform density will, given enough time, separate into two regions with different densities. The spinodal is a non-equilibrium concept as it demarcates a change in the kinetic process through which the phase transition occurs.

Some qualitative features of the transition may be inferred from Figure 1.3. Above the critical point, there is no real distinction between the liquid and gaseous states, and the system changes from a dense to a rarefied fluid continuously. Below the critical point, a transition occurs between one fluid phase and another with a discontinuity in density. The increasing width of the coexistence region at lower temperatures, indicates that the density difference between the coexisting phases is larger at lower temperatures.

It should be noted that the spinodal line obtained in this way is a result of an approximate calculation whereby a system is not only constrained to be globally homogeneous, but all microscopic inhomogeneities that result from correlations between the molecules have been neglected. It is also questionable whether a clear boundary such as the spinodal is an accurate description of realistic phase transitions [1]. Experimentally it is very difficult to define a clear spinodal boundary as the rate of formation of critical embryos in the coexistence region has a very strong dependence on the extent of penetration into the coexistence region. Superheated liquids evolve suddenly from a condition of relative stability (metastability) to a region in which the new phase is formed rapidly and spontaneously. This experimentally determined limit is called the superheat limit, and is not a sharp boundary like the spinodal.

1.3.2 Small systems

In large systems, interface effects can delay the occurrence of a phase transition. The free energy cost of formation of the interface may be substantial, acting as an activation barrier to the formation of the stable state. Surface effects influence the kinetics but not the thermodynamics of a system, which is governed by what happens over long timescales. The Gibbs approach outlined above, inherent in

the Maxwell or double-tangent construction, involves neglecting the surface between the two phases. This is justified when the equilibrium thermodynamic behaviour of large systems is required.

When the system itself is small in terms of the number of particles N, surface effects can make a substantial contribution to the total free energy, and therefore affect the equilibrium properties of the system. As a result of surface effects, small systems can violate the stability conditions discussed in Section 1.2.4. In these situations an exact (unconstrained) evaluation of the partition function results in regions where the free energy is a concave function of the volume V, and P-V diagrams exhibiting Van der Waals loops similar to those in Figure 1.3. Under these conditions, phase separation occurs within a small closed system, but the free energy cost of forming the interface between the phases causes the free energy to become concave.

Experiments on melting of small sodium clusters [4] have indicated that the heat capacity for such systems can be negative. Computer simulations of small molecular clusters have also produced P-V diagrams exhibiting Van der Waals-like loops [5, 6].

1.3.3 Thermodynamic ensembles and potentials

For the purposes of calculating the free energy from a microscopic theory, the microcanonical (NVE), canonical (NVT) and grand canonical (μVT) ensembles are the most convenient. Evaluation of the partition function for the Gibbs (constant pressure (NPT)) ensemble is difficult as it requires the imposition of nontrivial constraints on the microscopic configurations to give the required pressure [7]. Since temperature T is usually an experimentally controllable variable, we focus mainly on the canonical and grand canonical ensembles.

The grand canonical ensemble describes the configurations of a system at fixed volume V, temperature T, and chemical potential μ. The chemical potential $\mu = \partial F/\partial N$ regulates flow of particles between the system and an infinite reservoir with which it is at equilibrium. A change in μ therefore causes a change in the average number of particles in the system $\langle N \rangle$. The grand partition function Ξ is a sum over all possible occupancies of the system from $N = 0$ to infinity

$$\Xi = \sum_{N=0}^{\infty} \exp(\beta\mu N) Z_N \tag{1.14}$$

where μ is the chemical potential, and Z_N is the canonical partition function for a system containing N particles. The grand potential is given by $\Omega = -k_B T \ln \Xi$. The probability for the system to contain N particles is given by

$$W(N) = \frac{\exp(\beta\mu N) Z_N}{\Xi} \propto \exp(-\beta(F - \mu N)) \tag{1.15}$$

where F is the Helmholtz free energy for a system with N particles at volume V and temperature T. The size of fluctuations in particle number, is related to the width of the distribution $W(N)$. This is proportional to the isothermal compressibility κ_T

$$\langle N^2 \rangle - \langle N \rangle^2 = \frac{\langle N \rangle k_B T}{v} \kappa_T \tag{1.16}$$

where $\langle N \rangle$ is the mean number of particles in the system. As discussed before, at a liquid-vapour phase transition the P-V isotherms become flat so κ_T diverges. This indicates that the fluctuations in particle number for an open system become large at a phase transition, reflecting the large density fluctuations that occur during the phase transition.

It can be shown [8] that using the grand canonical ensemble, even an approximate treatment in which a system is constrained to have a homogeneous density throughout, will result in the correct coexistence isotherms. This is because the grand ensemble explicitly includes fluctuations in the total

density of the system, which are encoded in the sum over particle number (1.14).

1.4 Kinetics of first-order phase transitions

To illustrate the importance of interface effects, and the correct description of the inhomogeneities that occur in a system we will consider the kinetics of first-order phase transitions in this section. The kinetic process through which a system evolves from a phase of one density into a phase with a different density depends on the details of the inhomogeneities in density that bring about that change.

1.4.1 Nucleation

As described in Section 1.3.1, in the region between the binodal and spinodal the phase transition proceeds through the process of nucleation. A homogeneous system in this region is metastable because it costs a finite amount of free energy to create the nuclei that propagate the phase transition. Small nuclei have a large surface to volume ratio, and so generally shrink by decaying. However, once a nucleus of a certain critical size is formed, the free energy cost of forming more surface becomes less significant than the decrease in free energy of creating the new phase inside the cluster. Clusters of the new phase larger than the critical size grow spontaneously in a relatively short time. Therefore, the rate of phase transitions in this region is governed by the rate of nucleation of critical clusters.

Classical Nucleation Theory

As an example, we will consider the condensation of a vapour. In the classical nucleation theory (CNT), the clusters which are molecular aggregates of the new phase within the mother phase, are crudely represented as spherical droplets of liquid in contact with the supersaturated vapour. The interface between the droplet and the vapour is considered to be a well defined sharp surface, and is taken to have the same properties as a planar interface between the two bulk phases. This is known as the capillarity approximation. For a macroscopic planar interface between bulk phases, the surface free energy cost, or surface tension γ can be measured experimentally.

The free energy of formation of a cluster is the difference between the free energy of a system containing the cluster, and a uniform system fully occupied by the supersaturated vapour. The phase transition is considered to take place for a system at constant pressure P, particle number N, and temperature T. The appropriate thermodynamic potential for these constraints is the Gibbs free energy G. Within the framework of CNT, the free energy of formation of a cluster ΔG is given by [9]

$$\Delta G = -\frac{4\pi}{3} R^3 \Delta P + 4\pi R^2 \gamma \tag{1.17}$$

where $\Delta P = P_l - P_v$ the pressure difference between the bulk liquid and supersaturated vapour. Equation (1.17) clearly illustrates the competition between the favourable volume free energy (proportional to R^3) and the unfavourable surface free energy cost (proportional to R^2). The critical cluster is that for which ΔG is a maximum. Clusters larger than this grow spontaneously and propagate the phase transition. The free energy of formation ΔG at this point can be considered as an activation barrier for condensation. The radius of the critical cluster R_0 is obtained by setting $\partial \Delta G / \partial R = 0$. This has the result $R_0 = 2\gamma / \Delta P$. At low supersaturations, when the metastable system is close to the binodal (and far from the spinodal), the nucleation time is long relative to the relaxation time of the underlying microscopic processes. Under these conditions the nucleation process can be treated using equilibrium thermodynamic methods. The rate of formation of critical droplets per unit volume in

classical nucleation theory is given by

$$J = A\exp(-\Delta G(R_0)/k_B T) \tag{1.18}$$

There are various forms for the preexponential factor A, the details of which will not be discussed here.

Although classical nucleation theory contains the necessary ingredients to describe the competing effects that influence the rate of nucleation, the inadequate description of the cluster-vapour interface through the capillarity approximation, and the treatment of the cluster interior as a bulk liquid, make it quantitatively unreliable in many situations. The exponential dependence of J on the free energy of formation of the critical cluster $\Delta G(R_0)$, means that failure to accurately describe the critical cluster can lead to large errors in predicting the nucleation rate.

1.4.2 Spinodal decomposition

As described in Section 1.3.1, in the spinodal region arbitrarily small density fluctuations lead to growth of the new phase out of an unstable homogeneous phase. This is in contrast to the metastable region between the binodal and spinodal where only density fluctuations larger than the critical size go on to grow spontaneously. This is the difference between nucleation described above, and the process of spinodal decomposition. The following brief description of this process within the framework of Cahn-Hilliard theory is adapted from Jones in reference [10].

Even though all density fluctuations regardless of size will grow to propagate the phase transition, fluctuations of varying sizes grow at different rates. As before, we will consider a transition from a low density phase to a high density phase. Density fluctuations that conserve the overall density of the system can be decomposed into sinusoidal contributions characterised in terms of their wavelength. Long-wavelength fluctuations involve density changes over long distances, and short wavelength fluctuations involve density differences over short distances. Very long-wavelength fluctuations tend to grow slowly because this requires matter to diffuse over long distances. Very short range fluctuations do not grow quickly because of the comparatively high ratio of surface to volume they create, which involves a high free energy cost. Competition between these two effects means that one characteristic wavelength tends to grow fastest, and dominates the process of spinodal decomposition.

Cahn-Hilliard theory

The description of the process described above necessitates an expression for the free energy of a system with non-uniform order parameter which is the density in this case. This motivates the idea of a free energy functional, in which the free energy is expressed as a functional of a spatially varying order parameter. This kind of theory was first developed by Van der Waals, and subsequently by Cahn and Hilliard, and by Langer. It also features prominently in the Ginsburg-Landau theory of phase transitions. The total Helmholtz free energy of an inhomogeneous system is the integral of the free energy density f over the volume of the system. If the free energy can be expressed in terms of the local density $\rho(\mathbf{r})$ in an inhomogeneous system, then it is written as $f(\rho(\mathbf{r}))$. The total free energy of the system is then

$$F = \int f(\rho(\mathbf{r}))d\mathbf{r} \tag{1.19}$$

The most basic functionals are obtained by considering an expansion of the free energy density of a nonuniform fluid about the free energy density of a uniform fluid [11, 12]. This results in a series in terms of the local density gradients $\nabla\rho(\mathbf{r})$. For simplicity, most treatments keep terms only up to second order in $\nabla\rho(\mathbf{r})$, which is valid as long as the density gradients are not too large. The first order term in terms of $\nabla\rho(\mathbf{r})$ can be eliminated by symmetry arguments and the Helmholtz free energy

density is then

$$f(\rho(\mathbf{r})) = f_0(\rho(\mathbf{r})) + \frac{c}{2}(\nabla\rho(\mathbf{r}))^2 \tag{1.20}$$

where $f_0(\rho)$ is the Helmholtz free energy of the homogeneous fluid at the local density $\rho(\mathbf{r})$, and $\nabla\rho(\mathbf{r})$ is the local density gradient. The constant c is a measure of the free energy cost of creating inhomogeneities in the system. There are various ways of estimating c (which is related to the surface tension γ) from microscopic or empirical considerations. For the purposes of this section we assume a functional containing a free energy density of the form (1.20) and see how it is applied to the problem of spinodal decomposition.

In general, diffusion of material occurs along gradients in chemical potential μ, as a system attempts to reestablish the equilibrium situation of constant chemical potential throughout. In one dimension, the flux of material J is given by

$$J = -M\frac{d\mu(x)}{dx} \tag{1.21}$$

where M is the is the coefficient for diffusion along a chemical potential gradient. In many familiar situations, the chemical potential is lower in regions where the density ρ is lower, which means that material diffuses from regions of high concentration to regions of low concentration. This results in Fick's first law

$$J = -D\frac{d\rho}{dx} \tag{1.22}$$

where D is the diffusion coefficient. Conservation of the total amount of material is given by the continuity equation

$$\frac{d\rho}{dt} = -\frac{dJ}{dx} \tag{1.23}$$

where t is time. The combination of (1.22) and (1.23) yields the diffusion equation or Fick's second law

$$\frac{\partial\rho}{\partial t} = D\frac{\partial^2\rho}{\partial x^2} \tag{1.24}$$

To describe the kinetics of phase transitions, the more general form (1.21) is more useful. During a phase transition, the chemical potential may be lower in regions of high density. The spatially varying chemical potential is obtained from the spatially varying free energy density $f[\rho(x)]$ through the relation $\mu = \delta f/\delta\rho$. For a simple square-gradient functional of the form (1.20), the functional derivative reduces to

$$\mu(x) = \frac{df_0}{d\rho} + c\frac{\partial^2\rho}{\partial x^2}. \tag{1.25}$$

The flux is then given by

$$J = -M\left(f_0''\frac{\partial\rho}{\partial x} + c\frac{\partial^3\rho}{\partial x^3}\right) \tag{1.26}$$

where $f_0'' = d^2f_0/d\rho^2$. Substituting this J into the diffusion equation gives the Cahn-Hilliard equation

$$\frac{\partial\rho}{\partial t} = \frac{d}{dx}M\left(f_0''\frac{\partial\rho}{\partial x} + c\frac{\partial^3\rho}{\partial x^3}\right). \tag{1.27}$$

The problem is simplified by assuming that M, c and f_0'' spatially uniform and independent of the local density variations, which results in

$$\frac{\partial\rho}{\partial t} = D_{\text{eff}}\frac{\partial^2\rho}{\partial x^2} + Mc\frac{\partial^4\rho}{\partial x^4} \tag{1.28}$$

where $D_{\text{eff}} = Mf_0''$ is the effective diffusion coefficient. It can be shown that one set of solutions to

the differential equation (1.28) is given by

$$\rho(x,t) = \rho_0 + A\cos(qx)\exp\left[-D_{\text{eff}}q^2\left(1+\frac{cq^2}{f_0''}\right)t\right] \tag{1.29}$$

where ρ_0 is the mean density of the homogeneous phase, q is the wavenumber of an oscillatory fluctuation, and A is its magnitude. This shows that a density fluctuation will grow exponentially, depending on its characteristic wavenumber q. The q-dependent amplification factor $R(q) = q^2(1 + cq^2/f_0'')$ in the exponent is plotted in Figure 1.4. It can be seen that fluctuations of characteristic wavenumber q_{max} grow fastest, and will dominate the process of spinodal decomposition.

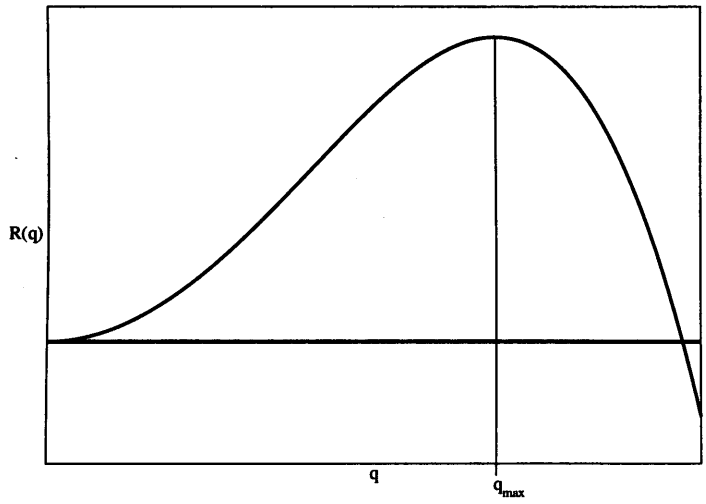

Figure 1.4: $R(q)$ amplification factor against wavenumber for characteristic fluctuations during spinodal decomposition. Fluctuations with wavenumber q_{max} will grow fastest, and dominate the process.

1.5 Description of inhomogeneous fluids

From the discussion above it can be seen that a good theory for the kinetics of a phase transition will depend on how accurately microscopic inhomogeneities can be described. Interface effects also make a large contribution to the equilibrium properties of small systems. These situations require the description of nonuniform fluids. Mean field density functional theory (MFDFT) provides a method for doing this. In the next chapter mean field density functional theory will be introduced generally. In principle, this theory does not require gradients in the density to be small as in the square gradient theory discussed above. This means MFDFT is applicable to systems away from the critical point where density gradients are larger. It also has the advantage of being constructed directly from the molecular interactions in the system, rather than incorporating macroscopic quantities such as the bulk surface tension. MFDFT is a powerful tool in the treatment of inhomogeneous fluids encountered when looking at phase transitions or inherently inhomogeneous systems.

After describing the basics of MFDFT applied to fluids in Chapter 2, the application to closed systems containing small numbers of particles is considered in Chapter 3, where MFDFT is applied to a simple one-dimensional system consisting of only two interacting particles.

In Chapter 4 the phase behaviour of charged colloidal suspensions is introduced, which is topic of the second part of this thesis. The microions that govern the effective interactions between charged colloidal particles comprise an inhomogeneous fluid. Chapters 5-8 deal with the mean field theory of interactions in charged colloidal suspensions. In Chapter 5 the mean field theory for these interactions is introduced generally in terms of the Poisson-Boltzmann (PB) equation. In Chapter 6 a new

linearisation scheme is introduced to tackle the nonlinear PB equation in the limit when the spacing between macroions is large (a dilute colloidal suspension). This approach is applied to the simple case of charged plates in Chapter 7 and to an array of spherical particles in Chapter 8.

Since colloidal suspensions have been observed to phase separate, there are also theories that describe suspensions that are inhomogeneous with respect to the colloid density distribution. The surface tension between colloidal phases has been calculated [13, 14] in order to be able to describe the kinetics of the phase separation processes in these systems. We have not touched upon this topic in this thesis, as our focus is on equilibrium calculations. We study the interactions between the colloidal particles themselves, which are mediated by an inhomogeneous fluid of smaller, more mobile microions.

Chapter 2

Mean field density functional theory

2.1 Free energy of a single-component fluid

In the absence of external fields, a set of N identical particles comprising a single-component fluid can be described by the Hamiltonian

$$H = \sum_{i=1}^{N} \frac{\mathbf{p}_i^2}{2m} + U(\mathbf{r}^N) \tag{2.1}$$

where m is the mass and $\mathbf{p}_i$ is the momentum of a particle. The first term is the kinetic energy K of the system. The second term $U(\mathbf{r}^N)$ is the potential energy of the inter-particle interactions, which depends on the positions of all N particles. If the interactions are assumed to be pairwise, then the potential energy in the absence of external fields can be recast into

$$U(\mathbf{r}^N) = \sum_{i>j} u(\mathbf{r}_i, \mathbf{r}_j) \tag{2.2}$$

For a system with a fixed number of particles, volume and temperature (NVT), the Helmholtz free energy is defined as

$$F(N, V, T) = -k_B T \ln Z \tag{2.3}$$

where the partition function Z is

$$Z = \frac{1}{N! h^{3N}} \int \exp(-H/k_B T) d^N\mathbf{p} d^N\mathbf{r} \tag{2.4}$$

The free energy F can be decomposed into two terms, one being the average energy of the system, and the second being the entropic contribution

$$F = \langle H \rangle - TS \tag{2.5}$$

where S is the entropy of the system.

The N-particle distribution function of the system is

$$f(\mathbf{r}^N, \mathbf{p}^N) = \frac{1}{Z} \exp(-H/k_B T) \tag{2.6}$$

which explicitly depends on the positions and momenta of all the particles. It is clear that the free

energy F is a functional of f. The entropy is defined as

$$S = -k_B \int f(\mathbf{r}^N, \mathbf{p}^N) \ln f(\mathbf{r}^N, \mathbf{p}^N) d^N\mathbf{r} d^N\mathbf{p} \tag{2.7}$$

The free energy (2.5) can be written as

$$F = \int f(\mathbf{r}^N, \mathbf{p}^N) \left(H + k_B T \ln f(\mathbf{r}^N, \mathbf{p}^N)\right) d^N\mathbf{r} d^N\mathbf{p} \tag{2.8}$$

2.1.1 n-particle distribution functions

In the canonical ensemble the mean kinetic energy $\langle K \rangle$ is fixed by the temperature T, and the particle momenta are distributed according to the Maxwell-Boltzmann distribution when the system is at equilibrium. The integrations over the momenta in the partition function Z, together with the $1/h^{3N}$ factor result in a constant factor of λ^{-3N}, where $\lambda = h/(2\pi m k_B T)^{1/2}$ is the thermal de Broglie wavelength. Of more interest are the spatial degrees of freedom which are distributed according to the N-particle distribution function $\rho^{(N)}(\mathbf{r}^N)$. This is obtained by integrating over all of the particle momenta in (2.6). The result is

$$\rho^{(N)}(\mathbf{r}^N) = \frac{1}{Z\lambda^{3N}} \exp(-U/k_B T) \tag{2.9}$$

which gives the probability for particles to be located at positions $\{\mathbf{r}^N\}$. By integrating over the positions of $N - n$ particles, it is possible to obtain a reduced distribution function for n particles in the system

$$\rho^{(n)}(\mathbf{r}^n) = \frac{N!}{(N-n)!} \int \rho^{(N)}(\mathbf{r}^N) d\mathbf{r}_{n+1} .... d\mathbf{r}_N \tag{2.10}$$

which gives the probability of finding any n of the N particles at positions $\{\mathbf{r}^n\}$. The factor in front of the integral accounts for the fact that identical particles can be exchanged leaving the result unchanged. Since any n of the N particles could be chosen to construct $\rho^{(n)}$, the normalisation condition is

$$\int \rho^{(n)}(\mathbf{r}^n) d\mathbf{r}^n = \frac{N!}{(N-n)!} \tag{2.11}$$

The n-particle distribution functions are particularly useful in calculating averages of quantities that depend on the positions of n particles [15]. Of particular importance are the single particle (or singlet) distribution function $\rho^{(1)}(\mathbf{r})$ and the two particle (or doublet) distribution function $\rho^{(2)}(\mathbf{r}, \mathbf{r}')$. For example if the potential energy is of the pairwise form as in (2.2), then the average potential energy $\langle U \rangle$ can be obtained by

$$\langle U \rangle = \frac{1}{2} \int \rho^{(2)}(\mathbf{r}, \mathbf{r}') u(\mathbf{r}, \mathbf{r}') d\mathbf{r}' d\mathbf{r} \tag{2.12}$$

If there is an external potential acting on all of the particles $V(\mathbf{r})$, then the mean energy due to this potential is

$$\langle V \rangle = \int \rho^{(1)}(\mathbf{r}) V(\mathbf{r}) d\mathbf{r} \tag{2.13}$$

Related to the n-particle distribution functions are the n-particle correlation functions defined as

$$g^{(n)}(\mathbf{r}^n) = \frac{\rho^{(n)}(\mathbf{r}^n)}{\rho^{(1)}(\mathbf{r}_1)\rho^{(1)}(\mathbf{r}_2)....\rho^{(1)}(\mathbf{r}_n)} \tag{2.14}$$

For the case of $n = 2$, the pair correlation function $g^{(2)}(\mathbf{r}, \mathbf{r}')$ relates $\rho^{(1)}(\mathbf{r})$ and $\rho^{(2)}(\mathbf{r}, \mathbf{r}')$

$$g^{(2)}(\mathbf{r}, \mathbf{r}') = \frac{\rho^{(2)}(\mathbf{r}, \mathbf{r}')}{\rho^{(1)}(\mathbf{r})\rho^{(1)}(\mathbf{r}')} \tag{2.15}$$

2.2 Density functional theory

2.2.1 The free energy is a unique functional of $\rho^{(1)}(\mathbf{r})$

The formal starting point of density functional theory is the statement that the free energy of a system F is a functional of the equilibrium single particle distribution function $\rho^{(1)}(\mathbf{r})$. The definition of $\rho^{(1)}(\mathbf{r})$ is

$$\rho^{(1)}(\mathbf{r}) = \left\langle \sum_i \delta^3(\mathbf{r}_i - \mathbf{r}) \right\rangle \tag{2.16}$$

where the angled brackets denote weighted averages. Using the N-particle distribution function of the canonical ensemble this may also be expressed as

$$\rho^{(1)}(\mathbf{r}) = \frac{N}{Z} \int \exp\left(-H/k_B T\right) \delta^3(\mathbf{r}_1 - \mathbf{r}) d^N\mathbf{r} d^N\mathbf{p} \tag{2.17}$$

since the N terms in the sum (2.16) are all equivalent.

It is remarkable that the free energy is a functional of $\rho^{(1)}(\mathbf{r})$ which appears to be much simpler than the full N-particle distribution function $f(\mathbf{r}^N, \mathbf{p}^N)$ which explicitly depends on the positions and momenta of all the particles. Hohenberg and Kohn [16] formulated a variational proof that the quantum mechanical ground state energy of an inhomogeneous electron fluid is a unique functional of the electron density $n(\mathbf{r})$. An analogous theorem underlies density functional theory for classical fluids. This theorem establishes that $f(\mathbf{r}^N, \mathbf{p}^N)$ is a unique functional of $\rho^{(1)}(\mathbf{r})$. Since the free energy F is clearly a functional of $f(\mathbf{r}^N, \mathbf{p}^N)$, it follows that the free energy is also a functional of $\rho^{(1)}(\mathbf{r})$. The proof for this theorem can be found in reference [17]. It is also shown that the equilibrium single particle distribution function $\rho^{(1)}(\mathbf{r})$, is the function that minimises the functional. For a different distribution function $\rho_x(\mathbf{r})$

$$F[\rho^{(1)}(\mathbf{r})] < F[\rho_x(\mathbf{r})] \tag{2.18}$$

From now on we will use $\rho(\mathbf{r})$ to denote single particle distribution functions. This will be used interchangeably to refer to arbitrary distributions or the equilibrium distribution where appropriate.

Unfortunately, for all but the simplest cases the form of the free energy functional $F[\rho(\mathbf{r})]$ is not known. If it were known, minimisation of the functional with respect to all possible single particle distribution functions $\rho(\mathbf{r})$ would yield the free energy F, which would be equivalent to calculating the system partition function.

The concept of the free energy density functional is useful in formulating approximate theories for inhomogeneous fluids. This is utilised in mean field density functional theory which will be introduced in Section 2.6.

2.2.2 Free energy functional for noninteracting particles in an external potential

One class of systems for which an exact free energy functional $F[\rho(\mathbf{r})]$ can be found is that of noninteracting ideal gas particles in an external potential. These systems have Hamiltonians of the form

$$H = \sum_{i=1}^{N} [K_i + V(\mathbf{r}_i)] \tag{2.19}$$

where K_i is the kinetic energy of the ith particle, and V is an external potential. This kind of system is particularly simple because there are no particle-particle interactions, and therefore no correlations between particles. This makes it possible to factorise the partition function into a product of N single

particle partition functions.

$$Z = \frac{1}{N!} z_1^N \tag{2.20}$$

where

$$z_1 = \frac{1}{\lambda^3} \int \exp(-V(\mathbf{r})/k_B T) d\mathbf{r} \tag{2.21}$$

For convenience we introduce a quantity I which is related to z_1 but has dimensions of volume defined by $z_1 = \lambda^{-3} I$. If Stirling's approximation is used in approximating $\ln N!$ for large N, the Helmholtz free energy can be expressed as

$$F = N k_B T \left[\ln \left(\frac{N\lambda^3}{I} \right) - 1 \right] \tag{2.22}$$

The equilibrium single particle distribution function $\rho(\mathbf{r})$ for this system is

$$\rho(\mathbf{r}) = \frac{N}{I} \exp(-V(\mathbf{r})/k_B T) \tag{2.23}$$

The average potential energy of the system $\langle V \rangle$ is

$$\langle V \rangle = \frac{N}{I} \int V(\mathbf{r}) \exp(-V(\mathbf{r})) d\mathbf{r} = \int \rho(\mathbf{r}) V(\mathbf{r}) d\mathbf{r} \tag{2.24}$$

Since $F = \langle K + V \rangle - TS$, the intrinsic free energy which is defined as the free energy excluding the potential energy due to the external field $F - \langle V \rangle = \langle K \rangle - TS$ is given by

$$F - \langle V \rangle = N k_B T \left[\ln \left(\frac{N\lambda^3}{I} \right) - 1 \right] - \int \frac{N \exp(-V(\mathbf{r}))}{I} V(\mathbf{r}) d\mathbf{r} \tag{2.25}$$

By looking at the definition of $\rho(\mathbf{r})$, it can be seen that the potential $V(\mathbf{r})$ can be expressed as

$$V(\mathbf{r}) = -k_B T \ln \rho(\mathbf{r}) \lambda^3 + k_B T \ln \left(\frac{N\lambda^3}{I} \right) \tag{2.26}$$

This allows the intrinsic free energy in (2.25) to be written as a functional of $\rho(\mathbf{r})$

$$F - U = k_B T \int \rho(\mathbf{r}) \left[\ln(\rho(\mathbf{r})\lambda^3) - 1 \right] d\mathbf{r} \tag{2.27}$$

The total free energy functional is then

$$F = k_B T \int \rho(\mathbf{r}) \left[\ln(\rho(\mathbf{r})\lambda^3) - 1 \right] d\mathbf{r} + \int \rho(\mathbf{r}) V(\mathbf{r}) d\mathbf{r} \tag{2.28}$$

This is the exact free energy functional for a system of N noninteracting point particles, each experiencing a single particle potential $V(\mathbf{r})$. Even though this system experiences no inter-particle correlations, it nevertheless possesses inhomogeneity of the particle distribution brought about by the external single particle potential.

2.2.3 Wide variety of systems studied using DFT

Approximate density functional theories have been used to model a wide variety of interesting systems that are distinct from simple fluids. Ashcroft [18] pioneered the use of density functional theory for the study of freezing of liquids. Talanquer and Oxtoby in particular have applied DFT to a very wide range of phenomena from freezing of liquids [19] to the formation of micelles from amphiphilic molecules [20].

Each situation necessitates a distinct approximate free energy functional to be constructed which

captures the competing energetic and entropic contributions to the free energy. For example, in their study of crystal nucleation Talanquer and Oxtoby constructed an approximate free energy as a functional of a spatially varying density $\rho(\mathbf{r})$ as well as structural order parameter $m(\mathbf{r})$. Their study of micelle formation involved a functional of the inhomogeneous density distributions of the hydrophobic $\rho_1(\mathbf{r})$ and hydrophilic $\rho_2(\mathbf{r})$ parts of the amphiphilic molecules, as well as the inhomogeneous distribution $\rho_0(\mathbf{r})$ of the solvent molecules. Density functional theory has also been used to study inhomogeneous fluids of polar molecules [21], which have been modelled as hard spheres with embedded dipoles. These studies involved $\rho(\mathbf{r},\omega)$ which is a positional and orientational probability distribution function for the molecules. Charged colloidal suspensions have been modelled [22] using mean field density functional theory, where the free energy is a functional of the set of distribution functions $\rho_\alpha(\mathbf{r})$ for ions of each charged species α. This is discussed Chapter 5, where the connection is made between MFDFT and the Poisson-Boltzmann mean field theory of charged colloidal suspensions.

2.3 Approximate treatment of fluids: separation of attractive and repulsive interactions

The starting point for many approximate treatments of fluids is the separation between the attractive and repulsive forces. The repulsive interactions can be dealt with approximately by treating the fluid molecules as hard spheres. The Hamiltonian is written as

$$H = K + \sum_{i>j} [u_R(\mathbf{r}_i, \mathbf{r}_j) + \phi(\mathbf{r}_i, \mathbf{r}_j)] \tag{2.29}$$

where the first term is the kinetic energy, $\phi(\mathbf{r}_i, \mathbf{r}_j)$ is the attractive portion of the pairwise molecular interaction, and $u_R = u_R(|\mathbf{r}_i - \mathbf{r}_j|)$ is the hard sphere interaction defined by

$$\begin{aligned} u_R(r) &= 0 \quad \text{for} \quad r \geq \sigma \\ u_R(r) &= \infty \quad \text{for} \quad r < \sigma \end{aligned} \tag{2.30}$$

where σ is the diameter of the hard spheres. Due to the nature of the hard-sphere interaction (2.30), the free energy for this system does not explicitly contain any potential energy terms due to $u_R(r)$. Any configuration for which $u_R(r)$ is nonzero for any pair of particles has zero probability, and does not contribute to the partition function.

Formally, if the form for the free energy functional of the system with purely repulsive interactions $F_{hs}[\rho(\mathbf{r})]$ were known, then the exact free energy functional for the full system could be obtained through thermodynamic integration [17]. This involves introducing a pair interaction $u_\alpha(\mathbf{r}_i, \mathbf{r}_j)$ which is a function of a 'charging up' parameter α

$$u_\alpha(\mathbf{r}_1, \mathbf{r}_2) = u_R(\mathbf{r}_1, \mathbf{r}_2) + \alpha\phi(\mathbf{r}_1, \mathbf{r}_2) \tag{2.31}$$

The free energy is then obtained from the free energy of the reference system and a second term involving an integration over α from 0 to 1.

$$F = F_{hs}[\rho(\mathbf{r})] + \frac{1}{2}\int_0^1 d\alpha \int d\mathbf{r} \int d\mathbf{r}' g_\alpha^{(2)}(\mathbf{r}, \mathbf{r}')\rho(\mathbf{r})\rho(\mathbf{r}')\phi(\mathbf{r}, \mathbf{r}') \tag{2.32}$$

where $g_\alpha^{(2)}(\mathbf{r}_1, \mathbf{r}_2)$ is the two-particle correlation function for a system with any given value of α between 0 and 1. This function is generally not known. In addition to this, F_{hs} is not known exactly and has to be approximated.

In principle, the procedure discussed here does not require $u_R(r)$ to be the hard-sphere interaction

or even the repulsive portion of the interaction. If a form of the functional for a reference system is known, together with a correlation function for all values of α, then the procedure can be applied generally. In practice, the hard-sphere reference system is frequently used because the nature of the correlations in a hard-sphere fluid are well understood. For Lennard-Jones fluids, a refinement to the hard sphere reference system is given by the Weeks, Chandler, Anderson (WCA) approach, whereby the reference system consists of hard spheres with a temperature-dependent diameter [23].

2.4 The Gibbs-Bogoliubov inequality

The Gibbs-Bogoliubov inequality plays an important role in the development of approximate statistical mechanical theories such as mean field density functional theory. This inequality asserts that when the free energy of a system with Hamiltonian H is estimated using the distribution of states from a different (possibly simpler) system with Hamiltonian H_0, then the resulting free energy will be greater than or equal to the exact free energy of the system.

To prove this principle, the original Hamiltonian is decomposed into $H = H_0 + H_1$, where H_0 corresponds to the Hamiltonian for which the free energy can be formulated. The system's partition function is

$$Z = \frac{1}{N!h^{3N}} \int d^N\mathbf{r} d^N\mathbf{p} \exp\left(-(H_0 + H_1)/k_BT\right) \tag{2.33}$$

The distribution of states in the system with Hamiltonian H_0 is

$$f_0 = \frac{1}{Z_0} \exp(-H_0/k_BT) \tag{2.34}$$

where Z_0 is the partition function for a system with H_0

$$Z_0 = \frac{1}{N!h^{3N}} \int d^N\mathbf{r} d^N\mathbf{p} \exp\left(-H_0/k_BT\right) \tag{2.35}$$

Dividing (2.33) through by Z_0 results in

$$\frac{Z}{Z_0} = \langle \exp(-H_1/k_BT) \rangle_0 \tag{2.36}$$

where the subscript indicates an average taken over the probability distribution f_0. Due to the convexity property [24] of the exponential function, averages obey the inequality $\langle \exp a \rangle \geq \exp\langle a \rangle$ so that

$$\frac{Z}{Z_0} \geq \exp\left(-\langle H_1 \rangle_0 / k_BT\right). \tag{2.37}$$

Taking logarithms we get

$$F \leq F_0 + \langle H_1 \rangle_0. \tag{2.38}$$

Now since $F_0 = \langle H_0 \rangle_0 - TS_0$, (2.38) can be re-written as

$$F \leq \langle H \rangle_0 - TS_0 \tag{2.39}$$

Where the first term is the average energy of the system, calculated using the distribution of states in H_0, and the second term contains the entropy of the system H_0.

The usefulness of this principle is that if the system with Hamiltonian H_0 contains some sort of parameter that can be varied, then minimisation of the quantity $F_0 + \langle H_1 \rangle_0$ with respect to this parameter, will tailor the H_0 system that gives the best distribution of states f_0 to approximate the free energy of the true system F. This variational principle is exploited in mean field density functional theory, where the approximate free energy is minimised with respect to all possible single

particle potentials $V(\mathbf{r})$ in order to find the one that best describes the full system of interacting particles.

2.5 Mean field theory for fluids

2.5.1 The mean field potential

In the mean field theory of fluids, the Hamiltonian (2.29) is split up into two parts $H = H_0 + H_1$ where

$$H_0 = K + \sum_{i>j} u_R(\mathbf{r}_i - \mathbf{r}_j) + \sum_{i=1}^{N} V(\mathbf{r}_i), \tag{2.40}$$

and

$$H_1 = \sum_{i>j} \phi(\mathbf{r}_i - \mathbf{r}_j) - \sum_{i=1}^{N} V(\mathbf{r}_i), \tag{2.41}$$

The potential $V(\mathbf{r})$ is a single particle potential that cancels out between the two terms and therefore does not feature in the full Hamiltonian H. The Hamiltonian H_0 describes a reference system of N hard spheres in an external potential $V(\mathbf{r})$. The mean field free energy for the system F_{MF} is calculated using the probability distribution of states in H_0

$$F_{MF} = F_0 + \langle H_1 \rangle_0 \tag{2.42}$$

where F_0 is the free energy of the system with Hamiltonian H_0 and $\langle H_1 \rangle_0$ is the average of H_1 evaluated using the probability distribution of states in H_0. The external potential $V(\mathbf{r})$ does not feature explicitly in the full Hamiltonian H, nor is it explicitly in the free energy F_{MF} since the average energy due to this external potential cancels out between the two terms in (2.42). Due to this cancellation, the free energy of the system can also be written as

$$F_{MF} = F_0 - \langle V \rangle_0 + \langle \phi \rangle_0 = \langle H \rangle_0 - TS_0 \tag{2.43}$$

where the averages evaluated over the probability of states in H_0 are the quantities

$$\langle V \rangle_0 = \left\langle \sum_{i=1}^{N} V(\mathbf{r}_i) \right\rangle_0 \qquad \text{and} \qquad \langle \phi \rangle_0 = \left\langle \sum_{i>j} \phi(\mathbf{r}_i - \mathbf{r}_j) \right\rangle_0 \tag{2.44}$$

The quantity $F_0 - \langle V \rangle_0 = \langle K \rangle_0 - TS_0$ is the intrinsic free energy of a hard-sphere fluid in an external potential. The last term $\langle \phi \rangle_0$ in Equation (2.43) is the average of the attractive energy evaluated in the distribution of states of the inhomogeneous hard-sphere fluid with Hamiltonian H_0.

The next task is to formulate a free energy functional for F_{MF}. Minimising this functional with respect to $\rho(\mathbf{r})$, is effectively equivalent to searching for the external potential $V(\mathbf{r})$ that minimises F_{MF}. The minimising $V(\mathbf{r})$ is the mean field potential- the single particle potential that best emulates the complicated pairwise interactions between the particles. According to the Gibbs-Bogoliubov inequality, the free energy F_{MF} will lie above the true free energy of the system, and so provides an upper bound to the free energy F.

2.5.2 The mean field approach seen as a perturbation theory

The approach outlined above may also be viewed as a form of thermodynamic perturbation theory. As before, the Hamiltonian is split up into $H = H_0 + H_1$ where $H_0 = K + U_R + V$ and $H_1 = \phi - V$ (we have used shorthand K, U_R, V, ϕ for the appropriate single particle and pairwise sums). For the

remainder of this chapter all energies will be given in units of k_BT. The partition function is

$$Z = \frac{1}{N!h^{3N}} \int d^N\mathbf{r} d^N\mathbf{p} \exp\left(-(H_0 + H_1)\right) \tag{2.45}$$

If H_1 can be considered to be small for all of the configurations in the integral, then the exponential in (2.45) may be expanded to first order

$$Z \simeq \frac{1}{N!h^{3N}} \int d^N\mathbf{r} d^N\mathbf{p} \exp(-H_0)\left(1 - H_1\right) = Z_0 - \langle H_1\rangle_0 Z_0 \tag{2.46}$$

taking the logarithm of Z, and expanding to first order in $\langle H_1\rangle_0$ gives the same result as the mean field free energy F_{MF}

$$F \simeq F_0 + \langle H_1\rangle_0 \tag{2.47}$$

This shows that the mean field potential $V(\mathbf{r})$ can be interpreted as the single particle potential that gives rise to a distribution of hard sphere particles optimised to make the perturbative term in this expansion $\langle H_1\rangle_0$ small

$$\langle H_1\rangle_0 = \left\langle \sum_{i>j} \phi(\mathbf{r}_i - \mathbf{r}_j) - \sum_{i=1}^{N} V(\mathbf{r}_i) \right\rangle_0 \tag{2.48}$$

2.6 Mean field free energy functional

The next task is to formulate a functional for F_{MF}. Even within the mean field approximation, further approximations need to be made to keep the functionals simple. The functional will be formulated in two steps. The first step is to obtain F_{hs}, the functional for the intrinsic free energy of the inhomogeneous hard sphere fluid $F_{hs} = F_0 - \langle V\rangle = \langle K\rangle_0 - TS_0$. The second step is to obtain a functional for the mean attractive energy in the H_0 distribution of states $\langle\phi\rangle_0$.

2.6.1 Approximate functional for the hard sphere fluid in the LDA

The hard-sphere interactions mean that the partition function does not trivially factorise into N single-particle partition functions as was the case for the ideal gas in an external potential (2.21). In fact, the hard sphere fluid has non-trivial correlations and even exhibits a phase transition to a solid phase at high densities. Certain simplifying approximations will be made here, that lead to the standard functional that is used in many treatments of inhomogeneous fluids.

For a homogeneous hard sphere fluid of uniform density ρ, a good approximation for the free energy is given by the Carnahan-Starling formula. This gives free energy density $f_{hs} = F_{hs}/V$ as

$$f_{hs}(\rho) = \rho\left[\ln\rho\lambda^3 - 1 + \frac{4\eta - 3\eta^2}{(1-\eta)^2}\right] \tag{2.49}$$

where η is the hard sphere packing fraction $\eta = (1/6)\pi\sigma^3\rho$ and σ is the hard sphere diameter. This formula is derived from a virial expansion of a uniform hard-sphere system. It accounts for the correlations in a dilute hard sphere fluid approximately, for the case when the fluid is homogeneous.

The next step involves invoking the local density approximation (LDA) to obtain F_{hs} for an inhomogeneous hard sphere fluid. The LDA applies the assumption that (2.49) is valid at every point in an inhomogeneous fluid of hard-spheres. It is implemented by simply replacing ρ by a spatially varying $\rho(\mathbf{r})$ everywhere in (2.49) to give $f_{hs}(\rho(\mathbf{r}))$. The free energy density is then integrated to give

the total intrinsic free energy for the inhomogeneous sphere free fluid

$$F_{hs} = \int \rho(\mathbf{r}) \left[\ln \rho(\mathbf{r})\lambda^3 - 1 + \frac{4\eta(\rho(\mathbf{r})) - 3\eta^2(\rho(\mathbf{r}))}{(1-\eta(\rho(\mathbf{r})))^2} \right] d\mathbf{r} \tag{2.50}$$

Essentially, the LDA corresponds to the assumption that the nature of the correlations in the hard sphere fluid is unaffected by the inhomogeneity. Note that F_{hs} is the intrinsic free energy of the hard sphere fluid, and does not contain $\langle V \rangle_0$ the energy of the potential causing the inhomogeneity.

2.6.2 Attractive energy in the RPA

The second term in equation F_{MF} is the average attractive energy evaluated in the probability distribution of states in H_0, which can be written in the form

$$\left\langle \sum_{i>j} \phi(r_i - r_j) \right\rangle_0 = \frac{1}{2} \int d\mathbf{r} \int d\mathbf{r}' g_0^{(2)}(\mathbf{r},\mathbf{r}')\rho(\mathbf{r})\rho(\mathbf{r}')\phi(\mathbf{r}-\mathbf{r}') \tag{2.51}$$

where $g_0^{(2)}(\mathbf{r},\mathbf{r}')$ is the two-particle correlation function for the inhomogeneous hard sphere system. The standard DFT treatment of this contribution involves a further simplification: the random phase approximation (RPA), according to which the hard sphere correlations in the reference system are neglected.

$$g_0^{(2)}(\mathbf{r},\mathbf{r}')\rho(\mathbf{r})\rho(\mathbf{r}') \approx \rho(\mathbf{r})\rho(\mathbf{r}') \tag{2.52}$$

It should be said at this point that since a functional constructed using the LDA and RPA is not strictly $F_{MF} = F_0 + \langle H_1 \rangle_0$, the variational principle $F_{MF} \geq F$ no longer necessarily holds. It must be assumed that the two approximations that lead to the formulation of the functional are valid, otherwise minimisation with respect to all $\rho(\mathbf{r})$ may result in a free energy that is lower than the true free energy.

2.6.3 Optimal distribution function and free energy

Combining the two terms (2.50) and (2.51) that make up F_{MF}, the final mean field functional is expressed as

$$F_{MF}[\rho(\mathbf{r})] = F_{hs}[\rho(\mathbf{r})] + \frac{1}{2} \int d\mathbf{r} \int d\mathbf{r}' \rho(\mathbf{r})\rho(\mathbf{r}')\phi(\mathbf{r}-\mathbf{r}') \tag{2.53}$$

This functional needs to be minimised with respect to $\rho(\mathbf{r})$, to find the distribution function that gives the best approximation to F. To obtain the optimal distribution function, the free energy (2.53) is functionally differentiated with respect to $\rho(\mathbf{r})$. For a closed system in the canonical ensemble (NVT), the minimisation needs to be subject to the constraint that the total number of particles is fixed to be N

$$\int \rho(\mathbf{r}) d\mathbf{r} = N \tag{2.54}$$

This constraint is imposed through the introduction of a Lagrange multiplier μ. The Euler Lagrange equation for the optimising density profile $\rho(\mathbf{r})$ is then

$$\frac{\delta}{\delta\rho(\mathbf{r})} \left[F_{MF}[\rho(\mathbf{r})] - \mu \int \rho(\mathbf{r}) d\mathbf{r} \right] = 0 \tag{2.55}$$

We denote the functional derivative of the hard sphere functional $\delta F_{hs}/\delta\rho(\mathbf{r}) = df_{hs}/d\rho(\mathbf{r}) = \mu_{hs}[\rho(\mathbf{r})]$, which is a spatially varying chemical potential for the inhomogeneous hard sphere fluid. The Euler-

Lagrange equation (2.55) becomes

$$\mu = \mu_{hs}[\rho(\mathbf{r})] + \int \rho(\mathbf{r}')\phi(\mathbf{r}-\mathbf{r}')d\mathbf{r}' \tag{2.56}$$

The second term on the right hand side may be viewed as an effective single particle potential $\phi_{\text{eff}}(\mathbf{r})$ that takes the place of the pairwise intermolecular attractions in the mean field approach. It is also worth noting that the two spatially varying terms on the right hand side of (2.56) add up to a spatially constant μ. The Lagrange multiplier is related to the chemical potential of the system. This is always expected to be constant throughout a system which is at equilibrium.

2.6.4 The grand potential functional

A system in the grand canonical ensemble (constant (μVT)) is open with respect to exchange of particles with a reservoir at a chemical potential μ. The appropriate thermodynamic potential is the grand potential Ω which is related to F through the Legendre transform $\Omega(\mu, V, T) = F(N, V, T) - \mu N$. The grand potential functional can be constructed from the Helmholtz free energy functional (2.53)

$$\Omega_{MF}[\rho(\mathbf{r})] = F_{MF} - \mu \int \rho(\mathbf{r})d\mathbf{r} \tag{2.57}$$

where μ is now the chemical potential of the system which is at equilibrium with the particle reservoir. Minimising $\Omega_{MF}[\rho(\mathbf{r})]$ with respect to $\rho(\mathbf{r})$ is somewhat easier than in the canonical ensemble, as μ is a pre-specified constant, rather than being determined by the constraint of constant particle number (2.54). The equation for the optimal profile is the same as (2.56), but with a fixed μ corresponding to the chemical potential of the reservoir. The total number of particles contained in the optimal density profile $\rho(\mathbf{r})$ will be the number that makes the chemical potential of the system have the required value $\mu = \partial F/\partial N$. This corresponds to the mean number of particles $\bar{N}$ in a system at equilibrium with a particle bath at chemical potential μ.

2.7 Relationship between DFT and the field theoretical approach

It is worth mentioning the parallels between DFT and the field theoretical approach (FT) in statistical mechanics. This approach underlies the Landau-Ginzburg model of phase transitions [24], and has been applied by Langer [25] to formulate a theory for the decay of metastable states, and by Langer and Turski [26] to vapour condensation specifically. Several authors have discussed various parallels between the DFT and FT approaches. Evans [11] compared and contrasted the two approaches in the description of planar liquid-vapour interfaces. Reguera and Reiss [27] discussed the role of fluctuations in the two approaches. Fluctuations are of particular importance in the study of small systems such as the molecular clusters that are the precursors to condensation. Barrett [28] made comparisons between the two approaches and suggested that adaptations need to be made to the DFT treatment of small molecular clusters to account for fluctuations.

In the field theoretical approach a system is divided into cells of a characteristic lengthscale Λ. These cells are large on the microscopic scale, and in the case of a fluid each cell would contain many molecules, but are small on a macroscopic scale. In this picture $\rho(\mathbf{r})$ is defined to be the mean density of particles in a cell centred at $\mathbf{r}$. In other words $\rho(\mathbf{r})$ is a coarse grained order parameter profile. The configurational part of the partition function for a system with Hamiltonian H is expressed as a

functional integral over all possible 'patterns' of the coarse grained order parameter $\rho(\mathbf{r})$

$$Z = \int d^N\mathbf{r} \exp(-H) = \int \mathcal{D}[\rho(\mathbf{r})] \exp\left(-E[\rho(\mathbf{r})]\right) \tag{2.58}$$

$\mathcal{D}[\rho(\mathbf{r})]$ denotes functional integration over all possible $\rho(\mathbf{r})$. $E[\rho(\mathbf{r})]$ is called the effective Hamiltonian describing a system constrained to have the coarse grained order parameter pattern $\rho(\mathbf{r})$. By comparing the left and right sides of (2.58) it can be seen that the effective Hamiltonian $E[\rho(\mathbf{r})]$ is defined through

$$\exp\left(-E[\rho(\mathbf{r})]\right) = \int d^N\mathbf{r} \exp(-H)\delta(\rho(\mathbf{r}) - \widehat{\rho}(\mathbf{r})) \tag{2.59}$$

The delta function allows only those configurations in the integral over the positions $d^N\mathbf{r}$ to be picked up for which $\rho(\mathbf{r})$ has the required pattern given by $\widehat{\rho}(\mathbf{r})$ (where $\widehat{\rho}(\mathbf{r})$ is a function of all of the molecular positions $\{\mathbf{r}_i\}$). From (2.59) it is clear that the effective Hamiltonian $E[\rho(\mathbf{r})]$ has properties of free energy rather than only energy. This is because one given pattern of the coarse grained order parameter $\rho(\mathbf{r})$, corresponds to a number of microscopic molecular configurations. A cell centred at a point $\mathbf{r}$ with average density $\rho(\mathbf{r})$ can have many different configurations of molecules. This means $E[\rho(\mathbf{r})]$ contains an entropic contribution as well as an energetic one.

The effective Hamiltonian $E[\rho(\mathbf{r})]$ is a functional of $\rho(\mathbf{r})$ and has different forms depending on the system. In most cases this has to be approximated in some way. Once a form for $E[\rho(\mathbf{r})]$ is obtained, the functional integral over $\mathcal{D}[\rho(\mathbf{r})]$ needs to be evaluated. In most cases this cannot be done exactly. This is where the saddle point approximation in FT comes in, which is also referred to as the mean field approximation. For a large system, the partition function (2.58) can be approximated by the contribution from the coarse grained order parameter profile $\rho^*(\mathbf{r})$ that gives the largest contribution to the functional integral

$$Z = \int \mathcal{D}[\rho(\mathbf{r})] \exp\left(-E[\rho(\mathbf{r})]\right) \simeq \exp\left(-E[\rho^*(\mathbf{r})]\right) \tag{2.60}$$

The 'mean field' profile $\rho^*(\mathbf{r})$ will be the one that minimises the effective Hamiltonian functional $E[\rho(\mathbf{r})]$, and therefore makes the largest contribution to the partition function. The free energy of the system in this approximation is then just $E[\rho^*(\mathbf{r})]$, which is the free energy of a system constrained to exhibit the optimising coarse grained order parameter profile $\rho^*(\mathbf{r})$. Systematic improvements to this estimate can be made by adding the contributions of fluctuations $\delta\rho(\mathbf{r})$ about the optimising profile $\rho^*(\mathbf{r})$ to the partition function Z [24]. This approach of adding fluctuations has also been used in various treatments of the effective interactions in colloidal suspensions [29, 30, 31, 32], where it has been shown that the mean field Poisson-Boltzmann equation corresponds to a saddle point approximation in a field theoretical representation of the free energy.

The free energy functional $F[\rho(\mathbf{r})]$ in DFT and the effective Hamiltonian $E[\rho(\mathbf{r})]$ in FT have very distinct definitions. If the exact form of a DFT free energy functional $F[\rho(\mathbf{r})]$ for a system were known, then the minimising density profile $\rho(\mathbf{r})$ would be the true equilibrium single particle distribution function, which is equivalent to a weighted average of the density profile over all possible microscopic configurations. The coarse grained order parameter $\rho(\mathbf{r})$ used in FT corresponds to a restricted subset of all microscopic configurations. The optimising distribution function $\rho^*(\mathbf{r})$ that minimises the effective Hamiltonian E is just the most likely order parameter profile. The equilibrium single particle distribution function $\rho(\mathbf{r})$ would be obtained from FT by performing a weighted average of $\rho(\mathbf{r})$ over all possible profiles.

$$\rho(\mathbf{r}) = \frac{1}{Z} \int \mathcal{D}[\rho(\mathbf{r})]\rho(\mathbf{r}) \exp\left(-E[\rho(\mathbf{r})]\right) \tag{2.61}$$

While the exact free energy F is a convex function of volume V, the free energy obtained from

the mean field or saddle point approximation in FT $E[\rho(\mathbf{r})^*]$ is not necessarily convex because it represents a system that is constrained to exhibit a certain coarse grained density profile $\rho(\mathbf{r})^*$.

The mean field approximation together with other approximations used to formulate the free energy in both FT and DFT make the two treatments become very similar. The two functionals $E[\rho(\mathbf{r})]$ and $F[\rho(\mathbf{r})]$ even take the same form in various treatments [27]. The question discussed extensively in the literature [11, 27, 28] is what subset of microscopic configurations of the true partition function Z are included in the different approximate functionals used in DFT and FT approaches. The nature of the mean field approximation may be different in the two treatments, however ultimately it involves the neglect of certain configurations in the partition function that are brought about by microscopic correlations between particles in the system.

Evans [11] argued that in the case of a planar interface between liquid and vapour phases, the square gradient free energy functional proposed by Van der Waals includes contributions to the free energy from long wavelength density fluctuations perpendicular to the interface known as capillarity fluctuations. He stated that field theoretical treatments that utilise the same functional and then add the effects of such fluctuations to the mean field profile are not consistent.

When the number of particles is small, deviations from mean field behaviour are large due to the increased importance of fluctuations. In the next chapter, the application of mean field density functional theory to systems containing a small number of particles will be considered.

Chapter 3

Application of Mean field density functional theory to small systems

3.1 Introduction

Small systems consisting of less than 100 particles exhibit unusual thermodynamic behaviour as a result of surface effects and the relative importance of fluctuations compared with larger systems. Examples of small systems include fluids confined to nanopores, which have been found to exhibit extremely rich phase behaviour [6], small metallic or semiconductor clusters that form quantum dots, and molecular clusters that can be isolated and studied in jets. In addition to this, small molecular clusters often characterise important transition states in phase transitions such as the condensation of vapours. In this situation, the embryos of the new phase or critical clusters whose formation governs the rate of the phase transition, can have sizes of less than 10 molecules.

Mean field density functional theory has been applied extensively over the past 20 years, to study the condensation of vapours [33, 9, 23, 34, 28, 35]. There are two main approaches. The approach of Oxtoby and Evans [9] involves treating an open system in the grand canonical ensemble. Using a free energy functional of the form (2.53), and employing an iterative procedure to find solutions to the Euler-Lagrange equation (2.56), they found that under the right conditions inhomogeneous density profiles corresponding to saddle-points in the functional space arise out of the procedure. These stationary solutions persisted for a few iterations before ultimately disappearing to be replaced with homogeneous density profiles corresponding to the stable global minima. The saddle point solutions were interpreted as critical clusters, the growth or evaporation of which are equally likely. The free energy difference between these clusters and the homogeneous vapour gives the free energy of formation of critical clusters that determine the nucleation rate.

The objection has been made that saddle point solutions are irrelevant. For given external conditions (say temperature and chemical potential) the system has a unique free energy and grand potential, and it is only the minimised free energy from the MFDFT approach that can be taken as an approximation to the free energy of an actual system. To counter this objection, it was shown by Talanquer and Oxtoby [23] that the metastable solutions in an open system (fixed chemical potential μ) can be mapped onto stable solutions of a closed system (with fixed N), for which the use of MFDFT to obtain the equilibrium solution is justified. Closed systems had been studied earlier in this context by Lee, Telo da Gamma and Gubbins [33].

Contributions to the free energy of a fluid that are negligible on a macroscopic scale become crucial on a more microscopic scale [6]. These contributions include surface effects, translational motion and especially fluctuations. Mean field theories are expected to be less successful in treating small systems due to the importance of fluctuations.

There has been relatively little work on validating MFDFT against other approaches. Lee *et. al.* [33] compared MFDFT results with molecular dynamics simulations for systems with N ranging from 100 to 30,000 particles. Reguera *et. al.* [6], compared results of MFDFT with Monte Carlo calculations for clusters of 80 argon atoms, with a discussion of the differences in density profiles and system pressures.

In this chapter a simple system is considered for which the exact free energy is available for comparison with MFDFT calculations [36]. The model system consists of just two interacting hard rods in one dimension. Exact calculations are possible since a small number of molecules is considered. On the other hand, this requires care to be taken in the application of the standard MFDFT approach, as inconsistencies arise when it is applied to systems containing small numbers of particles. The reduced dimensionality and small number of particles means that the problems in applying MFDFT should be most severe.

One dimensional hard-rods were studied by Percus, who derived an exact functional for the free energy of hard rods in an external potential $V(r)$ [37]. He also studied sticky hard rods [38], which have an infinitesimally short range attractive interaction between neighbouring rods. The rods studied in this chapter have an attractive interaction with a finite range. The system also differs from that studied by Percus due to the small number of particles considered. We pay particular attention to the finite size effects, and their consequences for the application of the standard approximate mean field density functional theory frequently applied to fluids.

3.2 Exact free energy of a simple model system

The model system consists of two hard rods each of length b, free to move on a line of length R, with periodic boundary conditions. The rods interact through a pair potential $\phi(r_{12})$ where r_{12} is the separation of the rod centres. The partition function is

$$Z = \frac{1}{2}\gamma^2 \int_0^R dr_1 \int_0^R dr_2 \exp(-U(r_1, r_2)/k_B T) \tag{3.1}$$

where $\gamma = (2\pi m k_B T)^{1/2}/h$ is the inverse thermal de Broglie wavelength (m is the rod mass and h is Planck's constant), k_B is Boltzmann's constant, T is the temperature, and $U(r_1, r_2)$ is the potential energy of the system: r_1 and r_2 are the positions of the centres of the rods.

The potential energy $U(r_1, r_2)$ can be separated into an attractive potential $\phi(r_1 - r_2)$, and a hard sphere (or in this one-dimensional case hard rod) repulsive potential $u_R(r_1 - r_2)$. Due to the periodic boundary conditions, the rods interact with each other and with periodic images. For the attractive potential we assume a form

$$\phi(r) = -\alpha \exp(-\lambda r) \tag{3.2}$$

For simplicity, we limit the range of this interaction so that there are only two terms in the exponent, an interaction between rod 1 and rod 2, and between rod 1 and the closest periodic image of rod 2. Further contributions to the interaction energy are neglected. The short range repulsive potential $u_R(r_1 - r_2)$ takes the form of a hard sphere interaction in one dimension:

$$\begin{aligned} u_R(r_1 - r_2) &= 0 \text{ when } |r_1 - r_2| \geq b \\ u_R(r_1 - r_2) &= \infty \text{ when } |r_1 - r_2| < b \end{aligned} \tag{3.3}$$

This repulsive interaction restricts the configurations that make a nonzero contribution to the partition

function, which reduces to $Z = \gamma^2 RI/2$ where

$$I = \int_b^{R-b} dr_2 \exp\left(\frac{\alpha}{k_B T}\exp(-\lambda r_2) + \frac{\alpha}{k_B T}\exp(-\lambda(R-r_2))\right) \tag{3.4}$$

The free energy is $F = -k_B T \ln Z$, but for convenience we focus on an excess free energy, obtained by subtracting the free energy of two non-interacting point particles for which $I = R$:

$$F_{\text{ex}} = F - F_{\text{id}} = -k_B T\left(\ln\frac{\gamma^2 RI/2}{\gamma^2 R^2/2}\right) = k_B T \ln(R/I) \tag{3.5}$$

The integral I can be calculated numerically once the parameters are specified. The distances R, r_2, b and λ^{-1} are taken to be dimensionless multiples of some length scale R_0. The energies α and F_{ex} are expressed in terms of the energy scale $k_B T$. To illustrate the qualitative differences between the interacting case and the noninteracting case, Figure 3.1 shows the full free energy (in arbitrary units) versus R of a system of two interacting particles ($\alpha = 5$, $b = 1$, $\lambda = 0.5$) as well as the free energy of an ideal gas of noninteracting particles ($\alpha = 0$ and $b = 0$). The free energy against volume curve for the interacting particles displays loop behaviour that is characteristic for small systems [5, 6]. Due to the short range repulsive and attractive forces the difference between the two curves becomes smaller for large R.

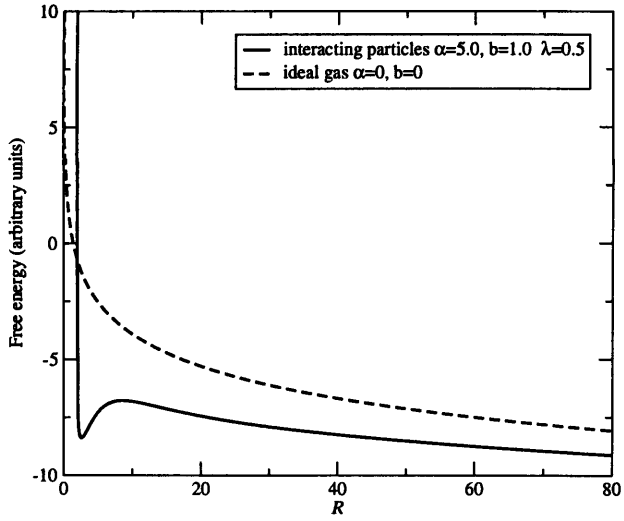

Figure 3.1: Comparison between the free energies of two non-interacting point particles and two interacting hard rods, as a function of ring circumference R. The difference between the two defines the excess free energy F_{ex}.

3.3 Mean field density functional theory

3.3.1 The standard free energy functional

To construct a mean field free energy functional for this model system, we follow the recipe laid out in Chapter 2. As is the case for many approximate treatments of fluids, the mean field theory involves the separation of the attractive and repulsive forces. The mean field approximation introduces an external single particle potential $V(r)$, tailored to mimic the effect of the pairwise attractive interactions. The mean field potential effectively facilitates the treatment of attractive interactions as a perturbation on the hard sphere system.

Following the mean field recipe, the Hamiltonian of the system is written [28]

$$H = K + H_0 + H_1. \tag{3.6}$$

where K is the kinetic energy part of the Hamiltonian, and H_0 is the potential energy of the mean field reference Hamiltonian

$$H_0 = \sum_{i>j} u_R(r_i - r_j) + \sum_{i=1}^{N} V(r_i) \tag{3.7}$$

where u_R is the hard sphere repulsive interaction potential. The $i > j$ denotes a sum over all pairs of particles. The Hamiltonian $K + H_0$ describes a reference system of N hard rods in a single particle mean field potential $V(r)$. The additional part of the Hamiltonian H_1 is

$$H_1 = \sum_{i>j} \phi(r_i - r_j) - \sum_{i=1}^{N} V(r_i) \tag{3.8}$$

where $\phi(r)$ is the attractive interaction potential. In mean field theory this contribution, which contains the attractive energy, is calculated using the distribution of states in the reference system $K + H_0$. The mean field free energy of the system is then given by

$$F_{MF} = F_0 + \langle H_1 \rangle_0 \tag{3.9}$$

where $F_0 = -k_B T \ln Z_0$ is the free energy of the reference system, with partition function

$$Z_0 = \frac{\gamma^N}{N!} \int d^N r \exp(-H_0/k_B T) \tag{3.10}$$

The second term in F_{MF} contains the average attractive energy estimated using the probability distribution of states in the reference system. Spatial integrations are over the entire ring of length R. The free energy depends on the choice made for the mean field potential $V(r)$. However, as discussed before, the average of $V(r)$ cancels out between the two contributions in equation (3.9), allowing the free energy to be rewritten as

$$F_{MF} = F_h + \left\langle \sum_{i>j} \phi(r_i - r_j) \right\rangle_0 \tag{3.11}$$

where F_h is the free energy of the reference system minus the contribution due to the mean field potential, and the second term contains the average of the pairwise attractive interactions in the ensemble of the reference system.

The mean field potential $V(r)$ appears neither in the full Hamiltonian in equation (3.6), nor explicitly in the free energy F_{MF} given by equation (3.11). The dependence on $V(r)$ is hidden in the weighting of configurations in the $\langle \ldots \rangle_0$ averages and in the entropic contribution to F_h. The main purpose of $V(r)$ is to mimic the effect of the attractive interactions. This approximation is best when the perturbative contribution to equation (3.9) is small. This is achieved by choosing $V(r)$ to minimise the free energy F_{MF}. The Bogoliubov inequality [24] ensures that the free energy calculated in this way will not lie below the true free energy of the system with Hamiltonian H.

Both terms on the right hand side of equation (3.11) may be regarded as functionals of the reference system single particle distribution function or density profile $\rho(r)$, defined by

$$\rho(r) = \left\langle \sum_{i=1}^{N} \delta(r_i - r) \right\rangle_0 = \frac{N}{Z_0} \frac{\gamma^N}{N!} \int d^N r \exp(-H_0/k_B T) \delta(r_1 - r). \tag{3.12}$$

This is itself a functional of the mean field potential $V(r)$, so the minimisation of the free energy F_{MF} with respect to the mean field potential may be done with respect to the density profile if F_{MF} is expressed as a functional of $\rho(r)$. This was the observation made by Barrett in his interpretation of the standard density functional approach [28].

Next, a density functional representation of the free energy F_{MF} for the two-rod system needs to be found. The term F_h is the intrinsic free energy of an inhomogeneous fluid of non-attractive hard rods. Percus [37, 38] developed an analytical functional for this, which is exact for the case when the number of particles N is large. It will be shown that this treatment breaks down for the case when $N = 2$. For the purposes of this study we employ the local density approximation (LDA), since this is the standard practice for developing MFDFT in higher dimensions, where exact solutions are not available.

Approximate functional for the intrinsic free energy of the reference system

The first step is to find an expression for the free energy of a homogeneous system of hard rods. By setting $\alpha = 0$ in the partition function obtained in the preceding section, we get the exact free energy of two non-interacting hard rods

$$F_h = -k_B T \ln\left(\frac{\gamma^2}{2} R(R-2b)\right) \tag{3.13}$$

The homogeneous one-particle density is $\rho = 2/R$ so we can rewrite this as

$$F_h = 2k_B T \ln\left(\frac{2}{\gamma R}\frac{1}{(2(1-2b/R))^{1/2}}\right) \tag{3.14}$$

and extract the free energy density

$$f_h = F_h/R = k_B T \rho \ln\left(\frac{\rho}{\gamma}\frac{1}{(2(1-b\rho))^{1/2}}\right) \tag{3.15}$$

The next step is to write the free energy, in the local density approximation, as a functional of a spatially varying single-particle distribution function $\rho(r)$:

$$F_h = \int_0^R f_h(\rho(r))dr = \int_0^R k_B T \rho(r) \ln\left(\frac{\rho(r)}{\gamma}\frac{1}{(2(1-b\rho(r)))^{1/2}}\right) \tag{3.16}$$

This is the intrinsic free energy of the system with Hamiltonian H_0, that is to say the contribution due to the interactions between the rods and the mean field has been subtracted. It is clearly a functional of $\rho(r)$.

Approximate functional for the mean attractive energy

The second term in equation (3.11) is the average attractive energy evaluated in the probability distribution of states in H_0, which can be written in the form [15]

$$\left\langle \sum_{i>j} \phi(r_i - r_j) \right\rangle_0 = \frac{1}{2}\int_0^R dr \int_0^R dr' \rho^{(2)}(r,r')\phi(r-r') \tag{3.17}$$

where $\rho^{(2)}(r,r')$ is the two-particle distribution function of hard rods in the reference system. As discussed in Chapter 2, the standard DFT treatment of this contribution employs a further simplification: the random phase approximation (RPA), which involves neglect of correlations in the hard-rod reference system.

$$\rho^{(2)}(r,r') \approx \rho(r)\rho(r') \tag{3.18}$$

Combining the two terms, the functional expression for F_{MF} is then

$$F_{MF} = \int_0^R dr k_B T \rho(r) \ln\left(\frac{\rho(r)}{\gamma} \frac{1}{(2(1-b\rho(r)))^{1/2}}\right) + \frac{1}{2}\int_0^R dr \int_0^R dr_2' \rho(r)\rho(r')\phi(r-r') \quad (3.19)$$

The free energy is now explicitly a functional of the reference system single-particle density profile $\rho(r)$. Minimising equation (3.19) with respect to $\rho(r)$ is equivalent to choosing the $V(r)$ which best mimics the attractive interactions. The optimal $V(r)$ can be reconstructed from the optimal density profile if required, though there are difficulties which will be discussed in Section 3.3.3.

The minimisation is achieved by solving the Euler-Lagrange equation associated with equation (3.19)

$$\mu_h(\rho(r)) = \mu - \int \rho(r')\phi(r-r')dr' \quad (3.20)$$

where $\mu_h(\rho(r)) = df_h/d\rho(r)$ is given by

$$\mu_h(\rho(r)) = k_B T \ln\left(\frac{\rho(r)}{\gamma\,(2(1-b\rho(r)))^{1/2}}\right) + k_B T\left(\frac{b\rho(r)}{2(1-b\rho(r))} + 1\right) \quad (3.21)$$

The Lagrange multiplier μ is adjusted to ensure that the density profile $\rho(r)$ satisfies the normalisation constraint

$$\int \rho(r)dr = 2 \quad (3.22)$$

The free energy of the system is then obtained by substituting the profile that satisfies equation (3.20) into the original free energy functional (3.19).

Comparison with Percus functional

It is worth comparing the intrinsic chemical potential of the inhomogeneous hard rod fluid μ_h to the exact formula obtained by Percus [38]

$$\mu_h^{\mathrm{P}}[\rho(r)]/k_B T = \ln\left(\frac{\rho(r)}{1-\int_r^{r+b}\rho(r')dr'}\right) + \int_{r-b}^{r} \frac{\rho(r')dr'}{\left(1-\int_{r'}^{r'+b}\rho(r'')dr''\right)} \quad (3.23)$$

Setting $\rho(r)$ to a constant ρ, this equals

$$\mu_h[\rho]/k_B T = \ln\left(\frac{\rho}{1-b\rho}\right) + \frac{b\rho}{1-b\rho} \quad (3.24)$$

For a homogeneous fluid, the formula (3.21) derived above should be exact. Substituting a homogeneous density ρ into (3.21), and eliminating additive constants, this gives

$$\mu_h(\rho(r))/k_B T = \ln\left(\frac{\rho}{(1-b\rho)^{1/2}}\right) + \frac{b\rho}{2(1-b\rho)} \quad (3.25)$$

The difference between the Percus formula (3.24) and the LDA formula (3.25) with $\rho(r) = \rho$ arises because the Percus formula was derived in the thermodynamic limit, while our result is for the case when $N = 2$.

3.3.2 Method of solution

There is a standard iterative approach to solving the integral equation (3.20) for $\rho(r)$. A trial profile is inserted into the right hand side, and a new profile is generated by inverting the function $\mu_h(\rho)$. For an open system with fixed μ this procedure leads ultimately to a free energy minimising profile,

but if the initial profile is chosen suitably, then a metastable saddle point solution may emerge and remain effectively unchanged for many iterations.

For a closed system such as the one studied here, the constraint (3.22) for a fixed number of particles needs to be imposed on the solution. This is achieved by updating μ at each iteration so that the normalisation condition is satisfied. This method is employed by Lee *et. al.* [33] and Talanquer and Oxtoby [23] to control the normalisation for closed systems. The Euler-Lagrange equation is altered to

$$\mu_h(\rho(r)) = -k_B T \ln\left(\frac{1}{2}\int dr \exp\left((-\mu_{h,c} - \phi_{\text{eff}})/k_B T\right)\right) - \phi_{\text{eff}} \tag{3.26}$$

where

$$\phi_{\text{eff}}(r) = \int \rho(r')\phi(r-r')dr' \tag{3.27}$$

and

$$\mu_{h,c}(r) = \mu_h - k_B T \ln(\rho(r)/\gamma) \tag{3.28}$$

The first term on the right hand side of equation (3.26) is the appropriate value of μ appearing in equation (3.20), to ensure normalisation. The density profile generated from this procedure is then inserted into the free energy functional, equation (3.19), to obtain the MFDFT estimate of the free energy of the system.

3.3.3 Higher order contributions to $\rho(r)$

The density profile that emerges from the above procedure will clearly be different from the exact single-particle density profile of the system, which we denote by $\rho_H(r)$ for clarity. Under certain conditions, the mean field density profile will be spatially varying. This occurs when the mean field free energy F_{MF} is lower for a spatially varying single particle distribution, corresponding to a reference system with a spatially varying $V(r)$. On the other hand, the single-particle density profile $\rho_H(r)$ in the real system is given by

$$\rho_H(r) = \frac{N}{Z}\frac{\gamma^N}{N!}\int d^N r \exp(-(H_0+H_1)/kT)\delta(r_1 - r), \tag{3.29}$$

where Z is the exact partition function. Due to the translational symmetry of the Hamiltonian $H = K + H_0 + H_1$, this profile should be uniform.

As discussed in Section 2.5.2, the mean field approach may be viewed as a thermodynamic perturbation of the free energy of the system with Hamiltonian $H = H_0 + H_1$ about the reference Hamiltonian H_0. The reference density profile $\rho(r)$ can be considered as the zeroth order approximation to $\rho_H(r)$ in an expansion in H_1. To check the validity of this approach, higher order contributions to ρ_H can be computed by expanding the $\exp(-H_1/kT)$ factor in equation (3.29). For example the first order density profile is given by

$$\rho_1(r) = \frac{N\int d^N r \exp(-H_0/kT)(1 - H_1/kT)\delta(r - r_1)}{\int d^N r \exp(-H_0/kT)(1 - H_1/kT)} \tag{3.30}$$

This can be calculated approximately, using the random phase approximation and the zero order density profile $\rho(r)$:

$$\rho_1(r) \approx \frac{\rho(r)\left[1 - \frac{1}{2}(N-1)(N-2)N^{-2}\mathrm{I}_1 + (N-1)N^{-1}\mathrm{I}_2 - (N-1)N^{-1}\int dr'\phi(r-r')\rho(r')/kT + V(r)/kT\right]}{1 - \frac{1}{2}(N-1)N^{-1}I_1 + I_2} \tag{3.31}$$

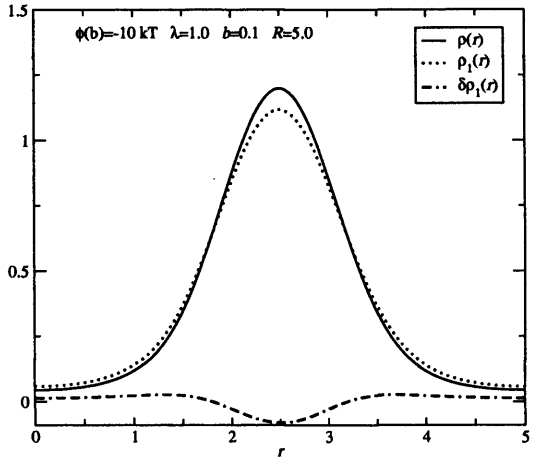

Figure 3.2: The zeroth (solid line) and first order density (dotted line) density profiles for the $b = 0.1$ case, and the difference between them (dash-dotted line), according to the perturbative expressions given in section 3.3.3.

where

$$\mathrm{I}_1 = \int dr'dr''\phi(r' - r'')\rho(r')\rho(r'')/kT, \tag{3.32}$$

and

$$\mathrm{I}_2 = \int dr'V(r')\rho(r')/kT. \tag{3.33}$$

One problem here is that the mean field $V(r)$ appears explicitly in equation (3.31). The inversion of the zeroth order profile $\rho(r)$ to give $V(r)$ is difficult, and also incomplete, since the mean field is necessarily uncertain up to a constant. However, we proceed using two approximations. First, hard sphere repulsions are neglected so we can use the point-particle formula $V(r) \approx -kT\ln\rho(r) + C$ where C is the arbitrary constant. Second, we fix the unknown constant by demanding that the perturbative second term in equation (3.9), evaluated using the approximate $V(r)$, vanishes. Once this is imposed, the first order density profile reduces to

$$\rho_1(r) \approx \rho(r)\left[1 - \frac{(N-1)}{N^2}\mathrm{I}_1 - \frac{1}{N}\mathrm{I}_2 - \frac{(N-1)}{N}\int dr'\phi(r-r')\rho(r')/kT - \ln\rho\right] \tag{3.34}$$

in which I_2 is now the integral in equation (3.33) with $V(r)$ replaced by $-kT\ln\rho$.

This result is still spatially varying. Indeed any expansion of equation (3.29) to finite order, and employing approximations to calculate the corrections, will lead to a density profile with spatial variation. Figure 3.2 shows a spatially varying density profile and the first order correction obtained using the procedure described. It can be seen that the correction is small, indicating that the perturbation expansion inherent in F_{MF} is valid.

The loss of translational symmetry is caused fundamentally by the need to choose an arbitrary location in space for the centre of the mean field potential well. By choosing a particular location, we obtain an inhomogeneous reference system single-particle density profile $\rho(r)$. This is the interpretation of Barrett [28]. The breakage of translational symmetry is associated with an undesirable error in the free energy. The MFDFT approach should be amended to take this effect into account. This will be addressed in Section 3.3.4.

3.3.4 Modifications for small systems

Small N effects

In applying MFDFT to small systems, several crucial modifications to the standard development should not be overlooked. These modifications are necessary to take account of finite size effects that

become increasingly important as the number of particles becomes small.

The first two corrections take us back to the random phase approximation (RPA) in equation (3.18). The correct relationship between the two-particle distribution function $\rho^{(2)}(r,r')$, and a product of two single particle distribution functions $\rho(r)\rho(r')$ is given by

$$\rho^{(2)}(r,r') = g(r,r')\rho(r)\rho(r'), \tag{3.35}$$

where $g(r,r')$ is the pair correlation function for the reference system. In the RPA, this function is set to unity irrespective of the positions r and r'. We will make corrections to this approximation in several stages. The first correction results from consideration of the normalisation condition for an n-particle distribution function:

$$\int_0^R d^n r \rho^{(n)}(r^n) = \frac{N!}{(N-n)!}. \tag{3.36}$$

For the case of $n = 2$ (the two-particle distribution function) the right hand side of equation (3.36) is equal to $N(N-1)$. On the other hand, the one-particle distribution functions are normalised to N, giving N^2 for the integral of the product $\rho(r)\rho(r')$. Therefore the RPA approximation $g = 1$ should be replaced by the more accurate form $g = (N-1)/N$, and equation (3.18) becomes

$$\rho^{(2)}(r,r') \approx \frac{N-1}{N}\rho(r)\rho(r'). \tag{3.37}$$

It is clear that this correction is only important for small N, but in the case of $N = 2$ it introduces a substantial correction factor of $1/2$. We have employed this correct normalisation in the derivation of equation (3.31) already.

A second modification of equation (3.18) addresses the neglect of spatial correlations between the two rods within the RPA. This will have consequences on the estimate for the attractive energy in the system $\langle\phi\rangle_0$. The most severe consequence of this is that the RPA fails to remove the attractive energy due to overlapping configurations of rods i.e. when $|r-r'| < b$. This leads to a substantial overestimation of the magnitude of the cohesive energy in the system. An approximate way to take account of this is to construct a correlation function from a pair of step functions

$$g(r,r') \propto \Theta(|r-r'|-b)\ \Theta(R-|r-r'|-b) \tag{3.38}$$

where $\Theta(z) = 0$ for $z < 0$ and unity otherwise. Now $g(r,r')$ is explicitly zero for overlapping hard rod configurations, and equation (3.18) is modified to

$$\rho^{(2)}(r,r') \approx \left(\frac{N-1}{N}\right)\left(\frac{R}{R-2b}\right)\rho(r)\rho(r')\Theta(|r-r'|-b)\ \Theta(R-|r-r'|-b) \tag{3.39}$$

An extra factor of $R/(R-2b)$ has been inserted to ensure that $\rho^{(2)}$ remains normalised for homogeneous profiles despite the exclusion of $2b$ from the available volume in the system. This pair distribution function is exact for a homogeneous fluid of two hard rod particles, however it is an approximation when an inhomogeneous external field is present giving rise to an inhomogeneous density profile. It is also an approximation when $N > 2$, as non-trivial hard rod correlations exist beyond $|r-r'| > b$ even for a homogeneous system. The correlations in one-dimensional hard rod fluids are described in reference [39] for systems with large N.

Taking these corrections into account, the MFDFT free energy function is now written

$$F_{DFT} = \int_0^R dr k_B T \rho(r) \ln\left(\frac{\rho(r)}{\gamma}\frac{1}{(2(1-b\rho(r))^{1/2}}\right) + \frac{1}{2}\int_0^R dr \int_0^R dr_2' \rho^{(2)}(r,r')\phi(r-r') \tag{3.40}$$

employing the two-particle distribution function from equation (3.39).

Centre of mass translation

The final correction we need to consider deals with the breakage of translational symmetry by the mean field potential utilised in MFDFT, which gives rise to an inhomogeneous distribution of the centre of mass of the system. A dynamical mode of the system, namely the motion of the centre of mass, is incorrectly described, which affects the free energy.

This issue has been the subject of some controversy in the literature. Talanquer and Oxtoby [23] have assumed that when MFDFT is applied to a system in a closed volume, the free energy obtained includes the full translational free energy for the centre of mass of the system within that volume. Simulations by Reguera *et. al.* [6], on the other hand, indicate that density profiles obtained from MFDFT correspond closely to a system modelled by Monte Carlo simulation with a fixed centre of mass. We take the view of Barrett [28], that the MFDFT approach limits the translational motion of the centre of mass of the system to a certain volume around the centre of the mean field potential well. For system sizes of a few tens of particles, this is a small volume compared with the extent of the profile itself, and so this interpretation is consistent with the observations made by Reguera *et. al.* [6]. However, the centre of mass is not fixed: it may be regarded as tethered to the midpoint of the mean field potential, and undergoing quasi-harmonic oscillations about it.

To make this clearer, consider a one dimensional closed system of length R, containing N particles interacting through a pair potential $U(r_i - r_j)$. With suitable periodic boundary conditions that avoid boundary effects, the probability distribution for the position of the centre of mass $\rho_c(R_{cm})$ should be uniform. Now, $\rho_c(R_{cm})$ is the expectation value of the operator

$$\hat{\rho}(R_{cm}) = \delta\left(\frac{1}{N}\sum_{i=1}^{N} r_i - R_{cm}\right) \tag{3.41}$$

so

$$\rho_c(R_{cm}) = \frac{1}{Z}\frac{\gamma^N}{N!}\int d^N r\, \delta\left(\frac{1}{N}\sum_{i=1}^{N} r_i - R_{cm}\right) e^{-(H_0+H_1)/k_BT} \tag{3.42}$$

where Z is the exact partition function. Transforming to centre of mass coordinates $r'_i = r_i - R_{cm}$, $\rho_c(R_{cm})$ becomes

$$\rho_c(R_{cm}) = \frac{1}{Z}\frac{\gamma^N}{N!}\int d^N r'\, \delta\left(\sum_{i=1}^{N}\frac{1}{N} r'_i\right) e^{-(H_0+H_1)/k_BT}. \tag{3.43}$$

The Hamiltonian $H = H_0 + H_1$ is unchanged by this transformation of coordinates since it depends only on particle separations, and with the correct boundary conditions the integration limits remain unchanged. We can therefore see that the right hand side of equation (3.43) does not depend the value of R_{cm}, resulting in a distribution ρ_c that does not depend on position.

As we have seen, in MFDFT the aim is to find the optimal form of the effective mean field potential $V(r)$ in the Hamiltonian H_0 to mimic the effect of the attractive interactions in H_1. The density profile $\rho(r)$ is the single particle distribution function corresponding to the reference system described by H_0 with this form of $V(r)$. The MFDFT approximation to the distribution of the centre of mass is determined by taking the trace of the operator $\hat{\rho}(R_{cm})$ in the reference ensemble, which we write as

$$\rho_c^0(R_{cm}) = \frac{1}{Z_0}\frac{\gamma^N}{N!}\int d^N r\, \delta\left(\frac{1}{N}\sum_{i=1}^{N} r_i - R_{cm}\right) \exp\left(-\frac{1}{k_BT}\left(\sum_{i>j} u_R(r_i - r_j) + \sum_{i=1}^{N} V(r_i)\right)\right) \tag{3.44}$$

Converting to the centre of mass coordinates $r_i' = r_i - R_{cm}$, we get

$$\rho_c^0(R_{cm}) = \frac{1}{Z_0}\frac{\gamma^N}{N!}\int d^N r'\,\delta\left(\sum_{i=1}^{N}\frac{1}{N}r_i'\right)\exp\left(-\frac{1}{k_BT}\left(\sum_{i>j}u_R(r_i'-r_j')+\sum_{i=1}^{N}V(r_i'+R_{cm})\right)\right) \tag{3.45}$$

The integrand now does depend upon R_{cm}, as a result of the spatial dependence of the mean field potential $V(r)$. Consequently the centre of mass distribution ρ_c^0 is spatially varying: we are more likely to find the centre of mass in some parts of the system than in others. This remains the case to higher order in perturbation theory, along the lines described in section 3.3.3. This unphysical result is an artifact of the mean field approximation, and will lead to an underestimation of the entropy of the system. Correcting this error is possible by changing the way the centre of mass dynamical degree of freedom is treated [40, 41]. In this treatment we do this by means of an approximate, ad hoc procedure *after* the optimal mean field density profiles are obtained.

We begin by writing the reference partition function Z_0 as

$$Z_0 = \frac{1}{h^N N!}\int d^N r\, d^N p \exp(-(K+H_0)/k_BT) \tag{3.46}$$

where the p_i are the particle momenta. This can be expressed with the insertion of integrations over the centre of mass position R_{cm} and momentum P_{cm}:

$$Z_0 = \int dR_{cm}dP_{cm}\frac{1}{h^N N!}\int d^N r\, d^N p\,\delta\left(\frac{1}{N}\sum_{i=1}^{N}r_i - R_{cm}\right)\delta\left(\sum_{i=1}^{N}p_i - P_{cm}\right)\exp(-(K+H_0)/k_BT) \tag{3.47}$$

or

$$Z_0 = \int dR_{cm}dP_{cm}\chi(R_{cm},P_{cm}) \tag{3.48}$$

which defines a distribution function for the centre of mass degrees of freedom $\chi(R_{cm},P_{cm})$, which is related to $\rho_c^0(R_{cm})$ through

$$\rho_c^0(R_{cm}) = \frac{1}{Z_0}\int \chi(R_{cm},P_{cm})dP_{cm}. \tag{3.49}$$

Equation (3.48) may be cast instead in the form

$$Z_0 = \frac{1}{h}\int dP_{cm}dR_{cm}\exp(-H_{\text{eff}}(R_{cm},P_{cm})/k_BT) \tag{3.50}$$

where H_{eff} is an effective Hamiltonian controlling the dynamics of the system centre of mass. In order to describe the freedom of motion of the centre of mass correctly we will replace this Hamiltonian with that of a free particle. The corrected partition function is

$$Z_0' = Z_0\frac{\int dR_{cm}}{\int dR_{cm}\exp(-U_{\text{eff}}(R_{cm})/k_BT)} \tag{3.51}$$

where $U_{\text{eff}}(R_{cm})$ is the effective potential in the effective Hamiltonian H_{eff}, that causes the centre of mass to be constrained. The origin $R_{cm}=0$ is chosen to lie at the centre of the mean field potential and we can choose $U_{\text{eff}}(0)$=0. Therefore the probability of finding the centre of mass at $R_{cm}=0$ is

$$\rho_c^0(0) = \frac{1}{hZ_0}\int dP_{cm}\exp(-H_{\text{eff}}(0,P_{cm})/k_BT) = \frac{1}{\int dR_{cm}\exp(-U_{\text{eff}}(R_{cm})/k_BT)} \tag{3.52}$$

and we can write the ratio of the two partition functions as

$$\frac{Z_0'}{Z_0} = \frac{\int dR_{cm}}{\int dR_{cm} \exp(-U_{\text{eff}}(R_{cm})/k_B T)} = \rho_c^0(0) R \tag{3.53}$$

which is in agreement with similar corrections suggested in the literature [40, 41]. The associated shift in reference free energy is given by

$$\Delta F = -k_B T \ln\left(\rho_c^0(0) R\right). \tag{3.54}$$

This free energy correction may be evaluated using the optimum single particle density profile $\rho(r)$ obtained from the Euler-Lagrange equation. We return to equation (3.44) which we write in the form

$$\rho_c^0(R_{cm}) = \frac{1}{N!} \int d^N r \, \delta\left(\frac{1}{N}\sum_{i=1}^{N} r_i - R_{cm}\right) \rho^{(N)}(r^N) \tag{3.55}$$

where $\rho^{(N)}$ is the N-particle distribution function. By employing the random phase approximation, we can proceed in terms of the single-particle density profile $\rho(r)$.

$$\rho^{(N)}(r^N) = \frac{N!}{N^N} \prod_{i=1}^{N} \rho(r_i) \tag{3.56}$$

so $\rho_c^0(0)$ is given by

$$\rho_c^0(0) = \frac{1}{N^N} \int d^N r \prod_{i=1}^{N} \rho(r_i) \, \delta\left(\frac{1}{N}\sum_{j=1}^{N} r_j\right) \tag{3.57}$$

which is readily calculable. For the case of $N = 2$, the result is simply

$$\rho_c^0(0) = \frac{1}{4} \int dr_1 \rho(r_1)\rho(-r_1) = \frac{1}{4} \int dr_1 \rho^2(r_1) \tag{3.58}$$

with the final form being a consequence of symmetry. A better approximation would be to use the more appropriate version of the RPA given in equation (3.39), but we will stick to the simplest form for the evaluation of this contribution to the free energy.

For general N, we can evaluate the integral in equation (3.57) by using the integral representation of the Dirac Delta function

$$\delta(x) = (2\pi)^{-1} \int_{-\infty}^{\infty} dw \, \exp(iwx) \tag{3.59}$$

in which case

$$\rho_c^0(0) = N^{-N}(2\pi)^{-1} \int_{-\infty}^{\infty} dw \, \widetilde{\rho}^N(w/N) \tag{3.60}$$

where $\widetilde{\rho}$ is given by

$$\widetilde{\rho}(q) = \int \rho(r) \exp(iqr) dr. \tag{3.61}$$

The translational free energy correction ΔF is therefore calculable, and should be added to the mean field free energy estimate F_{MF} in cases when translational motion of the centre of mass of the system makes a significant contribution to the system free energy. This will clearly be the case for systems with small N.

3.4 Comparison between exact and MFDFT free energy

The performance of MFDFT can be assessed by comparing the MFDFT excess free energy with the exact result obtained from numerical integration of the partition function in equation (3.1).

Calculations are performed here for two finite rod lengths $b = 0.1$, $b = 0.01$ and also point-like particles $b = 0$ in dimensionless units. For each rod length, equilibrium density profiles are found by solving the Euler-Lagrange equation (3.26), and the MFDFT free energy calculated for a range of 'volumes' R. This is then compared to the MFDFT free energy for a homogeneous density distribution $\rho = 2/R$, and to the exact free energy.

Homogeneous profiles are expected to be the solutions to the Euler-Lagrange equation as $\lambda R \to 0$, since in this limit, the spatial dependence in the attractive interaction vanishes, and it has the same effect as adding a constant potential to the system. It can be shown that the functional in equation (3.40) provides the exact free energy of the system in this limit. The error compared with the exact free energy increases with λ and α, as shown in Figure 3.3.

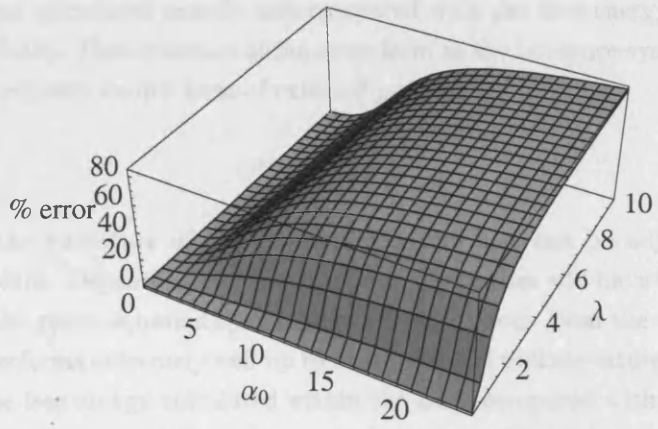

Figure 3.3: Percentage error of MFDFT free energy for a homogeneous profile as a function of the potential well depth at contact α_0, and inverse interaction range parameter λ. For this plot $b = 0.1$ and $R = 5.0$.

For this study, the parameters were adjusted to give a reasonably short range interaction, with considerable strength. The depth of the attractive potential energy well at contact (i.e. when the rod centres are separated by b) has been set to $\phi(b) = -10k_BT$, and the parameter $1/\lambda$, which determines the length scale of the attractive interaction, has been set to unity. In Figure 3.4 the excess free energy F_{ex} is plotted against R for three different rod sizes, using various MFDFT approaches as well as direct evaluation of the partition function.

The MFDFT free energies obtained by finding inhomogeneous optimal density profiles lie closer to the exact free energy than for the homogeneous density profiles, though there remains a large discrepancy. At small volumes ($R \sim 3$ for $b = 0$ and $b = 0.01$, and $R \sim 5$ for $b = 0.1$) the difference in free energy associated with the homogeneous and optimal inhomogeneous density profiles becomes very small, and eventually the homogeneous solutions to equation (3.26) become optimal. A similar development is expected at very large R, when the 'vapour' is very rarefied, however this limit is not observed in our calculations due to the large magnitude of $\phi(b)$.

The small rod lengths $b = 0$ and $b = 0.01$ give rise to more pronounced inhomogeneous density profiles than the larger rods $b = 0.1$, as is illustrated in Figure 3.5, and also display bigger difference between the homogeneous and inhomogeneous profile MFDFT free energies.

It can be seen from Figure 3.4 that the MFDFT free energies always lie above the exact free energy. For homogeneous density profiles neither LDA nor RPA approximations are made in the functional (3.40), and it becomes an exact representation of the reference system [1]. In this case, the Bogoliubov

[1]It should be noted that for the case when $N > 2$, the functional (3.40) does involve the RPA (but not the LDA) even when profiles are homogeneous. This is because the more complicated hard rod correlations for $N > 2$ have not been accounted for by the approximate two-particle distribution function (3.39).

inequality ensures that the MFDFT free energy lies above the exact free energy. The large discrepancy between the exact free energy and the MFDFT free energy for homogeneous profiles is due to the inadequacy of the homogeneous mean field representation of the system. This may also be seen as a breakdown of the perturbation expansion (3.9). The mean field $V(r)$, which in the homogeneous case is just a constant potential, is supposed to emulate the effect of attractive interactions $\phi(r-r')$ in order to make $\langle H_1^2/2\rangle_0$ and higher order moments of H_1 as small as possible. This does not seem to be accurate for the cases considered. As we are in a regime in which the interaction strength α is large, and the range $1/\lambda$ is finite, an inhomogeneous mean field and therefore an inhomogeneous density profile is expected to do better. However in this case there will also be an implicit error due to the LDA and RPA in the functional.

In order to quantify the error due to the LDA for inhomogeneous density profiles, a numerical investigation has been carried out in which the free energy of two hard rod particles in an external harmonic potential was calculated exactly and compared with the free energy calculated using the LDA approximation (3.16). This system is of the same form as the reference system with Hamiltonian $K+H_0$, but with an a priori known form of external potential

$$V(r) = \left(\frac{r}{\sigma}\right)^2 \tag{3.62}$$

where σ determines the curvature of the external potential and can be adjusted to give density profiles of different widths. Depending on the value of σ, the profiles will have different values for the expectation value of the mean square displacement $\langle r^2\rangle$ of the rods from the well minimum. It was found that the LDA performs extremely well up to high potential well curvature. Figure 3.6 shows the percentage error in the free energy calculated within the LDA compared with the exact free energy, against mean square displacement $\langle r^2\rangle$ of the resulting profiles. The parameters $b=0.1$ and $R=5$ were used, which corresponds to the highest packing fraction used in this study of attractive hard rods. The results on the test system indicate that the LDA error is negligible in the parameter ranges for which inhomogeneous profiles were obtained in this study.

From this result we can deduce that for inhomogeneous profiles, the difference between the MFDFT results and the exact free energy can be attributed to the mean field approximation, in which the correlations due to the attractive interaction are not properly taken into account. There is also an error due to the RPA approximation in the evaluation of $\langle H_1\rangle_0$, since the hard-sphere correlations in the inhomogeneous system have only been taken into account approximately.

The discrepancy between the exact and MFDFT free energy is due to the unsuitability of a mean field treatment for a system of low dimensionality, consisting of very few strongly interacting particles. For such a system large fluctuations or deviations from mean field behaviour are expected.

The correction ΔF for translational motion of the system centre of mass is significant for all three rod sizes. The profiles become narrower for smaller b, indicating that the mean field potential $V(r)$ is narrower, leading to stronger confinement of the centre of mass. This gives rise to a larger free energy correction factor for narrower profiles. It should be noted that once the translational correction ΔF is made, the Bogoliubov inequality is no longer valid regardless of the LDA and RPA approximations, since the confinement of the system centre of mass, the effect we are attempting to correct, is an inherent part of the H_0 reference system which includes an external field.

A numerical study on three profiles for $b=0.1, 0.01, 0$ with $R=5.0$ was carried out to evaluate the first order density profile $\rho_1(r)$ given by equation (3.31). This revealed that $\rho_1(r)$ is similar to $\rho(r)$ but is slightly flatter, as would be expected. This is illustrated in Figure 3.2 for the case of $b=0.1$. The free energy calculated from the resulting first order profiles did not vary significantly from the original zeroth order free energy obtained using the $\rho(r)$ profiles.

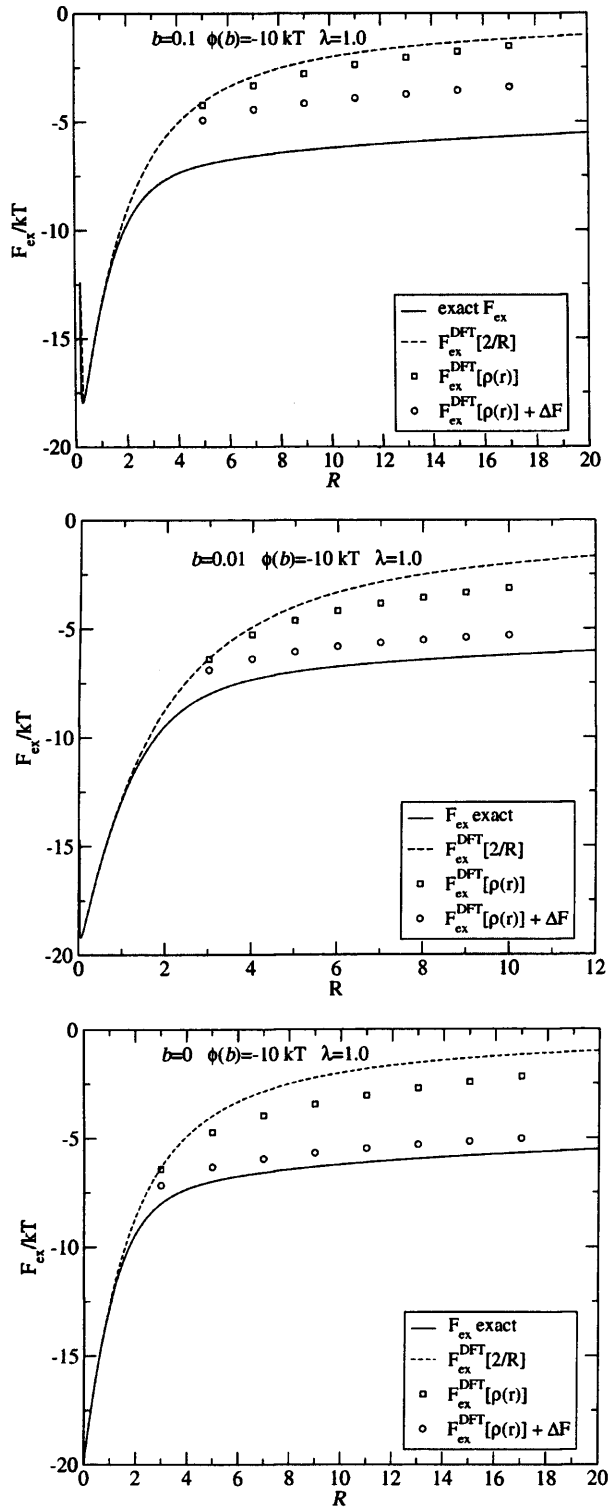

Figure 3.4: Excess free energy F_{ex} versus 'volume' R for attractive rods with length $b = 0.1$ (top graph), $b = 0.01$ (middle graph), and point particles $b = 0$ (bottom graph). The excess free energy is calculated exactly (solid line), and in three different variants of MFDFT. The dashed line results from inserting a homogeneous density profile $\rho = 2/R$ into equation (3.26), the free energy functional incorporating the modifications to the random phase approximation. The squares show the same free energy evaluated using the optimal inhomogeneous density profile. This free energy lacks the translational correction ΔF described in equation (3.54), and the substantial change that this introduces is shown by the further shift to the values shown by circles. For most values of R, inhomogeneous density profiles are favoured, but homogeneous profiles become more favourable for smaller R. The translational correction greatly improves the agreement between the MFDFT and exact free energies.

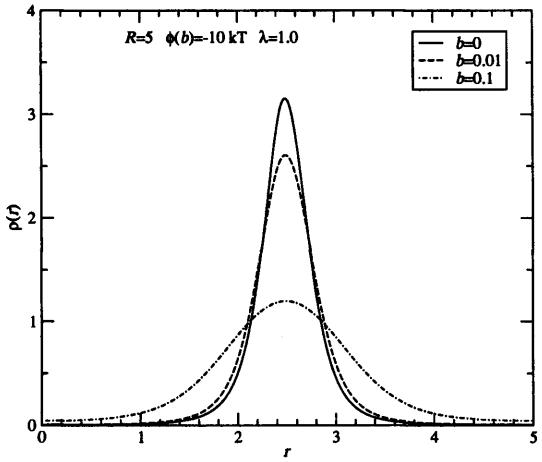

Figure 3.5: The optimal inhomogeneous density profiles for the three cases described in Figure 3.4 for $R = 5$. Note that the smaller rods are described by a more peaked profile, and consequently a narrower mean field potential.

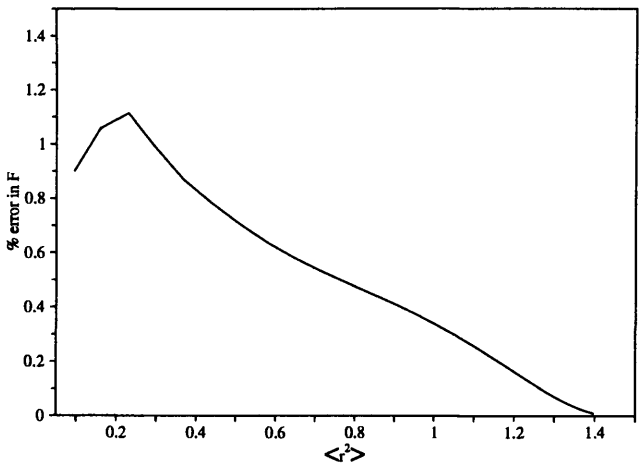

Figure 3.6: Percentage error in the free energy calculated within the LDA for a system of two particles in a harmonic external potential. This system has a Hamiltonian of the form $H = K + U_R + V(r)$, where $V(r) = (r/\sigma)^2$. Rod size $b = 0.1$ and volume $R = 5.0$ have been chosen for evaluation of the LDA, and the free energy compared with exact integration of the partition function.

3.5 Summary

We have investigated how well a mean field density functional theory performs in a very simple case of two attractive hard rods on a ring. Mean field theories are expected to be less successful in treating small systems due to the importance of fluctuations: they are better suited as a description of large systems. Reguerra and Reiss point out [27] that the neglect of certain fluctuations in MFDFT may be useful in the application to nucleation theory. This is because it allows MFDFT to capture stationary states of a system that do not correspond to equilibrium states, as for example the formation of critical molecular clusters in a condensing vapour. In this study the focus was on how well MFDFT can estimate the equilibrium free energy of a closed system, so this neglect of fluctuations represents a shortcoming highlighted in the difference between the MFDFT and exact free energies.

The standard MFDFT functional should be modified to deal with finite size effects. Two modifications involve changes to the random phase approximation, used to estimate the interaction free energy. The first is the need to ensure normalisation of the two-particle distribution function when it is replaced by a product of single distribution functions. The second correction is to prevent the inclusion of forbidden configurations with overlapping hard rods. Failure to remove these configurations leads to a substantial overestimation of the cohesive energy.

The final effect concerns the loss of translational symmetry due to the introduction of a mean field potential. This means that the free energy associated with the motion of the system centre of mass is not correctly treated, and for small systems, the error can be substantial. This loss of symmetry remains even if higher order terms are included in the evaluation of the density profile. The problem is resolved by the replacement of the effective Hamiltonian controlling the motion of the centre of mass. The correction to the free energy can be evaluated directly using the density distribution in the reference hard sphere system, and is added to the MFDFT free energy once an optimal density profile (or equivalently mean field potential $V(r)$) has been found.

The modifications lead to substantial changes in the MFDFT free energy. The free energies obtained from MFDFT were compared with exact values, which are easy to compute for the small system studied. The modification to the translational contribution to the free energy appears to be particularly important for the system studied. As expected, the correction is greatest when the optimal density profile departs most strongly from homogeneity.

We expect these various factors to be important in calculations of the free energy of small molecular clusters frequently made in nucleation studies using mean field density functional theory.

Chapter 4

Phase behaviour of charged colloidal suspensions: experiment and theory

4.1 Introduction to colloidal suspensions

4.1.1 Brief description of colloidal systems

The term colloid refers to a general class of complex systems containing inhomogeneities on length-scales between 10nm-1000nm consisting of matter of one phase dispersed in another. Colloids can be classified generally by the states that make up the dispersed phase and dispersion medium. In this thesis we are concerned with solid particles dispersed in liquids which are known as sols or dispersions. There are also colloids consisting of solid or liquid particles in gases (aerosols), liquids in liquids (emulsions), gases in liquids (foams). In addition to this there are solid-,liquid-, gas- in solid colloids known as solid dispersions, solid emulsions and solid foams.

In this study we are interested in suspensions of solid particles dissolved in polar solvents. In these systems, there is a large asymmetry in size between the solid particles and the molecules of the surrounding solvent. Depending on the specific system of interest, different types of interactions may be important, giving rise to different phenomena. These interactions include hydrodynamic, electrostatic and steric effects.

The study of colloids [42] as a scientific discipline dates back to the 1840s. The earliest studies were of solid in liquid colloids, and in the 1850s Michael Faraday made extensive studies of colloidal gold sols. The term *colloid* was coined in 1861 by Thomas Graham. Graham deduced that the low diffusion rate of colloidal particles implied the particles were fairly large- at least 1nm in diameter. He also deduced that the particles must have an upper size limit to prevent them from sedimenting under gravity which he set to approximately $1\mu m$. This range of lengthscales is still used in the definition of colloids today.

Colloidal sols can be broadly classed into two categories *lyophobic* and *lyophilic* colloids. Lyophobic or solvent-hating colloids are inherently unstable, and will eventually fall out of dispersion by aggregating. Lyophilic or solvent-loving colloids are stable and remain dispersed in solvent indefinitely. Aggregation of lyophobic particles occurs due to strong attraction at short range. These attractions are Van der Waals type interactions, and are sufficiently strong that when two particles meet, thermal agitation is not sufficient to separate them.

A very wide range of systems can be classified as colloidal suspensions, ranging from paints and toothpaste to protein solutions. Broadly speaking a dispersion of colloid sized particles may come

about in two ways. One way is that it is dispersed as a polymolecular aggregate, which is the case with silver and gold chloride particles. This is also the case for association colloids such as micelles formed from amphiphilic molecules. The second alternative is that the molecules themselves are macromolecules that are large enough to count as colloidal particles, which is the case with DNA or proteins. Such macromolecules are usually lyophilic.

4.1.2 Stabilisation of lyophobic colloids

There are two main methods of stabilisation for lyophobic colloids. Steric stabilisation involves coating the colloidal particles with polymeric molecules that are lyophilic and cause short range repulsions between the particles. The reduction in the available phase space for the polymer coils when particles approach each other causes a decrease in entropy, which results in an effective repulsion between the particles.

The second method of stabilisation is to coat the particles with ionisable salt groups. These groups preferentially dissociate, causing the particles to carry an overall surface charge. The chemical similarity of the coatings, means that the particles will carry the same sign of charge, giving rise to electrostatic repulsion between the particles. Michael Faraday used this method to produce suspensions of gold particles that have remained stable to this day [42].

In this study we are particularly interested in phenomena in charged colloidal suspensions. A typical system [43] consists of polystyrene sulphate spheres of diameter 650nm dispersed in deionised water. The spheres can be synthesised with a large number of ionisable sulphate salt groups chemically bonded to their surfaces. These groups dissociate in water, each leaving a single negative charge bound to the sphere's surface, and a compensating positive charge in solution. The resulting surface charge densities on the spheres are typically of the order $10^{-3} - 10^{-2}$ electron charges per square nanometre. This means that the spheres or macroions are highly charged, each carrying around $10^3 - 10^4$ electron charges. The hydrated counterions generally form neutralising clouds around the macroions referred to as double-layers [42], that screen the bare Coulomb interactions between the large particles

4.1.3 DLVO theory of colloidal stability

The classic theory of charged colloidal suspensions formulated by Derjaguin, Landau, Verwey and Overbeek (DLVO) in 1948 [44] expresses the effective interaction between large colloidal particles as the sum of a repulsive electrostatic term that takes the form of a screened Coulomb (Yukawa) potential, and an attractive Van der Waals interactions between the particles. The repulsive electrostatic interaction, which has a relatively long range, stabilises the colloids against coagulation due to shorter range van der Waals attractions which would otherwise cause irreversible coagulation of the particles.

The repulsive electrostatic interaction in the DLVO theory is derived using the linear Debye-Hückel approximation [45] in the mean field Poisson-Boltzmann theory which will be discussed in more detail in Chapter 5. Debye-Hückel theory was originally formulated to describe the interactions between microions in an electrolyte in the absence of the large, highly charged macroions present in a colloidal suspension. These microions are smaller and carry significantly less charge than the macroions referred to in the context of DLVO theory, and it is questionable whether a linear response treatment is valid when macroions are present in the system. In this theory, the electrostatic interaction between a pair of colloidal particles separated by a distance r, and carrying a charge Z is

$$V_R = \frac{Z^2 e^2}{4\pi\epsilon} \left(\frac{\exp \kappa a}{1 + \kappa a} \right)^2 \frac{\exp(-\kappa r)}{r} \tag{4.1}$$

where a is the radius of the particles, ϵ is the absolute dielectric permittivity of the solvent and κ is the inverse Debye screening length λ_D. The potential V_R is an effective electrostatic interaction

between two charged macroions that is mediated by the microions. The inverse screening length κ depends on the concentration of microions in the suspension. For the case where only one species of microion is present, the inverse screening length is given by

$$\kappa^2 = \frac{4\pi e^2 z n}{\epsilon k_B T} \tag{4.2}$$

where n is the mean density of microions, z is their valency, e is the elementary electron charge, k_B is Boltzmann's constant and T is the temperature. From (4.2) it can be seen that the Debye screening length decreases with microion density as $\lambda_D \propto 1/\sqrt{n}$. In the DLVO theory the mean microion concentration n is taken to be constant with respect to the separations between the macroions.

The attractive interaction in the DLVO theory results from Van der Waals interactions. The attraction between two identical spheres consisting of atoms which interact through Van der Waals interactions is obtained from Hamaker theory [46] , and is given by

$$V_A = -\frac{H}{12}\left[\frac{a^2}{r^2} + \frac{a^2}{r^2 - a^2} + 2\ln(1 - a^2/r^2)\right] \tag{4.3}$$

where H is the Hamaker constant, which depends on the material the colloidal spheres are made of, as well as the intervening medium between the particles. The general shape of the overall interaction $V_{DLVO} = V_R + V_A$ is plotted below for two different salt concentrations.

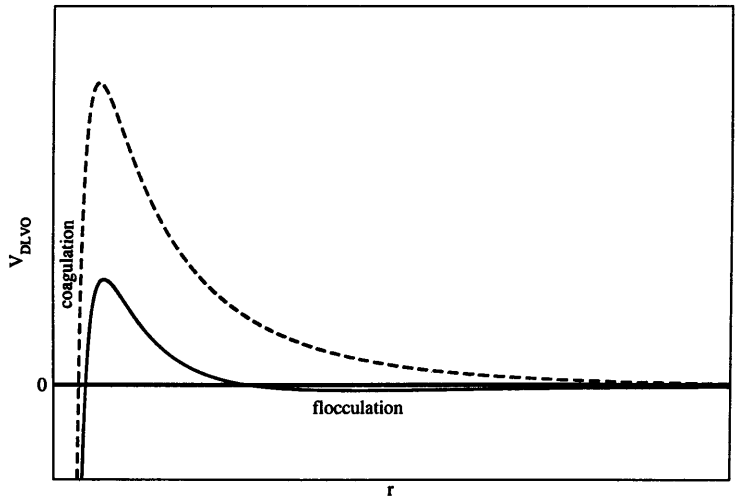

Figure 4.1: DLVO interaction potential between a pair of colloidal macroions. The full curve corresponds to a high concentration and the dashed curve to a low salt concentration. The secondary minimum responsible for flocculation is visible for the case with a higher salt concentration. Adapted from Knott [47].

DLVO theory asserts that the screened electrostatic repulsion stabilises the suspension against coagulation due to the strong Van der Waals interaction at short range. When the salt density is increased sufficiently, the repulsive interaction becomes more short ranged due to the enhanced screening, and the barrier to the primary minimum is overcome which leads to coagulation. This salting-out phenomenon was studied by Faraday. At intermediate salt densities a shallower secondary minimum appears. This secondary minimum, which is shallow relative to the thermal energy in the system, is responsible for the phenomenon of flocculation, the formation of a low density aggregate that is easily re-dispersed.

4.2 Experimental observations of inhomogeneous phase behaviour

The relatively large size of colloidal particles enables a wide range of experimental techniques to be used to study them. Colloidal particles can be imaged directly using optical microscopes [43, 48, 49], and scattering experiments to probe the structure of the suspensions are performed using lasers [50] or using small-angle X-ray scattering (SAXS) [51]. The low diffusion rate of colloidal particles also allows them to be tracked dynamically using time-resolved digital microscopy [43, 48, 52].

The formation of ordered structures in suspensions of latex spheres was observed as early as the 1950s [53]. Subsequent studies showed these structures coexisting with disordered phases [54]. Monovoukas and Gast found transitions between BCC and FCC structures, as well as the liquid-solid transitions [55].

The formation of ordered structures is compatible in principle with a purely repulsive pairwise interaction such as the Yukawa potential (4.3). Robbins *et. al.* studied the phase diagram of Yukawa fluids extensively by means of computer simulations [56, 57], and found them to display liquid-solid and solid-solid phase transitions. These transitions are driven by changes in the particle density (which would correspond to the macroion density in a colloidal system) as well as the inverse screening length κ (which in a colloidal system would be related to the mean density of microions).

Another example of a phase transition in a system in the absence of attractive interactions is that of hard-sphere crystallisation [10, 58]. A hard sphere system confined to a volume V can be characterised by the volume- or packing fraction ϕ which is the volume of one sphere divided by V. In hard sphere systems it is found that at a volume fraction of $\phi = 0.494$ there is an abrupt transition to a crystal with a volume fraction of $\phi = 0.545$. If a system is prepared at an intermediate volume fraction the system will separate into two coexisting phases. This transition occurs at packing fractions well below the maximum attainable packing fraction for random close packing of hard spheres which is around $\phi = 0.63$ and maximum packing fraction of a regular close packed structure $\phi = 0.7404$. The transition is entropically driven, and results from the fact that the volume available to the spheres when they are packed into a crystal is larger than at random packing. Phase coexistence in the hard sphere and repulsive Yukawa systems occurs between phases that do not differ substantially in density.

There is experimental evidence that attractive interactions exist in charged colloidal systems that have a much longer range than the Van der Waals interactions. Grier showed [43] that charged colloidal particles with packing fractions as low as $\phi = 0.01$ can order into crystals. The mean separation between macroions of radius $a = 330$nm at this packing fraction corresponds to approximately 3000nm. The Van der Waals interaction contributes less than $0.01 k_B T$ to the interaction potential between two polystyrene microspheres immersed in water separated by more than 100nm [43], and so is negligible at these packing fractions. Grier's study found that colloidal crystals persist for longer than expected in the absence of confinement if they had purely repulsive interactions. From the observation of metastable crystallites, he also deduced that the surface tension between the solid and liquid phases is much higher than would be expected for a purely repulsive interaction. This behaviour was attributed to an effective attractive interaction between the colloidal particles when they are near a container wall, but there is also evidence that effective attractions occur far from container walls.

Experiments showing the coexistence between phases with substantially different colloid densities add to the evidence for the existence of long range attractions between charged macroions. In 1979 Ise *et. al.* found evidence for the coexistence between solidlike and a very dilute gaslike phase in dilute suspensions of sodium polyacrylate [51]. The same effect was seen with highly charged latex spheres [59]. The coexistence behaviour was only observed for suspensions in which the particles carry a very high surface charge ($\sim 10^{-3} - 10^{-2}$ electron charges per nm^2), and the salt density in the electrolyte

is as low as a few μM (which equals about $10^{-7} - 10^{-6}$ ions per nm^{-3}).

Subsequent studies [60, 50, 61, 62, 63, 3] have found voids in liquidlike phases. These voids are indicative of a very low density gaslike phase, so that the observations may be interpreted as coexistence between dense and dilute fluid phases. Homogeneous fluids were observed to separate into dense liquidlike and rarefied gaslike phases over timescales of hours to days. This behaviour occurs at densities much lower than the range of densities for which flocculation due to the secondary minimum in the DLVO potential occurs. Reentrant behaviour was observed [50] with respect to the salt concentration of the electrolyte in the sense that the fluid remains homogeneous at lower and at higher salt concentrations but phase separates at intermediate salt concentrations. Palberg and Würth [64] disputed the claim that the observations correspond to equilibrium phenomena such as phase coexistence, and argued that the phase separation seen by Aurora *et. al.* correspond to nonequilibrium phenomena that result from a gradient in salt concentration in the system.

Unless the experiments mentioned above are flawed or have been misinterpreted they point to the existence of some form of long range interaction that is not covered by the DLVO theory. The inhomogeneous phase behaviour is difficult to explain otherwise.

Two more experimental observations are worth pointing out in this context. Matsuoka *et. al.* investigated the nearest neighbour macroion separation as a function of salt concentration and found that it first increased with increasing salt concentration, then decreased after passing through a maximum, indicating that the crystal density passed through a minimum [65]. When the surface groups on the macroions are acidic, then the concentration of base in the electrolyte determines the amount of charge titrated on the macroions. This allows control of the charge carried by the macroions. By varying the concentration of NaOH in suspensions, Yamanaka *et. al.* found a solid-liquid phase transition which was reentrant with respect to the macroion surface charge for a given salt density and macroion density [66].

4.3 Theoretical approaches

4.3.1 Discrepancy between DLVO theory and observations

The coexistence between dense and rarefied phases is not compatible with purely repulsive Yukawa interactions of the Debye-Hückel theory. Van der Waals attractions calculated within Hamaker or Lifshitz [42, 67] theory cannot account for this behaviour, as these interactions are too weak at the inter-particle separations for which coexistence behaviour is observed. The discrepancy between the DLVO theory and experimental observations leaves open a range of possibilities for the development of a theory to explain the phase behaviour described above. One such possibility is the existence of effective electrostatic *attractions* between the like-charged macroions induced by the microions, which are not captured by the the theory leading to the repulsive term in the DLVO theory.

4.3.2 The Primitive Model

There are several layers of complexity that have been shed on the way to formulation of the electrostatic repulsion term in the DLVO theory. The first level concerns the approximations in the so-called primitive model (PM), which is described in more detail in Chapter 5. This essentially involves neglecting the details of the effect of the solvent molecules on the microions and macroions in the system. Within the PM, the solvent is treated as a continuum (albeit with an adjusted dielectric permittivity to account for the polarity of the solvent), and so plays the role of a passive 'spectator' phase in the system [68]. This means that solvent polarisation and solvation-shell effects that play an important role in the phase behaviour of systems containing much smaller particles (compared to colloidal macroions), such as charged C_{60} molecules [69], are not included within the PM. The

neglect of solvent molecularity means that depletion effects that give rise to effective short-range interactions between colloidal particles [70], as well as solvent impurity effects are neglected. It should also be noted that hydrodynamic forces [42] that can mediate short-range interactions between colloidal particles are neglected, as they are inherently kinetic in nature, and therefore do not affect the equilibrium thermodynamic behaviour thought to be responsible for the observed phenomena.

4.3.3 Idealised geometry and other simplifying factors

Theoretical treatments using the PM usually make use of additional approximations to make the problem theoretically tractable. These include assumptions that the macroions are monodisperse in terms of size and have an idealised spherical geometry with little or no variation from one macroion to the next. The macroions are also usually assumed to be identical with respect to the amount of charge carried. In most treatments, the surface charge on the macroions is assumed to be homogeneously spread over the macroion surface.

Although some theories attempt to account for the variation of the total amount of surface charge carried by the macroions with external conditions [71, 72, 47], most assume that the amount of surface charge remains fixed with changes in salt density and macroion density over the relevant parameter ranges.

4.3.4 Mean field approximation

After the PM approximation together with the geometrical and monodispersity approximations have been made, the next major step in many theories involves a mean field approximation to describe the microions. There are different types of mean field theory, but the basic ingredient is the neglect of microion-microion correlations. In the mean field treatments, correlations brought about by long-range electrostatic interactions between the microions are neglected. There are also correlations due to forces with much shorter range, such as the repulsive $1/r^{12}$ interaction of the Lennard-Jones potential [70], however these will be less relevant at low macroion packing fraction and microion concentration. The Poisson-Boltzmann theory is a mean field theory in which the microions experience the electrostatic field due to the macroions together with a mean field due to all of the other microions. The approximations involved in formulating the mean field theory are less valid when the concentration of microions is high and the microion-microion spacings are small.

The Poisson-Boltzmann theory can be derived from a more complete field theory in which microion-microion correlations are included [29, 30, 31, 32]. Computer simulations have also pointed to the importance of such correlations [73, 74], especially when the microions are multivalent. However, for spherical macroions it has been found that although these correlations can induce effective attractions between like-charged macroions, these attractions are short ranged and therefore negligible at the low densities for which the inhomogeneous phase behaviour has been observed in experiments. There are other systems with different geometries such as charged cylinders [75, 32] (sometimes used as a model for DNA molecules) and charged plates [76, 32, 77] , in which electrostatic correlations induce attractions that are long ranged. In these cases too, the microion correlation effects are particularly important when the microionic species are multivalent [76]. For a review on correlations in electrostatic systems see reference [78].

4.3.5 Debye-Hückel approximation

The next approximation applied to many Poisson-Boltzmann treatments is to linearise the Poisson-Boltzmann equation. This is referred to as the Debye-Hückel approximation. The Poisson-Boltzmann equation is a differential equation for the mean field electrostatic potential, and contains terms that are nonlinear in this potential. Linearisation about a constant value of the mean field potential is

only valid when the spatial variations in the potential are small compared to k_BT. This translates to the requirement that the spatial modulations in the mean microion density are small. The Debye-Hückel approximation was originally proposed for the description of solutions containing microions only, and not the highly charged macroions encountered in colloidal suspensions which bring about greater spatial variations in the microion density.

4.3.6 Modified Poisson-Boltzmann theories

Several authors have produced theories based on modifications of the linearised Poisson-Boltzmann theory used in the DLVO formulation. These theories suggest the possibility that long-range effective attractions of electrostatic origin are obtainable within the approximations of the PM and mean field theory.

Van Roij, Dijkstra and Hansen (RDH) [22, 68] developed a mean field density functional theory for which the minimising microion distributions satisfy the linearised PB equation. Their approach lead to phase diagrams in the $\phi - n_s$ plane (ϕ is the colloid volume fraction, n_s is the mean salt density) that displayed solid- liquid- and gaslike phases, as well as coexistence between dense and rarefied phases. In addition to the pairwise repulsive interaction between macroions in the DLVO potential (4.3), the free energy contained terms that were independent of macroionic positions but depended on the macroion density. These structure-independent but state-dependent terms were responsible for driving the coexistence between phases of different density. Others had pointed to such 'volume terms' previously [79]. It should also be said that the earliest treatment based on modified Poisson-Boltzmann theory that contained effective electrostatic attractions was developed by Sogami and Ise [80], although their use of the Gibbs free energy G as the relevant thermodynamic potential was disputed [81].

Knott and Ford developed a theory based on linearised PB equation and constructed phase diagrams displaying dense and rarefied phases [47, 82]. Warren developed a theory [83] based on Debye-Hückel theory resulting in similar phase diagrams.

The phase diagrams calculated in these three modified PB treatments shared certain qualitative features in that they displayed coexistence only at very low salt density, and also showed the coexistence region in the $\phi - n_s$ plane to become smaller with decreasing macroion charge. This is in line with the experimental observations described in Section 4.2.

Importance of volume dependent inverse screening length κ

An important ingredient in all of the linearised Poisson-Boltzmann theories described above is that they allow the inverse screening length κ, which depends on the density of microions, to vary with macroion density. This effect causes regions of higher macroion density to have a higher density of microions, which means that the electrostatic forces are more effectively screened. This mechanism may provide a cohesive contribution to the effective interactions between the particles even when the pairwise interactions between particles are repulsive.

Dijkstra and van Roij [84] showed this mechanism leads to vapour-liquid coexistence for point-like Yukawa particles. Despite demonstrating the importance of a density dependent κ, this treatment missed out two important contributions to the free energy. Firstly the entropy of the microions did not depend on the change in inhomogeneity of the density distribution as screening is enhanced but only on the overall microion density, and secondly the macroion-microion energy (sometimes referred to as the self-energy of a macroion due to the presence of microions) was not included.

Another demonstration of this mechanism was provided by Löwen and Allayarov [85]. They used computer simulations on a triangular arrangement of macroions to demonstrate that 3-body interactions contribute a cohesive force to the effective interaction between the macroions. By approximately

evaluating a leading order correction to the truncated mean field free energy expansion about microion density distribution functions, they arrived at 3-body interactions as a natural extension to the linearised theory. In their theory, the local density modulations that arise in the vicinity of a macroion have an effect on the effective interaction with nearby macroions, but only when density modulations are taken beyond first-order. This may be seen as the 'local' equivalent to the many-body effects described by the modified linear PB theories, where the interaction between macroions is influenced by the 'global' density.

The volume dependence of κ, as well as the volume terms in the RDH treatment, can be viewed as many-body effects in that they depend on the density of macroions and therefore depend on the simultaneous position of several macroions rather than being the sum of pairwise interactions. The Wigner-Seitz cell model which will be outlined in the next chapter is an alternative method by which effective many-body interactions may be included.

Theories based on the volume dependence of κ may provide a clue as to why the phase separation phenomena are only observed at low salt densities. If the salt density is too high, then κ will not be strongly affected by the macroion density.

4.3.7 Problems with linearised theories

The linear PB theories are hampered by the problem that the coexistence phenomena are observed for highly charged spheres, which means that they occur beyond the limit of validity of the linearisation approximation. The linearised equations are not able to describe systems with large inhomogeneities in the mean field electrostatic potential and microion density distributions. Although Warren [83] states that the phase separation phenomena occur in the linear regime, work by some authors [86, 87] on spherical Wigner-Seitz cells (for which numerical solution of the full nonlinear PB equations is tractable without linearisation [88]) has suggested that the coexistence phenomena predicted by linearised PB theories may be spurious, and result from failure of the linearisation approximation.

One method that attempts to re-introduce nonlinear effects into the linearised PB treatment is by means of 'renormalisation', whereby oppositely charged microions very close to the macroionic surface are said to 'condense' onto the particle, giving it an effective charge that is significantly lower than the original charge. The lower macroionic surface charge means that the inhomogeneities in electrostatic potential are smaller, making the system more amenable to linearisation. Diehl *et. al.* developed a renormalisation theory [89] in which the free energy is minimised with respect to the number of 'condensed' microions. The conclusion drawn from this study was that counterion condensation stabilises the system against phase separation for a salt-free system, with a weak phase separation occurring when salt is added to the system. One disadvantage of the renormalisation theories is that it is not clear whether the reduction in entropy due to the tight confinement of the condensed counterions is properly accounted for.

In this thesis, we attempt to develop a different approach to capture the nonlinear screening properties of the Poisson-Boltzmann equation. This is based on a linearisation of the PB equation about the mean field distributions of widely separated macroions. The framework of this linearisation approach is laid out in Chapter 6, and is then applied to a system of two charged parallel plates in Chapter 7, and to a colloidal suspension of spherical particles in Chapter 8. The next chapter deals generally with the mean field theory of the effective interactions in charged colloidal suspensions.

Chapter 5

Mean field theory of charged colloidal suspensions

5.1 The primitive model of electrolytes and colloidal suspensions

The simplest representation of electrolytic solutions is the primitive model (PM) [45], in which the molecular nature of the solvent is neglected. In this model, the solvent is treated as a continuous medium with a bulk dielectric constant $\epsilon = \epsilon_0\epsilon_r$, where ϵ_0 is the permittivity of free space, and ϵ_r is the relative permittivity of the solvent. The dielectric constant is chosen to account for the response of the solvent to electric fields. This is particularly important for polar solvents such as water for which ϵ_r is approximately 78 at room temperature [42]. Within this approximation, an electrolyte consists of charged ions moving inside a continuous medium. The microions are modelled either as hard-sphere particles containing a point charge at the centre, or in even simpler cases simply as charged point particles.

Charged colloidal suspensions also contain particulate species of macroions. In the simplest models, these are represented as impenetrable hard-spheres with a uniform surface charge. The spheres are taken to have the same dielectric permittivity as the solvent, so that dielectric image effects can be neglected. Inhomogeneities in shape and surface charge are neglected within this framework. In addition, the particles are assumed to be monodisperse. These approximations will be better for some systems than others. The silica and latex spheres used in experiments by Yoshida [3] for example have a polydispersity in diameter of between $2\% - 6\%$. For suspensions of proteins irregularities in size and shape will be more significant.

All macroions are considered to carry an identical surface charge Z. The dissociation of surface groups that gives rise to charge Z on the macroions may vary depending on the experimental conditions. Theoretically it depends on the difference in free energy between the hydrated and bound states of the surface groups. As a first approximation Z is kept fixed (irrespective of changes in the system volume or other parameters) and identical for all macroions.

Overall a suspension will be charge neutral, so that

$$NZ + \sum_i q_i = 0 \tag{5.1}$$

N is the number of macroions, and q_i is the charge on the ith microion. A subset of the microions originates from the dissociation of the surface groups on the macroions- these are the counterions which have the opposite charge to the macroions. In addition to this, a suspension will contain positive

and negative microions resulting from the dissolution of salt. All microions will be considered to be similar in the sense that the counterions will be equivalent to salt ions of the same charge, with the remaining salt ions being different only in the sign of their valency.

The effective Hamiltonian for a colloidal suspension in the primitive model is a function of the macroion positions and momenta $\{\mathbf{R}_n, \mathbf{P}_n\}$ and the microion positions and momenta $\{\mathbf{r}_i, \mathbf{p}_i\}$. It consists of the kinetic energy of macroions K_F, kinetic energy of microions K_M, the electrostatic potential energy of macroion-macroion interactions, microion-microion interactions and microion-macroion interactions. In addition to this there is the hard-sphere interaction between macroions, and macroions and microions, which makes it impossible for macroions to overlap or the microions to penetrate into the interiors of the macroions. In what follows subscripts F refer to the macroions, and M to microions. Writing the Hamiltonian for the primitive model as a sum of the macroion and microion kinetic energies (K_F and K_M respectively) together with the macorion-macroion V_{FF}, micorion-microion V_{MM} and macroion-microion V_{MF} potential enegies, gives

$$H_{PM} = K_F + K_M + V_{FF} + V_{MM} + V_{MF} \tag{5.2}$$

It should be noted that since the microions and macroions are bathed in a solvent, H_{PM} cannot be thought of as the Hamiltonian of a closed system for which energy is conserved, but rather as an effective Hamiltonian of a system in contact with a heat bath. This heat bath will absorb any latent heats resulting from transitions between phases of different macroionic order or density. Since water has a high heat capacity, we can be confident that the temperature will remain constant after such transitions.

H_{PM} results as a consequence of integrating out the solvent degrees of freedom from an 'original' Hamiltonian H, comprising of

$$H = K_F + K_M + V^0_{FF} + V^0_{MM} + V^0_{MF} + K_s + V_{ss} + V_{sM} + V_{sF} \tag{5.3}$$

where V^0_{FF}, V^0_{MM} and V^0_{MF} contain the interactions in vacuo (with dielectric constant ϵ_0 for the electrostatic interactions), and $K_s, V_{ss}, V_{sM}, V_{sF}$ are the solvent kinetic energy, solvent-solvent, solvent-microion and solvent-macroion interaction energies respectively. For a closed system with energy E_0, the microcanonical probability distribution of states can be written [15]

$$\rho(\{\mathbf{r}_i, \mathbf{p}_i\}, \{\mathbf{R}_n, \mathbf{P}_n\}, \{\mathbf{r}_s, \mathbf{p}_s\}) = const\ \delta(H - E_0) \tag{5.4}$$

A trace over solvent positions and momenta is assumed to result in a canonical distribution for the colloidal degrees of freedom

$$Tr_s\left[\rho(\{\mathbf{r}_i, \mathbf{p}_i\}, \{\mathbf{R}_n, \mathbf{P}_n\}, \{\mathbf{r}_s, \mathbf{p}_s\})\right] = \frac{1}{Z}\exp(-H_{PM}(\{\mathbf{r}_i, \mathbf{p}_i\}, \{\mathbf{R}_n, \mathbf{P}_n\})/k_BT) \tag{5.5}$$

Where Tr_s denotes an integral over positions and momenta of all the solvent molecules, H_{PM} is the primitive model effective Hamiltonian, k_B is Boltzmann's constant, T is the temperature, and Z is the corresponding canonical partition function. Since most experiments on colloidal phase transitions are done at room temperature, T is approximately $300K$.

Clearly, the dynamics of the macro and microions are not governed by H_{PM}, as the solvent degrees of freedom have been integrated out. The primitive model Hamiltonian H_{PM} is required to calculate the thermodynamic, equilibrium behaviour of the colloidal suspension. The important assumption in the PM is that the interactions of the solvent with the micro and macroions are correctly accounted for through the relative dielectric permittivity in the electrostatic interactions in V_{FF}, V_{MM} and V_{MF}.

There are situations in which the molecular nature of the solvent is very important, especially

when the dissolved particles are very small [69], or when the spacing between particles contains room for only a few solvent particles [90]. The approximation is also problematic near the surface of a highly charged macroion. The strong electric field near such a surface causes the polar solvent molecules nearby to have strongly preferential orientations. This severely reduces the dielectric permittivity near the surface. This is exacerbated by the high density of counterions in the vicinity of the surface. The dissolved microions are typically surrounded by a solvation shell of preferentially orientated water molecules. The high density of counterions near a charged surface restrict the orientations of the solvent molecules even more and cause a further reduction of the permittivity. In addition to this, the high density of ions near a charged surface means that the typical distance between the ions becomes comparable to their diameter which is typically $\sim 3-6\mathring{A}$, so that the short-range repulsion becomes important.

Some treatments of charged surfaces in water attempt to take account of these molecular effects by treating a thin layer near the surface (which contains a large number of counterions) separately, so that a more diffuse layer beyond this can be treated within mean field theory. This somewhat arbitrary construct is called the Stern layer [67], in which the charged surface and a layer of counterions are treated as a capacitor. The permittivity of the solvent inside this layer is strongly reduced compared to the bulk. For water this is typically taken to be of the order of $\epsilon_r \approx 6-32$.

For the purposes of this study, the PM approximations are assumed to be valid even near highly charged surfaces. Solvent effects such as the overlap of hydration shells between two microions are neglected. A uniform dielectric permittivity for water is assumed throughout, and microion molecularity is neglected.

5.2 Adiabatic potential for macroions: mapping to a one-component system

Since the mass of the macroions is much larger than the mass of the microions, the assumption can be made that the motion of macroions is adiabatically cut off from the motion of the microions. The macroions move so slowly compared with the microions, that for each macroionic configuration the microions can be considered to have reached thermodynamic equilibrium. This requires that $\tau_F >> \tau_M$, the relaxation time of the microions to be much shorter than that of the macroions.

For the purposes of calculating the equilibrium thermodynamic properties of a colloidal suspension, this criterion does not have to be satisfied, as timescales do not feature in the equilibrium thermodynamic description of a system. However, the construction of an effective Hamiltonian for the macroionic degrees of freedom only, is useful as a first step towards calculating the equilibrium free energy of a colloidal suspension. An adiabatic effective Hamiltonian for the macroions $H^{\text{eff}}(\{\mathbf{R}_n, \mathbf{P}_n\})$ is formed by performing a weighted sum over all possible microionic configurations.

$$\exp\left[-\beta H^{\text{eff}}\left(\{\mathbf{R}_n, \mathbf{P}_n\}\right)\right] = Tr_M\left[\exp\left[-\beta H_{PM}\left(\{\mathbf{r}_i, \mathbf{p}_i\}, \{\mathbf{R}_n, \mathbf{P}_n\}\right)\right]\right] \tag{5.6}$$

The trace over M is over all microionic positions and momenta and $H_{PM} = K_F + K_M + V_{FF} + V_{MM} + V_{MF}$. The resulting effective Hamiltonian consists of

$$H^{\text{eff}} = K_F(\{\mathbf{P}_n\}) + V_{FF}(\{\mathbf{R}_n\}) + F_M(\{\mathbf{R}_n\}) \tag{5.7}$$

where $F_M(\{\mathbf{R}_n\})$ is the free energy of the microions, for a given set of fixed macroionic positions. The Helmholtz free energy F_M is obtained from the trace over microionic positions and momenta

$$\exp[-\beta F_M(\{\mathbf{R}_n\})] = Tr_M\left[\exp[-\beta(K_M + V_{MM} + V_{MF})]\right] \tag{5.8}$$

This is the same trace as that performed in (5.6). Since the macroions are fixed during the trace, the terms involving only macroions K_F and V_{FF} may be factored out of (5.6), leaving the trace (5.8).

The macroion-macroion interaction V_{FF} together with F_M produce an effective many-body potential for the macroions $V^{\text{eff}} = V_{FF} + F_M$ that depends on all of the macroionic positions $\{\mathbf{R_n}\}$. The resulting effective Hamiltonian for the one-component system of macroions is

$$H^{\text{eff}}(\{\mathbf{R}_n\},\{\mathbf{P}_n\}) = \sum_l \frac{\mathbf{P}_l^2}{2M} + V^{\text{eff}}(\{\mathbf{R}_n\}) \tag{5.9}$$

where M is the mass of a macroion. It is this Hamiltonian from which the thermodynamic behaviour of the suspension may be calculated, which is the topic of the next section.

5.3 Thermodynamics and phase stability of a suspension

In theory, the thermodynamic behaviour of the colloidal suspension within the primitive model is derived from the free energy of macroions F_F with the effective one-component Hamiltonian H^{eff} in Equation (5.9). This free energy involves a trace over all possible macroionic configurations Tr_F

$$\exp\left[-\beta F_F\right] = Tr_F\left[\exp\left[-\beta H^{\text{eff}}\left(\{\mathbf{R}_n\},\{\mathbf{P}_n\}\right)\right]\right] \tag{5.10}$$

The free energy F_F is the equilibrium free energy of a system of macroions interacting through an effective potential mediated by microions. As discussed in Chapter 1, the stability of a uniform phase with respect to phase separation can be inferred from the free energy of a hypothetical system *constrained* to be of uniform density and order corresponding to the phase in question. Here we are interested in finding out whether a system with a uniform colloidal density η_F is unstable with respect to phase separation into two coexisting phases with substantially differing densities, say η_{FL} and η_{FG}. The criterion for this is that the isothermal compressibility χ_{Tc} of the constrained, homogeneous system becomes negative making it thermodynamically unstable

$$\chi_{Tc} = -\frac{1}{V}\left(\frac{\partial V}{\partial P_c}\right)_T < 0 \tag{5.11}$$

V is the volume of the system and P_c is the pressure of the constrained system defined as

$$P_c = -\frac{\partial F_{Fc}}{\partial V} \tag{5.12}$$

The free energy F_{Fc} refers to the Helmholtz free energy of the constrained system of macroions with uniform density, which is given by

$$F_{Fc} = \langle H^{\text{eff}}\rangle_c - TS_c \tag{5.13}$$

where the subscript c denotes the ensemble of macroionic configurations corresponding to a restricted uniform macroionic phase. Theoretically F_{Fc} would be obtained by taking the trace in (5.10) over an ensemble of constrained macroionic configurations corresponding to the uniform phase in question.

As discussed in Chapter 4, various experiments and theoretical treatments point toward coexistence between dilute fluid phases with substantially denser fluid as well as solid phases. This indicates that a theoretical treatment should account for both fluid and crystalline phases of various macroionic densities. Knott [47] found that the configurational entropy S_c associated with macroionic positions in the fluid phase makes a negligible contribution to F_{Fc}. The dominant terms in F_{Fc} are a result of the strong electrostatic interactions, as well as the entropy of the microions which are typically of the order of $10^3 - 10^4$ times more numerous than the macroions. Therefore both solid and fluid phases were represented using a perfect lattice of static macroions.

Van Roij and co-workers (RDH) took account of macroion motions approximately using simplified fluid and solid reference systems in conjunction with the Gibbs-Bogoliubov inequality [68]. The free energy evaluated using the reference system ensemble was minimised with respect to one or more parameters characterising the reference system, in order to obtain the best possible estimate to F_{Fc}. Uniform FCC and BCC solid phases were estimated within the Einstein model, with the Einstein phonon frequency ω_0 and mean square displacement of macroions as variational parameters. The liquid phase was approximated using an uncharged hard-sphere liquid reference system, with the hard sphere diameter d (or equivalently the reference system system packing fraction ϕ_{ref}) as the variational parameter. This scheme enabled the authors to produce solid-liquid-gas phase diagrams for colloidal suspensions, which exhibited fluid-fluid and fluid-solid coexistence with large density differences. Under some conditions fluid-solid coexistence was found to be preempted by a metastable fluid-fluid phase transition following a roughly similar contour in the $n_s - \phi$ plane. In other words, even though the equilibrium phase diagram exhibits solid-fluid phase coexistence, a hypothetical fluid-fluid coexistence covering roughly the same region in $n_s - \phi$ space is seen if only fluidlike configurations for the macroions are used to calculate F_{Fc}.

This indicates that the mechanism underlying phase transitions between phases with significantly different densities is qualitatively independent of the configurational entropy of the macroions, so that solid and liquid phases are broadly interchangeable for the purposes of finding out whether this kind of coexistence occurs. MC simulations performed by RDH also indicate that the difference in free energy between solid and fluid phases of the same packing fraction ϕ are very small (less than $1k_BT$ per macroion), again supporting the assertion that it is not differences in macroionic entropy that cause fluid-fluid or fluid-solid coexistence between phases of substantially different densities.

For these reasons, calculations of F_{Fc} for the constrained, homogeneous density system can be performed on a perfect lattice of macroions. Neither lattice vibrations nor configurational disorder for fluidlike phases have to be considered. This greatly simplifies the problem to the calculation of F_{Fc} for a perfect lattice of macroions interacting through $V^{\text{eff}}(\{\mathbf{R_n}\})$ at different homogeneous densities η_F.

5.4 Mean field description of the microions

5.4.1 Mean field density functional theory

Within the approximation laid out above, the constrained free energy F_{Fc} consists of the free energy of microions F_M and the macroion-macroion potential energy V_{FF} for a perfect static lattice of macroions with a uniform density η_F. The entropy and kinetic energy of the macroions are neglected. We will drop the subscript F and refer to F_c as the free energy of the homogeneous system of macroions arranged in a perfect lattice.

$$F_c = F_M + V_{FF} \tag{5.14}$$

This section is concerned with the evaluation of $F_M(\{\mathbf{R}_n\})$. This is the Helmholtz free energy of a system of microions interacting with a fixed set of macroions located at positions $\{\mathbf{R}_n\}$. So it is the Helmholtz free energy of a system with the Hamiltonian

$$H_M(\{\mathbf{p}_i, \mathbf{r}_i\}; \{\mathbf{R}_n\}_{\text{fixed}}) = K_M + V_{MM} + V_{MF} \tag{5.15}$$

Clearly this is the Hamiltonian of a many body system, for which the partition function cannot be evaluated exactly. For this reason most approaches to this problem are variations on mean field theory. A mean field theory along the lines of Chapter 2 can be developed for the microions. In this framework, the microions are modelled as non-interacting point particles in an external mean field

potential. Microion-microion correlations are neglected within this approximation.

To begin with, we will consider an idealised system containing only counterions of a single species carring a charge q. The free energy is expressed as a functional of the single particle probability distribution function for these microions $\rho(\mathbf{r})$. The kinetic and entropic contribution to the free energy for this class of distribution functions is given (as in Section 2.2.2) by

$$\langle K_M \rangle_0 - TS_0 = k_B T \int \rho(\mathbf{r})[log(\rho(\mathbf{r})\lambda^3) - 1]d\mathbf{r} \tag{5.16}$$

Where 0 denotes the probability distribution function of the mean field ensemble corresponding to the distribution function $\rho(\mathbf{r})$, and λ is the thermal de Broglie wavelength of the microions $h/(2\pi m k_B T)^{1/2}$, where m is the mass of a microion.

One component of the macroion-microion interaction V_{MF} is a hard-sphere interaction that prevents the microions from penetrating the macroions. Therefore the integral in (5.16) and all subsequent configurational integrals are restricted to be over the available space for the microions, excluding the regions inside the macroions. Restricting the integrals in this way means the only remaining component in V_{MF} is the electrostatic interaction.

The next task is to evaluate the mean potential energy contributions $\langle V_{MF} \rangle_0$ and $\langle V_{MM} \rangle_0$ using the trial probability distribution $\rho(\mathbf{r})$. Since the trial probability distributions are based on non-interacting particles inside an external potential, there are no correlations in the two-particle probability distribution function, so that the pair distribution function reduces to

$$\rho^{(2)}(\mathbf{r}_1, \mathbf{r}_2) = g^{(2)}(\mathbf{r}_1, \mathbf{r}_2)\rho(\mathbf{r}_1)\rho(\mathbf{r}_2) = \rho(\mathbf{r}_1)\rho(\mathbf{r}_2) \tag{5.17}$$

where $g^{(2)}(\mathbf{r}_1, \mathbf{r}_2)$ is the pair correlation function and equals unity for the trial ensemble, in which correlations between the particles are neglected. As a result of this simplification, averages of quantities that depend on the positions of pairs of particles such as V_{MM}, are evaluated as

$$\langle V_{MM} \rangle_0 = \frac{q^2}{2} \int d\mathbf{r} \int d\mathbf{r}' \rho(\mathbf{r})\rho(\mathbf{r}')G(\mathbf{r} - \mathbf{r}') \tag{5.18}$$

where $G(\mathbf{r} - \mathbf{r}')$ is the electrostatic Green's function satisfying the Poisson equation

$$\nabla^2 G(\mathbf{r} - \mathbf{r}') = -\frac{1}{\epsilon}\delta^3(\mathbf{r} - \mathbf{r}') \tag{5.19}$$

The mean macroion-microion interaction $\langle V_{MF} \rangle_0$ is given by

$$\langle V_{MF} \rangle_0 = q \int d\mathbf{r} \rho(\mathbf{r})\psi_F(\mathbf{r}) \tag{5.20}$$

where $\psi_F(\mathbf{r})$ is the electrostatic potential due to all of the macroions. In this model, we consider all of the macroions to be identical, with a smooth surface charge density $\sigma = Z/4\pi a^2$ (Z is the total charge carried by a macroion and a is the macroion radius). The charge distribution due to a single macroion centred at $\mathbf{R_n}$ is represented using a spherical delta function as

$$n_1(\mathbf{r} - \mathbf{R_n}) = \sigma\delta(|\mathbf{r} - \mathbf{R_n}| - a) \tag{5.21}$$

The electrostatic potential $\psi_F(\mathbf{r})$ can be expressed in terms of the total macroionic charge distribution

$$\psi_F(\mathbf{r}) = \int d\mathbf{r}' n_F(\mathbf{r}')G(\mathbf{r} - \mathbf{r}') \tag{5.22}$$

where the total macroionic charge distribution $n_F(\mathbf{r})$ is the sum over all macroions (labelled n)

$$n_F(\mathbf{r}) = \sum_n n_1(\mathbf{r} - \mathbf{R}_n) \tag{5.23}$$

Combining these terms, the mean field free energy of the microions is expressed as

$$\begin{aligned} F_M[\rho(\mathbf{r})] = &\int k_B T \rho(\mathbf{r})[log(\rho(\mathbf{r})\lambda^3) - 1]d\mathbf{r} + \frac{q^2}{2}\int d\mathbf{r}\int d\mathbf{r}'\rho(\mathbf{r})\rho(\mathbf{r}')G(\mathbf{r}-\mathbf{r}') \\ &+q\int d\mathbf{r}\int d\mathbf{r}'\rho(\mathbf{r})n_F(\mathbf{r}')G(\mathbf{r}-\mathbf{r}') \end{aligned} \tag{5.24}$$

As mentioned previously, all integrals are understood to be over the volume outside of the colloidal spheres.

The free energy (5.24) is functionally differentiated in order to find the $\rho(\mathbf{r})$ that minimises it, and hence gives the best possible approximation to the true free energy. A Lagrange multiplier μ to constrain the total number of microions and ensure charge neutrality is required. The optimal density profile satisfies

$$\begin{aligned} \frac{\delta}{\delta\rho(\mathbf{r})}\left[F - \mu\int d\mathbf{r}\rho(\mathbf{r})\right] = &k_B T\, log(\rho(\mathbf{r})\lambda^3) - q^2\int d\mathbf{r}'\rho(\mathbf{r}')G(\mathbf{r}-\mathbf{r}') \\ &- q\int d\mathbf{r}' n_F(\mathbf{r}')G(\mathbf{r}-\mathbf{r}') - \mu = 0 \end{aligned} \tag{5.25}$$

The second term is $\langle\psi_M(\mathbf{r})\rangle_0$, the average electrical potential at $\mathbf{r}$ due to microions, evaluated within the mean field ensemble. The third term is the electrostatic potential due to the fixed macroions $\psi_F(\mathbf{r})$. Equation (5.25) for the optimal profile may be written as

$$\rho(\mathbf{r}) = \frac{1}{\lambda^3}\exp\left[\beta\left(\mu - q\left\langle\psi_M(\mathbf{r})\right\rangle_0 - q\psi_F(\mathbf{r})\right)\right] \tag{5.26}$$

The average potential due to microions $\langle\psi_M(\mathbf{r})\rangle_0$ is a functional of $\rho(\mathbf{r})$, and (5.26) is a non-linear equation for the self-consistent density profile satisfying

$$\rho(\mathbf{r}) = \frac{1}{\lambda^3}\exp\left[\beta\left(\mu - q\int G(\mathbf{r}-\mathbf{r}')\rho(\mathbf{r}')d\mathbf{r}' - q\psi_F(\mathbf{r})\right)\right] \tag{5.27}$$

5.4.2 The Poisson-Boltzmann equation

The Poisson-Boltzmann approach is an alternative representation of the equation for the mean field distribution of microions. Instead of solving for an optimal mean field density distribution of microions $\rho(\mathbf{r})$ as in (5.27), the objective in the PB approach is to solve for the total mean field electrical potential

$$\psi = \langle\psi_M(\mathbf{r})\rangle_0 + \psi_F(\mathbf{r}) \tag{5.28}$$

For a fixed configuration of microions, the electrostatic potential satisfies the Poisson equation

$$\nabla^2\hat{\psi}_M(r) = -\frac{q}{\epsilon}\hat{\rho}(r) \tag{5.29}$$

where the hats indicate that the quantities relate to particles at fixed positions. It can be shown that this relation holds for thermal averages. For averages taken over the mean field ensemble the result is

$$\nabla^2\langle\psi_M(r)\rangle_0 = -\frac{q}{\epsilon}\rho(r) \tag{5.30}$$

where $\rho(r)$ is the optimising mean field distribution function. Equation (5.26) may be written in terms of $\langle\psi_M(\mathbf{r})\rangle_0$ as

$$\nabla^2\langle\psi_M(\mathbf{r})\rangle_0 = -\frac{q}{\lambda^3\epsilon}\exp\left[\beta\left(\mu - q\langle\psi_M(\mathbf{r})\rangle_0 - q\psi_F(\mathbf{r})\right)\right] \tag{5.31}$$

The fixed macroion electrostatic potential is related to the fixed macroionic charge distribution through the Poisson equation

$$\nabla^2\psi_F(\mathbf{r}) = -\frac{1}{\epsilon}n_F(\mathbf{r}) \tag{5.32}$$

The equation satisfied by the total mean field potential (5.28) is

$$\nabla^2\psi(\mathbf{r}) = -\frac{1}{\epsilon}\left(qn_0\exp[-\beta\, q\,\psi(\mathbf{r})] + n_F(\mathbf{r})\right) \tag{5.33}$$

where the normalisation constant $n_0 = \exp(\beta\mu)/\lambda^3$ has been introduced. This is the nonlinear Poisson-Boltzmann equation that has to be solved to find $\psi(\mathbf{r})$, which is equivalent to finding the density distribution that minimises the functional (5.24).

5.4.3 Multiple microionic species

The mean field Helmholtz free energy (5.24) may be generalised to account for the presence of differently charged species of microion. This situation arises for example when salt is added to the deionised solution containing the colloidal suspension. We introduce $\rho_i(\mathbf{r})$, the probability distribution for microions carrying charge q_i. Each species of microion may have a different mass, so the thermal de Broglie wavelength (which depends on mass) for species i is denoted by λ_i. F_M is now a functional of the full set of distribution functions $\{\rho_i(\mathbf{r})\}$

$$\begin{aligned}F_M[\{\rho_i(\mathbf{r})\}] = \sum_i\Bigg[&k_BT\int\rho_i(\mathbf{r})[log(\rho_i(\mathbf{r})\lambda_i^3) - 1]d\mathbf{r} + q_i\sum_j q_j\frac{1}{2}\int d\mathbf{r}\int d\mathbf{r}'\rho_i(\mathbf{r})\rho_j(\mathbf{r}')G(\mathbf{r}-\mathbf{r}')\\ &+ q_i\int d\mathbf{r}\int d\mathbf{r}'\rho_i(\mathbf{r})n_F(\mathbf{r}')G(\mathbf{r}-\mathbf{r}')\Bigg]\end{aligned} \tag{5.34}$$

where the sums in i, j run over all of the different microionic species. Generalising to account for multiple species, the average mean field potential due to all of the microions is

$$\langle\psi_M(\mathbf{r})\rangle_0 = \sum_j q_j\int d\mathbf{r}'\rho_j(\mathbf{r}')G(\mathbf{r}-\mathbf{r}') \tag{5.35}$$

The potential due to the fixed charges $\psi_F(\mathbf{r})$ remains the same, so that (5.34) may be expressed as

$$F_M[\{\rho_k(\mathbf{r})\}] = \sum_i\left[k_BT\int\rho_i(\mathbf{r})[log(\rho_i(\mathbf{r})\lambda_i^3) - 1]d\mathbf{r} + \frac{q_i}{2}\int\rho_i(\mathbf{r})\langle\psi_M(\mathbf{r})\rangle_0 d\mathbf{r} + q_i\int\rho_i(\mathbf{r})\psi_F(\mathbf{r})d\mathbf{r}\right] \tag{5.36}$$

A functional derivative with respect to $\rho_i(\mathbf{r})$ is taken to find the optimal distributions. Lagrange multipliers μ_i that regulate the number of microions of each species i are introduced, and total mean field potential at $\mathbf{r}$ is again defined as $\psi(\mathbf{r}) = \langle\psi_M(\mathbf{r})\rangle_0 + \psi_F(\mathbf{r})$

$$\frac{\delta}{\delta\rho_i(\mathbf{r})}\left[F_M - \mu_i\int d\mathbf{r}\rho_i(\mathbf{r})\right] = k_BT\, log(\rho_i(\mathbf{r})\lambda_i^3) + q_i\,\psi(\mathbf{r}) - \mu_i = 0 \tag{5.37}$$

The profiles satisfying this condition are

$$\rho_i(\mathbf{r}) = \frac{1}{\lambda_i^3} \exp\left[\beta(\mu_i - q_i\psi(\mathbf{r}))\right] \tag{5.38}$$

or

$$\rho_i(\mathbf{r}) = n_{0i} \exp\left[-\beta q_i \psi(\mathbf{r})\right] \tag{5.39}$$

where $n_{0i} = \exp(\beta\mu_i)/\lambda_i^3$. The form of n_{0i} must be chosen to ensure the correct abundance of ions of each species. Equation (5.39) represents a set of coupled equations (one for each microionic species i), with each ρ_i contributing to the total mean field potential $\psi(\mathbf{r})$ through (5.35).

The Poisson-Boltzmann approach utilises the relationship between the total electrostatic potential $\psi(\mathbf{r})$ and the total (microionic and macroionic) charge density. The microionic contribution to the charge density which we denote by $\rho(\mathbf{r})$ couples all of the profiles ρ_i together

$$\rho(\mathbf{r}) = \sum_i q_i \rho_i(\mathbf{r}) \tag{5.40}$$

Using (5.40) as the total microionic contribution to the charge density, the Poisson-Boltzmann equation is generalised to

$$\nabla^2\psi(\mathbf{r}) = -\frac{1}{\epsilon}\left(\sum_i q_i\, n_{0i}\, \exp[-\beta q_i \psi(\mathbf{r})] + n_F(\mathbf{r})\right) \tag{5.41}$$

The charge on a microion of species i may be written as $q_i = e\ z_i$ where e is the elementary charge of the electron and z_i is the valency of microion species i. For convenience, we introduce the dimensionless reduced potential $\Phi = e\psi/k_BT$ and change the macroion charge density $n_F(\mathbf{r})$ to a number density through $n_F(\mathbf{r}) \to n_F/e$. In terms of these quantities the PB equation can be rewritten as

$$\nabla^2\Phi(\mathbf{r}) = -4\pi l_B\left(\sum_i z_i\, n_{0i}\, \exp[-z_i\Phi(\mathbf{r})] + n_F(\mathbf{r})\right) \tag{5.42}$$

where l_B is the Bjerrum length $l_B = e^2/4\pi\epsilon k_BT$. This is the length at which the potential energy between two elementary charges (in a medium with dielectric permittivity ϵ) equals their thermal kinetic energy. With $\epsilon = 78\epsilon_0$, and $T = 300K$, $l_B = 0.72$ nm.

5.4.4 Salt content of a suspension

The concentration of ions in electrolytes greatly affects the collective electrostatic interactions in the system. A high concentration of ions enhances the screening capability of the solution. The Debye screening length λ_D quantifies the lengthscale on which a charge is effectively screened within the *linear* Debye Hückel theory [45]. The inverse Debye screening length $\kappa = 1/\lambda_D$ is defined as

$$\kappa^2 = 4\pi l_B \sum_i z_i^2 n_{oi} \tag{5.43}$$

This indicates that the screening length is proportional to the inverse square root of the total ionic concentration in the electrolyte. A higher concentration of ions n_{0i} enhances screening, so that the electrostatic potential of a charge in the electrolyte is screened over a shorter distance. Even the purest deionised solvent will contain a small number of salt ions, which will reduce the screening length from that of a suspension containing only the counterions dissolved from the surfaces of the colloidal particles.

So far we have only said that the number of ions of each species is regulated by a Lagrange multiplier μ_i. However there are two distinct physical situations that will determine the form of μ_i.

The system may be in contact with a large reservoir of electrolyte containing a fixed concentration of salt, or it may be closed containing a fixed number of salt ions. These two situations give rise to the grand canonical and canonical ensemble for the microions respectively. The grand-canonical ensemble is sometimes referred to the semi-grand canonical ensemble [86] in this context, to indicate that the system is open to microion exchange with a reservoir but with the number of macroions in the system remaining fixed.

For the case of the grand canonical ensemble, μ_i is the chemical potential of the species i inside an infinite salt bath. When the system reaches equilibrium with the bath, the chemical potential for species i in the system must equal the chemical potential inside the bath μ_i. In the canonical ensemble, μ_i takes a form that ensures that the number of ions of species i equals the fixed amount present in the closed system.

In the grand canonical ensemble, where the number of microions in the system is not fixed, the Helmholtz free energy F is not the correct thermodynamic potential for the microions. It is replaced by the grand potential $\Omega(\{\mu_i\}, V, T)$, which is related to $F(\{N_i\}, V, T)$ through the Legendre transform

$$\Omega(\{\mu_i\}, V, T) = F(\{N_i\}, V, T) - \sum_i \mu_i N_i \tag{5.44}$$

where μ_i is the fixed chemical potential of species i in the reservoir, and N_i is the mean number of i-ions in the system when it is at equilibrium with the reservoir.

The mean field theory presented here neglects microion-microion correlations. Since these correlations are expected to be stronger for higher valency microions [73], we restrict ourselves to the case of univalent $z = \pm 1$ microions in this study. $N|Z|$ counterions result from dissolution of surface groups from the N macroions. From now on we will take the macroionic charge to be negative $Z < 0$, though this choice is arbitrary. The $N|Z|$ counterions (of valency $z = +1$) are joined by N_s additional $z = +1$ ions, and N_s coions (with $z = -1$) resulting from the presence of N_s dissolved salt particles in the system. In both ensembles the system must be charge neutral overall so that the total number of positive microions in the system is $N_+ = N|Z| + N_s$ while the total number of negative microions is $N_- = N_s$.

5.4.5 Charge neutrality

In both thermodynamic ensembles, the suspension must satisfy overall charge neutrality

$$\sum_n \int n_1(\mathbf{r} - \mathbf{R}_n) d\mathbf{r} + \sum_i \int z_i \rho_i(\mathbf{r}) d\mathbf{r} = 0 \tag{5.45}$$

This constraint may be imposed through the use of an additional Lagrange multiplier [86] μ_{el}, to ensure overall charge neutrality, so that the Euler-Lagrange equation (5.37) is changed to

$$\frac{\delta}{\delta \rho_i(\mathbf{r})} \left[F_M - \mu_i \int d\mathbf{r} \rho_i(\mathbf{r}) - \mu_{el} \int d\mathbf{r} \sum_i z_i \rho_i(\mathbf{r}) \right] = log(\rho_i(\mathbf{r})\lambda_i) + z_i \left(\Phi(\mathbf{r}) - \mu_{el}\right) - \mu_i = 0 \tag{5.46}$$

Although μ_{el} and μ_i are clearly interrelated, they have distinct roles. The electroneutrality Lagrange multiplier μ_{el} enforces overall charge neutrality, while μ_i ensures the correct abundance of each species of ion either through straightforward normalisation for the canonical ensemble of ions, or by maintaining equilibrium with a salt bath at chemical potential μ_i for the grand canonical ensemble of ions. For a system containing two species of microion $z = \pm 1$, the constraint on the number of microions can be imposed by either a Lagrange multiplier for each species $\mu_\pm$, or one for the number of salt particles μ_s and one to impose charge neutrality μ_{el}.

In terms of the Poisson-Boltzmann equation, the charge neutrality condition takes the form of

conditions on the mean field potential $\Phi(\mathbf{r})$. Gauss's Theorem relates the total charge in the system to the flux through a bounding surface. If the total charge in the volume V is zero, then the net flux through the surface S enclosing it must also be zero

$$\int_S \nabla\Phi \cdot d\mathbf{s} = \int_V \nabla^2\Phi dV \tag{5.47}$$

where S is a surface bounding the volume V, $d\mathbf{s} = \hat{\mathbf{n}}ds$ and $\hat{\mathbf{n}}$ is a vector perpendicular to the surface element ds.

In certain, simplified geometries, the charge neutrality condition translates to simple boundary conditions on $\Phi(\mathbf{r})$. As an example consider a single spherical colloidal particle with radius a, carrying charge Z, located at the centre of a spherical volume of radius R. The particle is immersed in an electrolyte containing an excess of counterions that neutralise the charge on the macroion. For the system to be charge neutral, the charge density distribution of microions must satisfy

$$\sum_i \int_a^R z_i \rho_i(\mathbf{r}) d\mathbf{r} = -Z \tag{5.48}$$

Now we assume a spherically symmetric charge distribution, so that any electrostatic field is purely in the radial direction, and the electrostatic potential depends only on the radial coordinate r, so that $\Phi(\mathbf{r}) = \Phi(r)$. Integrating the microionic charge density given by the PB equation between radial positions $r = a$ and $r = R$, and requiring the total microionic charge to satisfy (5.48), results in

$$4\pi R^2 \frac{d\Phi}{dr}\bigg|_{r=R} - 4\pi a^2 \frac{d\Phi}{dr}\bigg|_{r=a} = 4\pi l_B Z \tag{5.49}$$

where Z is the total amount of surface charge divided by e (i.e. the valency of the macroion). If condition (5.45) is met, then the field at R and beyond must vanish

$$\frac{d\Phi}{dr}\bigg|_{r=R} = 0 \tag{5.50}$$

inserting this in (5.49) gives the boundary condition at $r = a$

$$\frac{d\Phi}{dr}\bigg|_{r=a} = -4\pi l_B \sigma \tag{5.51}$$

which relates the gradient of the potential at the surface of the macroion to the surface charge density $\sigma = Z/4\pi a^2$. If the boundary conditions (5.50) and (5.51) are met by the potential satisfying the Poisson-Boltzmann equation, then the charge neutrality condition is satisfied.

The simple relationship between charge neutrality and the gradient of the potential is a result of the simple, spherically symmetric geometry in this example. In general the form of the boundary condition will be more complicated.

5.5 The Wigner-Seitz cell model

5.5.1 Symmetry and periodicity of the mean field distribution of microions

The Hamiltonian for microions in the primitive model is given in Equation (5.15). More explicitly, for the case of a salt-free suspension containing univalent ($z = +1$) counterions only, this takes the form

$$H_M(\{\mathbf{p}_i, \mathbf{r}_i\}; \{\mathbf{R}_n\}_{\text{fixed}}) = \sum_{i=1}^{NZ} \left[K_i + \Phi_F(\mathbf{r}_i) + \sum_{j=1}^{NZ} u(\mathbf{r}_i - \mathbf{r}_j) \right] \tag{5.52}$$

K_i is the kinetic energy of the ith microion, $u(\mathbf{r}_i - \mathbf{r}_j)$ is the Coulomb interaction between two microions, and $\Phi_F(\mathbf{r}_i)$ is the Coulomb potential of a microion at $\mathbf{r}_i$ due to the surface charge on all of the macroions. From now on energies will be given in units of k_BT.

We have established that it suffices to calculate the free energy of a perfect lattice of static macroions to estimate F_{Fc} for various packing fractions. The microionic contribution F_M requires the solution of the mean field equation for the optimal distribution of microions

$$\rho(\mathbf{r}) = \lambda^{-3} \exp\left[\mu - \int G(\mathbf{r} - \mathbf{r}')\rho(\mathbf{r}')d\mathbf{r}' - \Phi_F(\mathbf{r})\right] \tag{5.53}$$

with the appropriate electrostatic potential $\Phi_F(\mathbf{r})$ due to macroions centred at lattice sites $\{\mathbf{R}_n\}_{\text{lattice}}$.

The next step is to assume that the optimising density profile of microions will have the same symmetry inherent in the geometry of the fixed macroions. In other words the mean field distribution $\rho(\mathbf{r})$ and potential $\Phi(\mathbf{r})$ will have the same symmetry as $\Phi_F(\mathbf{r})$. Distributions with a lower symmetry are expected to result in a higher free energy, and are therefore not the optimising mean field solutions.

With this assumption $\rho(\mathbf{r})$ turns into a periodic function that is invariant with respect to lattice translations $\rho(\mathbf{r} + \mathbf{L}) = \rho(\mathbf{r})$, where $\mathbf{L}$ is a lattice vector [1]. This means a solution for $\rho(\mathbf{r})$ can be restricted to lie within a single Wigner-Seitz (W-S) cell of the lattice [91]. This cell is a regular polyhedron reflecting the point group symmetry of the lattice of macroions, containing a single macroion at the centre [92, 93]. The volume of each cell is the system volume divided by the total number of macroions $V_W = V/N$ which is equivalent to $V_W = 1/\eta_F$ the inverse of the macroionic number density.

The Wigner-Seitz cell concept ties in with the condition of local or mesoscopic charge neutrality. It is assumed that the most likely solution for $\rho(\mathbf{r})$ is one that creates charge neutral regions on the length scale of the macroionic spacings. This is expected to be the case because the formation of charged regions would be energetically and entropically unfavourable. This behaviour is expected in an exact statistical mechanical treatment of the system as well: the configurations that contribute most to the canonical partition function are those that split the system up into charge neutral regions that interact weakly with each other. Therefore the W-S cells are charge neutral, with each cell containing the correct number of excess counterions to neutralise the charge on one macroion.

The W-S cell treatment is clearly a mean field concept. In a computer simulation of a system with many fixed macroions arranged in a lattice, we would expect there to be a net charge in the different cells at any given instant. Geometrically, this could be thought of as deformations of the charge neutral volumes about the macroions. However on average, the geometry of the neutralising volumes is expected to be identical about each macroion- namely the W-S cells.

An inherent feature of the mean-field theory is the neglect of microion-microion correlations. This means local microscopic fluctuations due to microion-microion correlations are neglected. In addition to this, long-wavelength fluctuations of the microionic distribution functions on the length scale of the W-S cells are excluded too. Some fluctuations about the mean-field solution may make a substantial contribution to the partition function, with the result that the mean field approximation to the free energy will not be accurate. Correlations between microions on the length-scale of the W-S cells can be imagined in which for example adjacent cells contain a small excess charge of opposite signs. The fluctuations could even be on a longer length-scale with groups of adjacent cells containing excess charge.

The W-S cell model introduces an additional approximation in that microion-macroion correlations between cells are neglected in addition to the microion-microion correlations. Situations can be imagined in which the microion distribution about a macroion in a charge neutral W-S cell is skewed

[1] To be precise, the additional assumption that the number of macroions is large has been introduced. The invariance holds for the case of an infinite lattice. If the number of macroions is sufficiently large, distortions due to finite size of the colloidal crystal can be neglected.

and breaks the symmetry. This would set up dipole or higher order multipole fields emanating from the cell. Correlations between cells could bring about asymmetries in adjacent cells. These effects are neglected in the W-S cell model, as well as most field theories that do not involve W-S cells.

Despite the neglect of inter-cell correlations in the W-S cell model, it is important to recognise that inter-cell interactions are inherent within the model. The microions in a cell are confined to the cell by virtue of their interactions with the microions and macroions in the surrounding cells. The W-S cell construction constrains the form of the mean field electrostatic potential $\Phi(\mathbf{r})$ and microion distribution function $\rho(\mathbf{r})$ as a result of interactions with an infinite lattice of identical cells surrounding it.

The interactions between the cells manifest themselves in boundary conditions on the mean field potential $\Phi(\mathbf{r})$ on the cell boundary. This is a typical feature of electrostatic problems: the interaction of a bounded region with its surroundings is encoded in the boundary conditions of the electrostatic potential on the surface enclosing the region [94]. In the W-S cell treatment, the symmetry and periodicity imposed on the mean field potential, means that the flux out of each cell boundary exactly cancels with the flux into the cell from all of the identical adjacent cells in the lattice. This means that on the W-S cell boundary, the mean field potential must satisfy

$$\nabla\Phi \cdot \hat{\mathbf{n}} = 0 \tag{5.54}$$

where $\hat{\mathbf{n}}$ is a unit vector perpendicular to the cell boundary. It is important to note that conditions for periodicity, symmetry and charge neutrality are interrelated, and the combination of all three gives rise to the condition (5.54) on the W-S cell boundary. It is impossible to construct an infinitely periodic lattice of W-S cells containing a net charge. It is equally impossible to have an infinite, periodic lattice consisting of cells with electrostatic fields of a different symmetry to the lattice. In both of these cases, when the infinite cell limit is taken, electrostatic fields build up at the outer boundaries of the lattice, breaking the periodicity property.

A mean field potential $\Phi(\mathbf{r})$ that satisfies (5.54) on the boundary of the W-S cell, implicitly accounts for inter-cell interactions with an infinite set of identical cells in the lattice. The W-S cell treatment replaces the problem of a lattice containing many macroions and their respective microions, into one of a single macroion with microions in a W-S cell with the appropriate boundary conditions to account for the interactions with microions and macroions in all other cells. Using this approach, the electrostatic energy per macroion of the infinite lattice U_{el}/N where $U_{el} = V_{MM} + V_{FF} + V_{MF}$ may be calculated from the charge distribution and electrostatic potential within a single W-S cell. The same is true for the mean field free energy F_M.

5.5.2 Simple cubic geometry

A comparatively easy lattice structure to deal with is the simple cubic (SC) lattice [92], which possess a high degree of symmetry. If the spacing between macroions centred at lattice sites is D, the volume of each cell is $V_W = D^3$. The lattice sites are described by the position vectors $\mathbf{R}_{lmn} = l\mathbf{r_1} + m\mathbf{r_2} + n\mathbf{r_3}$, where $\mathbf{r_1}, \mathbf{r_2}, \mathbf{r_3}$ are lattice vectors which may be taken to be $D\hat{\mathbf{i}}, D\hat{\mathbf{j}}, D\hat{\mathbf{k}}$ for this geometry, and l, m, n are integers.

The Wigner-Seitz cell for this geometry is a cube with sides of length D. For the cell centred at the origin (with $l = m = n = 0$), the faces of the cubic cell are composed of the $x - y$ planes at $z = \pm D/2$, the $x - z$ planes at $y = \pm D/2$ and the $y - z$ planes at $x = \pm D/2$. The boundary conditions satisfied by the mean field potential at the faces of the W-S cube are

$$\nabla\Phi(\pm D/2, y, z) \cdot \hat{\mathbf{i}} = \left.\frac{\partial\Phi}{\partial x}\right|_{x=\pm D/2} = 0 \tag{5.55}$$

and

$$\nabla\Phi(x, \pm D/2, z) \cdot \hat{\mathbf{j}} = \left.\frac{\partial\Phi}{\partial y}\right|_{y=\pm D/2} = 0 \tag{5.56}$$

and

$$\nabla\Phi(x, y, \pm D/2) \cdot \hat{\mathbf{k}} = \left.\frac{\partial\Phi}{\partial z}\right|_{z=\pm D/2} = 0 \tag{5.57}$$

These boundary conditions are direct reflection of the symmetry and periodicity imposed on the mean field potential $\Phi(\mathbf{r})$ in the W-S treatment.

The mean field potential $\Phi(\mathbf{r})$ and distribution of microions $\rho(\mathbf{r})$ are assumed to possess the full symmetry of the simple cubic structure of macroions, and the respective macroionic electrostatic potential $\Phi_F(\mathbf{r})$. For the SC geometry, this corresponds to the full octahedral group O, which contains 48 symmetry operations (24 operations which take a cube onto itself, together with the inversion operation I) [93]. These symmetry conditions may be expressed as

$$\Phi(\mathbf{s} \cdot \mathbf{r}) = \Phi(\mathbf{r}) \tag{5.58}$$

and

$$\rho(\mathbf{s} \cdot \mathbf{r}) = \rho(\mathbf{r}) \tag{5.59}$$

where $\mathbf{s}$ are any of the operations that make up the symmetry group of the lattice. These may be expressed as matrix operators that take a point $\mathbf{r}$ in the cell to a different point within the cell $\mathbf{r}' = \mathbf{s} \cdot \mathbf{r}$. By construction, the function $\Phi_F(\mathbf{r})$ also satisfies these symmetry conditions.

The high degree of symmetry in the simple cubic W-S cell, allows us to focus on a small irreducible portion of the cell, that corresponds to 1/48th of the cell volume, in the solution of the mean field equations.

Experimental observations of colloidal crystals show that these systems tend to crystallise into close-packed BCC or FCC lattice structures. These structures have lower symmetries than the SC structure, so for convenience we restrict ourselves to the SC lattice structure.

5.5.3 Spherical approximation

An appreciable simplification is brought about if the W-S cells, which are regular polyhedra for a colloidal crystal, are approximated as being spherical. In this case the W-S cell is taken to be a spherical volume with radius R and volume $V_W = (4/3)\pi R^3$, containing a single macroion at the centre. The microion distribution $\rho(\mathbf{r})$ and the mean field potential $\Phi(\mathbf{r})$ follow the symmetry of the cell, and turn into radially symmetric functions $\rho(r)$ and $\Phi(r)$ depending only on the radial distance from the centre of the cell r.

This allows the PB equation to be converted into an ordinary differential equation (with r being the only variable) as opposed to a partial differential equation. The boundary conditions satisfied by $\Phi(r)$ are those in equations (5.50) and (5.51). If results from the spherical approximation are to be compared to those from a SC W-S cell of the same volume, then a radius of $R = (3/4\pi)^{1/3} D \approx 0.62D$ must be taken, where D is the length of the sides of the SC W-S cube.

It should be noted that although the spherical W-S cell geometry can be seen as an approximation to a cubic W-S cell, in situations where the macroions are in a positionally disordered (liquidlike) state, the spherical W-S cell may actually be more appropriate. In this situation a spherical W-S cell may be interpreted as representing the 'average' environment arround one macroion in the disordered system.

5.6 The Boundary Density Theorem

5.6.1 Pressure of a suspension from a single Wigner-Seitz cell

The stability of a homogeneous phase with respect to phase separation can be deduced from the pressure P_c of a constrained homogeneous system. In the W-S cell mean field theory, the free energy per macroion of the system $f_c = F_c/N$ is obtained from the free energy of microions and a macroion within a single W-S cell. The pressure P_c is the derivative of f_c with respect to the cell volume V_W

$$P_c = -\frac{\partial F_c}{\partial V} = -\frac{\partial f_c}{\partial V_W} \tag{5.60}$$

This pressure is related to the osmotic pressure which is the difference between the pressure of a solution and a pure solvent, but we refer to it simply as the pressure.

For the simple cubic cell the volume is $V_W = D^3$ and the differential $dV_W = 3D^2 dD$, so that the pressure is

$$P_c = -\frac{1}{3D^2}\frac{\partial f_c}{\partial D} \tag{5.61}$$

For the spherical approximation, $V_W = (4/3)\pi R^3$ and $dV = 4\pi R^2$, so the pressure is

$$P_c = -\frac{1}{4\pi R^2}\frac{\partial f_c}{\partial R} \tag{5.62}$$

Due to the specific form that the free energy functional f_c takes within mean field theory, specific cancellations occur between the entropic and energetic terms that give rise to particularly simple expressions for P_c. This result is given by the Boundary Density Theorem (BDT), which relates P_c to the density of microions at the W-S cell boundary.

The BDT is valid for systems containing one or several species of microion, and systems that are open or closed with respect to a salt bath. In addition to this, similar results can be obtained for different W-S cell geometries. In order to illustrate the nature of the cancellations clearly, we will first derive the BDT for a salt-free system in the spherical W-S cell approximation. Subsequently we will show how the result can be extended to open and closed systems containing salt, and finally to the simple cubic W-S cell geometry.

5.6.2 Salt-free system in the spherical approximation

In the spherical approximation the W-S cell is a sphere of radius R, containing a single macroion of radius a and charge Z. The macroion is positioned at the centre of the W-S cell. For a closed, salt-free system, there will also be $N|Z|$ neutralising univalent counterions. The boundary conditions satisfied by the mean field potential $\Phi(\mathbf{r})$ are (5.50) and (5.51).

For a static lattice of macroions, F_c consists of the free energy of the microions F_M and V_{FF} the macroion-macroion potential energy. The entropy and kinetic energy of the macroions are neglected. The free energy per macroion is given by

$$f_c = \int_W \rho(\mathbf{r})\left(\ln\rho(\mathbf{r})\lambda^3 - 1\right)d\mathbf{r} + \frac{1}{2}\int_W \left(\rho(\mathbf{r}) + n_F(\mathbf{r})\right)\left(\rho(\mathbf{r}') + n_F(\mathbf{r}')\right)G(\mathbf{r}-\mathbf{r}')d\mathbf{r}'d\mathbf{r} \tag{5.63}$$

W indicates integration over the volume of the W-S cell, excluding the interior volume of the central macroion. The double integral on the right is the total electrostatic energy per macroion U_{el}/N where $U_{el} = V_{MM} + V_{FF} + V_{MF}$.

In the spherical geometry, the distribution of microions and the total mean field potential are assumed to be spherically symmetric, so $\rho(\mathbf{r}) = \rho(r)$ and $\Phi(\mathbf{r}) = \Phi(r)$. The integrations in (5.63) are best done in spherical coordinates using the volume element $d\mathbf{r} = r^2 \sin\theta dr d\theta d\phi$. When taking the

derivative with respect to the cell radius R in (5.62) it is important to account for the R-dependence of the upper limit of the integral over r in (5.63). Taking the derivative of f_c with respect to R, and subsequently performing some of the integrations over $d\mathbf{r}'$ and some of the angular integrals results in

$$\begin{aligned}\frac{\partial f_c}{\partial R} &= 4\pi R^2\rho(R)\lambda^3\left(\ln\rho(R)\lambda^3-1\right)+\int_W\frac{\partial\rho}{\partial R}\ln\rho(\mathbf{r})d\mathbf{r}\\ &+4\pi R^2\left(\rho(R)+n_F(R)\right)\Phi(R)+\int_W\left(\frac{\partial\rho}{\partial R}+\frac{\partial n_F}{\partial R}\right)\Phi(\mathbf{r})d\mathbf{r}\end{aligned} \tag{5.64}$$

where

$$\Phi(\mathbf{r})=\int\left(\rho(\mathbf{r}')+n_F(\mathbf{r}')\right)G(\mathbf{r}-\mathbf{r}')d\mathbf{r}' \tag{5.65}$$

Clearly $n_F(R)=0$ since there is no macroionic charge at the cell boundary, and $\partial n_F/\partial R$ is also zero since the macroionic distribution is assumed to be fixed with respect to changes in R. We now substitute $\rho(\mathbf{r})=n_0\exp(-\Phi(\mathbf{r}))$, which results in the cancellation of some of the terms originating from the entropic and energetic portions of f_c to give

$$\frac{\partial f_c}{\partial R}=-4\pi R^2\rho(R)+\ln n_0\left[4\pi R^2\rho(R)+\int_W\frac{\partial\rho}{\partial R}d\mathbf{r}\right] \tag{5.66}$$

The term in the square brackets can be identified as the derivative of the total microionic charge, which for this case is fixed at $N|Z|$ to conserve charge neutrality

$$\frac{\partial}{\partial R}\int_W\rho(\mathbf{r})d\mathbf{r}=0 \tag{5.67}$$

Using (5.67) in (5.66) and substituting the outcome into (5.62) gives the result that the pressure equals the density of microions at the W-S cell boundary

$$P_c=\rho(R) \tag{5.68}$$

in units of k_BT per unit volume.

5.6.3 System containing fixed amount of salt

A similar result is obtained for a system with N_s dissolved salt particles per macroion in addition to the $|Z|$ counterions. Each salt particle dissolves into one univalent coion $z=-1$ and one univalent counterion $z=+1$. We take the mass of all of the microions, and therefore the respective thermal de Broglie wavelengths, to be the same. The free energy in this case is

$$f_c=\int_W\rho_+(\mathbf{r})\left(\ln\rho_+(\mathbf{r})\lambda^3-1\right)+\rho_-(\mathbf{r})\left(\ln\rho_-(\mathbf{r})\lambda^3-1\right)d\mathbf{r}+\frac{1}{2}\int_W\left(\rho(\mathbf{r})+n_F(\mathbf{r})\right)\left(\rho(\mathbf{r}')+n_F(\mathbf{r}')\right)G(\mathbf{r}-\mathbf{r}')d\mathbf{r}'a \tag{5.69}$$

where ρ in the energy term is the charge density distribution $\rho=\rho_+-\rho_-$. The optimal distributions of positive and negative microions are

$$\rho_\pm=n_{0\pm}\exp(\mp\Phi) \tag{5.70}$$

where the normalisation factors $n_{0\pm} = \lambda^{-3}\exp(\mu_\pm)$ fix the number of microions of each species. Taking the derivative with respect to R results in similar cancellations, with the result

$$\frac{\partial f_c}{\partial R} = -4\pi R^2\left(\rho_+(R)+\rho_-(R)\right)+\ln n_{0+}\left[4\pi R^2\rho_+(R)+\int_W \frac{\partial \rho_+}{\partial R}d\mathbf{r}\right]+\ln n_{0-}\left[4\pi R^2\rho_-(R)+\int_W \frac{\partial \rho_-}{\partial R}d\mathbf{r}\right] \tag{5.71}$$

Again, the terms in the square brackets are identified with derivatives of the total number of microions of each species. Since these are fixed with respect to changes in volume in the closed system, the final result is

$$P_c = \rho_+(R)+\rho_-(R) \tag{5.72}$$

The pressure equals the total density of microions at the W-S cell boundary.

5.6.4 System in contact with salt reservoir

As discussed in Section 5.4.4, for a system which is open with respect to exchange of microions with a salt reservoir, the required thermodynamic potential for the microions is the grand potential

$$\Omega_M(\mu_+,\mu_-,V,T) = F_M(N_+,N_-,V,T)-\mu_+N_+-\mu_-N_- \tag{5.73}$$

$\mu_\pm$ are the chemical potentials of the microions in the salt bath, and $N_\pm$ is the mean number of ions of each species in the system at equilibrium with the salt bath.

For this situation, the semi-grand canonical ensemble (number of microions is variable, while the number of macroions is fixed) the free energy per macroion is $f_c = \Omega_M + V_{FF}$ which is just the Legendre transform of the functional (5.69)

$$f_c(\mu_+,\mu_-,\eta_c,T) = f_c(N_+,N_-,\eta_c,T)-\mu_+\int_W \rho_+(\mathbf{r})d\mathbf{r}-\mu_-\int_W \rho_-(\mathbf{r})d\mathbf{r} \tag{5.74}$$

Now the optimal density profiles $\rho_\pm(\mathbf{r})$ contain the normalisation factors $n_{0\pm} = \lambda^{-3}\exp(\mu_\pm)$ with $\mu_\pm$ fixed at the salt bath chemical potentials. When the derivative $\partial f_c/\partial R$ is taken at fixed chemical potentials $\mu_\pm$, the terms subtracted from f_c in (5.74) exactly cancel those in the square brackets in (5.71) leaving the result for the pressure unchanged

$$P_c = \rho_+(R)+\rho_-(R) \tag{5.75}$$

5.6.5 Simple cubic Wigner-Seitz cell geometry

To illustrate that a similar result for the pressure is obtained in the cubic geometry, we will go back to the salt-free scenario. As before, the simple cubic W-S cell consists of a cubic cell with sides of length D, containing a central spherical macroion with radius a, carrying charge Z. In this geometry the integrations over the W-S cell are performed using cartesian coordinates as follows

$$\int_W d\mathbf{r} = \int_{-D/2}^{D/2}dx\int_{-D/2}^{D/2}dy\int_{-D/2}^{D/2}dz\Theta(|\mathbf{r}|-a) \tag{5.76}$$

To ensure the region inside the spherical colloidal particle is exluded, a unit step function $\Theta(x)$ has been introduced for which $\Theta(x)=1$ if $x>0$ and $\Theta(x)=0$ otherwise.

When taking the derivative of f_c, the symmetry of the SC geometry comes into play. The D-dependence of the integration limits in x, y, z will each give rise to two terms in the derivative (one from the lower and one from the upper limit). If the symmetry of the mean field distribution follows the SC symmetry of the macroionic field, then $\rho(\mathbf{r})$ and $\Phi(\mathbf{r})$ are invariant under all of the relevant point-group symmetry operations. One consequence of this is that $\rho(\mathbf{r})$ and $\Phi(\mathbf{r})$ will look the same on each

face of the cubic W-S cell boundary. In other words, integrals over the W-S cell boundary involving $\rho(\pm D/2, y, z)$, $\rho(z, \pm D/2, z)$ and $\rho(x, y, \pm D/2)$ will all be equivalent, giving rise to 6 identical terms. When taking the derivative of f_c with respect to D, we group all of the identical terms as a 6-fold multiple of the term obtained from the integration over the cubic face at $x = +D/2$ in the $y - z$ plane.

$$\begin{aligned}\frac{\partial f_c}{\partial D} =& 6 \times \frac{1}{2} \int_{-D/2}^{D/2} dy \int_{-D/2}^{D/2} dz \rho(D/2, y, z) \left(\ln \rho(D/2, y, z)\lambda^3 - 1\right) + \int_W d\mathbf{r} \ln \rho \frac{\partial \rho}{\partial D} \\ &+ 6 \times \frac{1}{2} \int_{-D/2}^{D/2} dy \int_{-D/2}^{D/2} dz \rho(D/2, y, z)\Phi(D/2, y, z) + \int_W d\mathbf{r}\Phi \frac{\partial \rho}{\partial D}\end{aligned} \tag{5.77}$$

Substituting the optimal density profile $\rho(\mathbf{r}) = n_0 \exp(-\Phi(\mathbf{r}))$ into the functional, finding the usual cancellations, and setting the derivative of the total number of microions with respect to D to zero, we get

$$\frac{\partial f_c}{\partial D} = 3 \int_{-D/2}^{D/2} dy \int_{-D/2}^{D/2} dz \rho(D/2, y, z) = 3D^2 \langle \rho \rangle_{\text{surf}} \tag{5.78}$$

where the angled brackets denote the average of the microionic density over one face of the W-S cell. This gives the nice result that the pressure is given by the mean density of microions at the W-S cell boundary

$$P_c = \langle \rho \rangle_{\text{surf}} \tag{5.79}$$

As for the spherical W-S cell, this result may be generalised to systems containing a fixed amount of salt or to systems in contact with a salt reservoir, in which case (5.79) is generalised to

$$P_c = \langle \rho_+ + \rho_- \rangle_{\text{surf}} \tag{5.80}$$

In the next chapter, a new linearisation scheme for the PB equation will be introduced. This will be applied in the subsequent chapters to calculate pressures using the BDT.

Chapter 6

New linearisation scheme for dilute suspensions

6.1 Introduction

The non-linear nature of the mean field integral and corresponding Poisson-Boltzmann differential equations makes finding solutions very challenging. Numerical techniques for these equations usually involve cumbersome iterative procedures that become computationally expensive for all but the simplest geometries. These techniques require a good initial guess for the solution in order for convergence to be efficient, and a poor initial guess might not converge at all. For these reasons it is often attractive to look for some kind of limiting principle that allows the equations to be linearised. In some cases this may even enable the equations to be solved analytically. Otherwise, the huge arsenal of relatively simple and efficient techniques for solving linear equations can be applied [95].

The traditional linearisation of the PB equation is the Debye-Hückel (D-H) approximation, which was initially intended for electrolytic solutions containing microions without the highly charged, large macroions present in colloidal suspensions. In this approximation the mean field potential is linearised about a constant value. This approximation is good as long as deviations from this constant potential are not too large throughout the system. This will be the case if the charge carried by the macroions $|Z|$ is not very large, and if the distance between them is small compared to the Debye screening length λ_D. These situations give rise to mean field potentials and density distributions with comparatively small spatial inhomogeneities.

As discussed in Chapter 4, phase coexistence is typically observed for very dilute suspensions of highly charged macroionic particles with $|Z| \sim 10^3 - 10^4$, containing a low density of salt. The diluteness means that even the 'high density' phase has a packing fraction that is typically no higher than $\phi \sim 0.1$. This packing fraction corresponds to a macroion separation of approximately 4 macroion radii a. The low salt density on the other hand means that λ_D may be large. However, even in the low salt density regime the salt density is of the order of a few μM, corresponding to screening lengths of the order of $\lambda_D \sim 300\text{nm}/\sqrt{n_s}$ (where the salt concentration n_s has units of μM). This means that for particles with $a = 100\text{nm}$, even a $1\mu M$ salt concentration will give rise to screening lengths that are smaller than the macroion spacings. In the low density phase of a phase separated suspension the macroion spacings will correspond to many screening lengths.

This suggests that in the regime in which colloidal suspensions phase separate, spatial inhomogeneities in $\rho(\mathbf{r})$ and $\Phi(\mathbf{r})$ are expected to be large, and the D-H approximation is expected to fail. This has caused several authors [86, 96, 87] to call into question conclusions drawn from theoretical treatments based on the linearised PB equation [80, 22, 82, 83, 68].

The approximations underlying the primitive model and mean field treatment are pushed hardest

when $|Z|$ is large and λ_D is small. The high density of microions in these situations means that microion correlations (neglected in the mean field approximation) and solvent effects (neglected in the PM approximations) become important. Nevertheless, several authors have produced theoretical phase diagrams based on the linearised PB equation, displaying coexistence in this regime. It is important to establish whether this is a result of the failure of the D-H linearisation approximation, or whether such coexistence is inherent in the mean field theory of colloidal suspensions.

Here we propose a new linearisation based on the use of a superposition of mean field potentials for isolated macroions as a reference potential. This linearisation is expected to be successful for dilute suspensions for which η_F is small, and the macroionic separations are large compared to the screening length λ_D.

6.2 New linearisation scheme

6.2.1 Charge neutral sectors

We focus on the limit of a dilute colloidal suspension where the macroion density η_F is small, and the spacing between the fixed macroions at positions $\{\mathbf{R}_n\}$ is large in comparison with the Debye screening length λ_D. Although the presence of salt is important in this limit as it has the effect of decreasing the screening length, the equations will be derived for a salt-free suspension for clarity. As discussed in Chapter 5, the optimising mean field distribution of microions is expected to give rise to regions that are charge neutral on the length scale of the macroionic spacings. Anticipating that the most likely solution to the mean field equations is one that creates charge neutral regions, we proceed with the mean field treatment of the dilute colloidal suspension by splitting it into N charge neutral sectors, one for each macroion labelled n. We choose the macroion labelled as $n = 1$ to be centred at the origin. Each sector is a charge neutral volume with a macroion centred at $\mathbf{R}_n$ along with neutralising microions. For the idealised salt-free case, each sector contains $|Z|$ counterions. For each sector n we define the distribution of microions $\rho_n(\mathbf{r})$ within that sector

$$\rho(\mathbf{r}) = \rho_n(\mathbf{r}) \qquad \text{if} \quad \mathbf{r} \quad \in \quad \mathrm{S_n} \tag{6.1}$$

where S_n defines the space containing all points in the nth sector. For a salt-free system containing N macroions in total, overall normalisation dictates

$$\int_{\text{all S}} \rho(\mathbf{r}) d\mathbf{r} = N|Z| \tag{6.2}$$

and charge neutrality of each sector requires

$$\int_{\mathrm{S_n}} \rho_n(\mathbf{r}) d\mathbf{r} = |Z| \qquad \forall \quad \mathrm{n} \tag{6.3}$$

In a similar vein we denote the part of the total macroion charge distribution $n_F(\mathbf{r})$ that lies in the nth sector by $n_n(\mathbf{r})$. Since all of the macroions are identical we may say $n_n(\mathbf{r}) = n_1(\mathbf{r} - \mathbf{R}_n)$, where $n_1(\mathbf{r})$ is the charge distribution for a macroion centred at the origin, and $\mathbf{R}_n$ is the position vector to the centre of the nth cell.

Now the free energy functional $F_M[\rho(\mathbf{r})]$ in (5.24) is split up into contributions from within each

cell S_n and the inter-cell interaction energy.

$$F_M[\rho(\mathbf{r})] = \sum_n \int_{S_n} \rho_n(\mathbf{r}) \left[(\ln \rho_n(\mathbf{r})\lambda^3 - 1) + \frac{1}{2}\int_{S_n} \rho_n(\mathbf{r}')G(\mathbf{r}-\mathbf{r}')d\mathbf{r}' + \int_{S_n} n_n(\mathbf{r}')G(\mathbf{r}-\mathbf{r}')d\mathbf{r}' \right] d\mathbf{r}$$
$$+ \sum_n \sum_{m\neq n} \int_{S_n} \rho_n(\mathbf{r}) \left[\frac{1}{2}\int_{S_m} \rho_m(\mathbf{r}')G(\mathbf{r}-\mathbf{r}')d\mathbf{r}' + \int_{S_m} n_m(\mathbf{r}')G(\mathbf{r}-\mathbf{r}')d\mathbf{r}' \right] d\mathbf{r} \tag{6.4}$$

In more compact notation

$$F_M = \sum_n F_{Mn} + \sum_n \sum_{m\neq n} U_{nm} \tag{6.5}$$

Taking the functional derivative of F_M with respect to the microion distribution in the nth cell gives the equation for the optimising $\rho_n(\mathbf{r})$ within S_n

$$\rho_n(\mathbf{r}) = \frac{1}{\lambda^3} \exp\Big[\mu - \int_{S_n} \rho_n(\mathbf{r}')G(\mathbf{r}'-\mathbf{r})d\mathbf{r}' - \int_{S_n} n_n(\mathbf{r}')G(\mathbf{r}'-\mathbf{r})d\mathbf{r}'$$
$$- \sum_{m\neq n} \left(\int_{S_m} \rho_m(\mathbf{r}')G(\mathbf{r}'-\mathbf{r})d\mathbf{r}' + \int_{S_m} n_m(\mathbf{r}')G(\mathbf{r}'-\mathbf{r})d\mathbf{r}' \right) \Big] \tag{6.6}$$

The inter-cell interactions couple the mean field equations for the N sectors. As a result, the optimal ρ_n in sector n depends on the ρ_m in every other sector.

We define $\Phi_n(\mathbf{r})$ to be the electrostatic potential due to the total charge distribution inside the nth sector. It is important to note that while $\rho_n(\mathbf{r})$ is defined for $\mathbf{r}$ in S_n, $\Phi_n(\mathbf{r})$ is defined as the potential at $\mathbf{r}$ in any sector anywhere in the system, due to charge in the nth sector. The corresponding Poisson-Boltzmann equation is

$$\nabla^2\Phi_n(\mathbf{r}) = -4\pi l_B \left(n_0 \exp\left[-\Phi_n(\mathbf{r}) - \sum_{m\neq n} \Phi_m(\mathbf{r}) \right] + n_1(\mathbf{r}-\mathbf{R}_n) \right) \tag{6.7}$$

where the normalisation constant to ensure the correct number of microions is $n_0 = \exp(\mu)/\lambda^3$. The second derivative $\nabla^2\Phi_n(\mathbf{r})$ is related to the total (macroionic and microionic) charge density in the nth cell through

$$\nabla^2\Phi_n(\mathbf{r}) = -4\pi l_B \left(\rho_n(\mathbf{r}) + n_1(\mathbf{r}-\mathbf{R}_n)\right) \tag{6.8}$$

Even if $\Phi_n(\mathbf{r})$ is nonzero beyond S_n, the charge density $\nabla^2\Phi_n(\mathbf{r}) = 0$ if r is not in S_n.

6.2.2 Symmetry and periodicity: Wigner-Seitz cells

If the identical macroions are positioned at lattice sites, the macroionic charge distribution will have the translational property $n_m(\mathbf{r}) = n_n(\mathbf{r}-\mathbf{R}_{nm})$, where $\mathbf{R}_{nm}$ is a translation vector from the centre of the nth cell to the centre of the mth cell.

If the approximation is made that the microionic mean field takes the same symmetry as the field due to the fixed macroions, then the mean field potential in each charge neutral sector will be equivalent. In this case the charge neutral sectors correspond to Wigner-Seitz cells discussed in Section 5.5. The microionic charge distribution then possess the periodicity property $\rho_m(\mathbf{r}) = \rho_n(\mathbf{r}-\mathbf{R}_{nm})$. With this assumption, Equation (6.6) becomes

$$\lambda^3\rho_n(\mathbf{r}) = \exp\Big[\mu - \int_{S_n} \rho_n(\mathbf{r}')G(\mathbf{r}'-\mathbf{r})d\mathbf{r}' - \int_{S_n} n_n(\mathbf{r}')G(\mathbf{r}'-\mathbf{r})d\mathbf{r}'$$
$$- \sum_{m\neq n} \left(\int_{S_m} \rho_n(\mathbf{r}'-\mathbf{R}_{nm})G(\mathbf{r}'-\mathbf{r})d\mathbf{r}' + \int_{S_m} n_n(\mathbf{r}'-\mathbf{R}_{nm})G(\mathbf{r}'-\mathbf{r})d\mathbf{r}' \right) \Big] \tag{6.9}$$

Alternatively all of the integrals may be performed over a single W-S cell S_n as follows

$$\lambda^3\rho_n(\mathbf{r}) = \exp\Big[\mu - \int_{S_n}\rho_n(\mathbf{r}')G(\mathbf{r}'-\mathbf{r})d\mathbf{r}' - \int_{S_n} n_n(\mathbf{r}')G(\mathbf{r}'-\mathbf{r})d\mathbf{r}' \\ - \sum_{m\neq n}\left(\int_{S_n}\rho_n(\mathbf{r}')G(\mathbf{r}'+\mathbf{R}_{nm}-\mathbf{r})d\mathbf{r}' + \int_{S_n} n_n(\mathbf{r}')G(\mathbf{r}'+\mathbf{R}_{nm}-\mathbf{r})d\mathbf{r}'\right)\Big] \tag{6.10}$$

This is a reassertion of the fact that the W-S cell approximation reduces the multi-cell problem to a single cell problem with appropriate boundary conditions. Equation (6.10) may be re-written as

$$\lambda^3\rho_n(\mathbf{r}) = \exp\left[\mu - \int_{S_n}\rho_n(\mathbf{r}')G_g(\mathbf{r}'-\mathbf{r})d\mathbf{r}' - \int_{S_n} n_n(\mathbf{r}')G_g(\mathbf{r}'-\mathbf{r})d\mathbf{r}'\right] \tag{6.11}$$

where the generalised Green's function $G_g(\mathbf{r}-\mathbf{r}')$ is

$$G_g(\mathbf{r}'-\mathbf{r}) = G(\mathbf{r}'-\mathbf{r}) + \sum_m G(\mathbf{r}'+\mathbf{R}_{nm}-\mathbf{r}) \tag{6.12}$$

The generalised Green's function [94] contains one component to account for charge within the cell, and a second component representing charge outside the W-S cell. The second component, which satisfies the Laplace equation inside the cell, imposes the required conditions on the W-S cell boundary to account for all of the surrounding cells. This is the same approach that underlies the method of images for the electrostatic potential near conducting surfaces.

6.2.3 Infinitely dilute suspension: the isolated macroion

When $\eta_F \to 0$ each sector becomes infinite in extent, and the interaction between sectors vanishes. The free energy then consists of independent contributions

$$F_M = \sum_n F_{Mn} \tag{6.13}$$

Each F_{Mn} is equivalent, and for the infinite sector centred at the origin F_{M1} is given by

$$F_{M1}[\rho_1(\mathbf{r})] = \int \rho_1(\mathbf{r})\left[(\ln\rho_1(\mathbf{r})\lambda^3 - 1) + \frac{1}{2}\int\rho_1(\mathbf{r}')G(\mathbf{r}-\mathbf{r}')d\mathbf{r}' + \int n_1(\mathbf{r}')G(\mathbf{r}-\mathbf{r}')d\mathbf{r}'\right]d\mathbf{r} \tag{6.14}$$

where the integrals extend over all space, reflecting the infinite volume of the sectors in this limit. The optimal profile, denoted $\rho_1^{(0)}(\mathbf{r})$ in this limit, satisfies

$$\lambda^3\rho_1^{(0)}(\mathbf{r}) = \exp\left[\mu - \int\rho_1^{(0)}(\mathbf{r}')G(\mathbf{r}-\mathbf{r}')d\mathbf{r}' - \int n_1(\mathbf{r}')G(\mathbf{r}-\mathbf{r}')d\mathbf{r}'\right] \tag{6.15}$$

The corresponding Poisson-Boltzmann equation is

$$\nabla^2\Phi_1^{(0)}(\mathbf{r}) = -4\pi l_B\left(n_0\exp\left[-\Phi_1^{(0)}(\mathbf{r})\right] + n_1(\mathbf{r})\right) \tag{6.16}$$

Since the macroions are spherical and possess a uniform surface charge density σ, the distribution of microions $\rho(\mathbf{r})$ and mean field potential $\Phi(\mathbf{r})$ in the infinite-dilution limit are expected to be spherically symmetric. The boundary conditions on the mean field potential for the cell centred at the origin $\Phi_1^{(0)}(r)$ are

$$\left.\frac{d\Phi_1^{(0)}}{dr}\right|_{r=a} = -4\pi l_B\sigma \tag{6.17}$$

and

$$\left.\frac{d\Phi_1^{(0)}}{dr}\right|_{r\to\infty} = 0 \tag{6.18}$$

As discussed in Chapter 5 the constant $n_0 = \exp(\mu)/\lambda^3$ is related to the charge neutrality condition and to the constraint on salt ions in the system. In the hypothetical salt-free case, μ can be chosen in order to set a desired zero for the potential $\Phi(\mathbf{r})$. Since the number of counterions in the salt-free case is finite $|Z|$, the concentration of counterions far away from the macroion in an isolated system must tend to zero. This requires either $\Phi(r) \to \infty$ as $r \to \infty$, or alternatively $\mu \to -\infty$ as the volume per macroion tends to infinity, allowing for the choice $\Phi(r) \to 0$ as $r \to \infty$ which is more convenient. For an open system in contact with a salt bath, the density far away from an isolated macroion will tend to the salt bath density n_b.

6.2.4 Approximate solutions for dilute suspensions

We will now focus on finding approximate solutions to equation (6.10) for situations in which the macroionic density is low, so that the cells are very large, and the density profiles ρ_n resemble those for completely isolated macroions in effectively infinite cells $\rho_n^{(0)}$.

The crudest approximation in this regime is to solve (6.15) for a single, isolated macroion (in an infinite volume) and use the resulting distribution function $\rho_1^{(0)}(\mathbf{r})$ to estimate the free energy of a system with finite cells. This would be done by plugging $\rho_1^{(0)}(r)$ into the free energy functional (6.4), where the integration limits for each sector extend only over the finite cell volumes S_n

$$F_M \approx \sum_n F_n[\rho_n^{(0)}(r)] + \sum_n \sum_{m\neq n} \langle U_{nm}\rangle_{(0)} \tag{6.19}$$

where $\rho_n^{(0)}(r) = \rho_1^{(0)}(|\mathbf{r} - \mathbf{R}_n|)$. We do not expect this isolated-cell approximation to be very successful even for relatively low macroion densities. One deficiency is that the normal derivative of $\Phi_n^{(0)}$ at the nth cell boundary will not be zero unless the cell volume is infinite, whereas an exact solution to (6.10) possesses zero field perpendicular to the cell boundaries. In addition to this, the charge neutrality condition for the cells would be violated, as the neutralising charge in $\rho_n^{(0)}$ extends over all space.

To improve on this approximation, the isolated-cell solution $\rho_n^{(0)}(\mathbf{r})$ is inserted into equation (6.6). This can be thought of as the next iteration of the self-consistent field procedure for solving the mean field equations. The resulting density profile is given by

$$\begin{aligned}\lambda^3\rho_n^{(1)}(\mathbf{r}) = \exp\Big[\mu &- \int\rho_n^{(0)}(\mathbf{r}')G(\mathbf{r}'-\mathbf{r})d\mathbf{r}' - \int n_n(\mathbf{r}')G(\mathbf{r}'-\mathbf{r})d\mathbf{r}' \\ &- \sum_{m\neq n}\left(\int\rho_m^{(0)}(\mathbf{r}')G(\mathbf{r}'-\mathbf{r})d\mathbf{r}' + \int n_m(\mathbf{r}')G(\mathbf{r}'-\mathbf{r})d\mathbf{r}'\right)\Big]\end{aligned} \tag{6.20}$$

where the integrals extend over all space. The exponent corresponds to a superposition of mean field potentials, each satisfying the Poisson-Boltzmann equation for an isolated macroion in infinite cell centred at different $\mathbf{R}_n$. Writing the exponent in terms of potentials (6.20) can be re-written as

$$\lambda^3\rho_n^{(1)}(\mathbf{r}) = \exp\left[\mu - \Phi_n^{(0)}(\mathbf{r}) - \sum_{m\neq n}\Phi_m^{(0)}(\mathbf{r})\right] \tag{6.21}$$

Unlike $\rho_n^{(0)}(\mathbf{r})$, the charge distribution $\rho_n^{(1)}(\mathbf{r})$ is not spherically symmetric, but possesses the symmetry and periodicity of the underlying macroionic lattice. This is also true for superposition of potentials in the exponent. As a result, the perpendicular gradient of the superposition of potentials at the W-S

cell boundary is zero, even when the cells are finite.

6.2.5 Linearisation scheme in the dilute limit

Although $\rho_n^{(1)}$ is not a solution to the self-consistent mean field equation (6.6), it serves as a good reference distribution about which to linearise the free energy functional for a dilute suspension. A linearisation of the optimal density profile in

$$\Delta(\mathbf{r}) = \rho(\mathbf{r}) - \rho^{(1)}(\mathbf{r}) \tag{6.22}$$

is related to a linearisation of the mean field potential in

$$\epsilon(\mathbf{r}) = \Phi(\mathbf{r}) - \sum_n \Phi_n^{(0)}(\mathbf{r}) \tag{6.23}$$

in the Poisson-Boltzmann approach. Note that this ϵ is not the dielectric permittivity.

Differential equation approach

Substituting $\Phi(\mathbf{r})$ from (6.23) into the PB equation gives

$$\sum_n \nabla^2 \Phi_n^{(0)}(\mathbf{r}) + \nabla^2 \epsilon(\mathbf{r}) = -4\pi l_B \left(\frac{1}{\lambda^3} \exp\left[\mu - \sum_n \Phi_n^{(0)}(\mathbf{r}) - \epsilon(\mathbf{r}) \right] + n_F(\mathbf{r}) \right) \tag{6.24}$$

In the dilute suspension limit, the sectors are large, and the deviation ϵ will be small, so the exponential in (6.24) can be linearised about the superposition of potentials.

$$\sum_n \nabla^2 \Phi_n^{(0)}(\mathbf{r}) + \nabla^2 \epsilon(\mathbf{r}) = -4\pi l_B \left(\frac{1}{\lambda^3} \Big(1 - \epsilon(\mathbf{r}) \Big) \exp\left[\mu - \sum_n \Phi_n^{(0)}(\mathbf{r}) \right] + n_F(\mathbf{r}) \right) \tag{6.25}$$

which is a linear differential equation for $\epsilon(\mathbf{r})$. The deviation of the exact microionic charge density from the superposition of charge densities from the isolated solutions $\rho_n^{(0)}$ is defined by

$$\nabla^2 \epsilon(\mathbf{r}) = -4\pi l_B \Delta\rho(\mathbf{r}) \tag{6.26}$$

or equivalently

$$\Delta\rho(\mathbf{r}) = \rho(\mathbf{r}) - \rho_s(\mathbf{r}) \tag{6.27}$$

where ρ_s is defined as the superposition of microionic charge densities from the isolated solutions

$$\rho_s(\mathbf{r}) = \sum_n \rho_n^{(0)}(\mathbf{r}) \tag{6.28}$$

Microionic and macroionic contributions to the potential and charge density

The isolated solutions $\Phi_n^{(0)}$ may be decomposed into a macroionic $\Phi_{Fn}^{(0)}$ and a microionic $\Phi_{Mn}^{(0)}$ portion, giving rise to macroionic n_{Fn} and microionic charge densities $\rho_n^{(0)}$ for isolated systems centred at $\{\mathbf{R}_n\}$. These two portions satisfy the equations

$$\nabla^2 \Phi_{Fn}^{(0)} = -4\pi l_B n_1(\mathbf{r} - \mathbf{R}_n) \tag{6.29}$$

and

$$\nabla^2 \Phi_{Mn}^{(0)} = -4\pi l_B \rho_n^{(0)}(\mathbf{r}) \tag{6.30}$$

in the regions containing macroions and microions respectively. The macroionic charge distribution is contained in the solution for isolated systems through the boundary condition (6.17) at the macroion surface. The charge distribution $n_{Fn}(\mathbf{r})$ corresponds to the uniform surface charge on the macroions σ, which is assumed not to be altered by the presence of other macroions in a finite-volume system. So it is only the microionic portion of the charge distribution which needs to be altered in the description of a finite density system.

The charge density ρ_s refers only to the superposition of microionic contributions, and may be written as

$$\rho_s(\mathbf{r}) = -4\pi l_B \sum_n \nabla^2 \Phi_n^{(0)}(\mathbf{r}) - n_F(\mathbf{r}) \tag{6.31}$$

Note that while the exact charge density for sector n and therefore $\nabla^2\Phi_n = -4\pi l_B \rho_n$ is zero outside of S_n, the charge densities for infinite sectors $\nabla^2\Phi_n^{(0)} = -4\pi l_B \rho_n^{(0)}$ are non-zero beyond their respective S_n, since the isolated solution extends over all space.

Integral equation approach

It is tempting to say that the linearisation carried out about the superposition of potentials in $\epsilon(\mathbf{r})$ is equivalent to a linearisation in the density profile deviation $\Delta\rho(\mathbf{r})$ defined in (6.27). Actually the linearisation is equivalent to a linearisation in the density deviation $\Delta(\mathbf{r})$ defined in (6.22). This linearisation is consistent with an expansion of the free energy functional $F_M[\rho^{(1)} + \Delta]$ to second order in $\Delta(\mathbf{r})/\rho^{(1)}(\mathbf{r})$.

$$\begin{aligned} F_M[\rho^{(1)}(\mathbf{r}) + \Delta(\mathbf{r})] \simeq & \int \rho^{(1)}(\mathbf{r}) \left[\ln\left(\rho^{(1)}(\mathbf{r})\lambda^3\right) - 1\right] d\mathbf{r} + \int \ln\left(\rho^{(1)}(\mathbf{r})\lambda^3\right) \Delta(\mathbf{r}) d\mathbf{r} + \frac{1}{2}\int \frac{\Delta^2(\mathbf{r})}{\rho^{(1)}(\mathbf{r})} d\mathbf{r} \\ & + \frac{1}{2}\int\int \left(\rho^{(1)}(\mathbf{r}) + \Delta(\mathbf{r})\right)\left(\rho^{(1)}(\mathbf{r}) + \Delta(\mathbf{r}')\right) G(\mathbf{r}-\mathbf{r}') d\mathbf{r}' d\mathbf{r} + \\ & \int d\mathbf{r} \left(\rho^{(1)}(\mathbf{r}) + \Delta(\mathbf{r})\right) \Phi_F(\mathbf{r}) + O\left(\Delta/\rho^{(1)}\right)^3 \end{aligned} \tag{6.32}$$

To find the optimising profile, the functional derivative with respect to $\Delta(\mathbf{r})$ is taken. The constraint

$$\int \left[\Delta(\mathbf{r}) + \rho^{(1)}(\mathbf{r})\right] d\mathbf{r} + Z = 0 \tag{6.33}$$

is imposed by introducing a Lagrange multiplier γ. Adding $\rho^{(1)}(\mathbf{r})$ to the equation for the optimising $\Delta(\mathbf{r})$ results in a linear integral equation for optimising profile $\rho(\mathbf{r}) = \rho^{(1)}(\mathbf{r}) + \Delta(\mathbf{r})$

$$\rho^{(1)}(\mathbf{r}) + \Delta(\mathbf{r}) = \rho^{(1)}(\mathbf{r}) \left[1 + \gamma - \ln\rho^{(1)}(\mathbf{r})\lambda^3 - \int \left(\rho^{(1)}(\mathbf{r}) + \Delta(\mathbf{r}')\right) G(\mathbf{r}-\mathbf{r}') d\mathbf{r}' - \Phi_F(\mathbf{r})\right] \tag{6.34}$$

To show that is equivalent to the PB expansion in (6.25), we substitute $\rho = \rho^{(1)} + \Delta = \rho_s + \Delta\rho$ into (6.34). Since

$$\sum_n \Phi_n^{(0)}(\mathbf{r}) = \int \rho_s(\mathbf{r}') G(\mathbf{r}-\mathbf{r}') d\mathbf{r}' + \sum_n \Phi_{Fn}(\mathbf{r}) \tag{6.35}$$

and

$$\epsilon(\mathbf{r}) = \int \Delta\rho(\mathbf{r}') G(\mathbf{r}-\mathbf{r}') d\mathbf{r}' \tag{6.36}$$

cancellations occur between the logarithmic term and the integral involving ρ_s, so that in terms of $\Delta\rho$ and ρ_s Equation (6.34) becomes

$$\rho_s(\mathbf{r}) + \Delta\rho(\mathbf{r}) = \rho^{(1)}(\mathbf{r}) \left[1 + \gamma - \mu - \epsilon(\mathbf{r})\right] \tag{6.37}$$

which is the same as the microionic portion of Equation (6.25) if the constant $\mu - \gamma$ is absorbed into $\epsilon(\mathbf{r})$.

6.2.6 Charge neutrality and boundary conditions

The PB equation (6.25) must give rise to charge neutral cells. In the cell labelled $n = 1$, the only source of macroionic charge is $n_F = n_1(\mathbf{r})$. This is correctly contained in the total electrostatic potential for the isolated system centred at the origin $\Phi_1^{(0)}(\mathbf{r})$. Since the macroions corresponding to isolated potentials centred at the other cells $\Phi_n^{(0)}$ do not lie anywhere within S_1, writing the PB equation in terms of microionic and macroionic contributions to the charge density gives

$$\nabla^2\Phi_{F1}^{(0)}+\nabla^2\Phi_{M1}^{(0)}+\sum_{n\neq 1}\nabla^2\Phi_{Mn}^{(0)}+\nabla^2\epsilon = -4\pi l_B\frac{1}{\lambda^3}\exp\left[\mu-\sum_n\Phi_n^{(0)}(\mathbf{r})\right]\Big(1-\epsilon(\mathbf{r})\Big)-4\pi l_B n_{F1} \quad (6.38)$$

Since the macroion charge density in cell $n = 1$ is

$$\nabla^2\Phi_{F1}^{(0)} = -4\pi l_B n_{F1} \quad (6.39)$$

the macroionic terms cancel, leaving an equation for the microionic charge densities

$$\nabla^2\Phi_{M1}^{(0)}+\sum_{n\neq 1}\nabla^2\Phi_{Mn}^{(0)}+\nabla^2\epsilon = -4\pi l_B\frac{1}{\lambda^3}\exp\left[\mu-\sum_n\Phi_n^{(0)}(\mathbf{r})\right]\Big(1-\epsilon(\mathbf{r})\Big) \quad (6.40)$$

The mean field potential for an isolated system with a macroion centred at the origin $\Phi_1^{(0)}(\mathbf{r})$ gives rise to a neutralising microion distribution over an infinite volume

$$\int\rho_1^{(0)}(\mathbf{r})d\mathbf{r} = -Z \quad (6.41)$$

where the integral is over all space. An integral over the finite volume corresponding to the $n = 1$ cell volume S_n results in a deficient number of counterions, leading to a non-neutral cell.

However if we take the finite cell $n = 1$ and look at the function $\rho_s(\mathbf{r})$ i.e. the superposition of microionic charge densities from isolated solutions centred at lattice sites of an infinite lattice, we see that the tails of all $n \neq 1$ charge distributions penetrate the $n = 1$ cell and compensate for the deficiency

$$\int\rho_1^{(0)}(\mathbf{r})d\mathbf{r} = \int_{S_1}\sum_n\rho_n^{(0)}(\mathbf{r})d\mathbf{r} = -Z \quad (6.42)$$

Microions cannot penetrate the interiors of the colloidal particles, so the true solution must have $\nabla^2\Phi = 0$ inside the colloidal sphere centred at the origin. The system is split up into the inner region R_i comprising the inner volume of the colloidal particle, and the outer region R_o comprising the rest of the W-S cell. The linearised PB equation (6.40) is satisfied in R_o for dilute suspensions, but in the inner region R_i we require

$$\nabla^2\epsilon = -\sum_n\nabla^2\Phi_{Mn}^{(0)} \quad \text{in} \quad R_i \quad (6.43)$$

The exclusion of charge density in the inner volume R_i through (6.43) means that the superposition of charge densities ρ_s will no longer be sufficient to neutralise the W-S cell as in Equation (6.42). If the amount of charge 'removed' from the inner volume is Q_i, then

$$-4\pi l_B Q_i = \int_{R_i}\nabla^2\epsilon d\mathbf{r} = -\int_{R_i}\sum_n\nabla^2\Phi_n^{(0)}d\mathbf{r} \quad (6.44)$$

the deviation $\nabla^2\epsilon = -4\pi l_B\Delta\rho$ needs to account for this amount of microion charge to neutralise the

W-S cell in the outer region. The amount of charge represented by ϵ in the outer region Q_o is given by

$$-4\pi l_B Q_o = \int_{R_o} \nabla^2 \epsilon d\mathbf{r} = + \int_{R_i} \sum_n \nabla^2 \Phi_n^{(0)} d\mathbf{r} \tag{6.45}$$

The total amount of charge represented by ϵ over both regions adds up to zero so $Q_o + Q_i = 0$

An equivalent statement of this condition is that the superposition of potentials satisfies

$$\sum_n \nabla \Phi_n^{(0)} \cdot \mathbf{n} = 0 \tag{6.46}$$

on the W-S cell boundary. This is a result of symmetry, periodicity of the superposition of potentials and the charge neutrality of the respective superposition of charge densities within each cell. Since the exact solution of the PB equation also satisfies the condition $\nabla\Phi \cdot \mathbf{n} = 0$ on the cubic boundary, it must be true that $\nabla\epsilon \cdot \mathbf{n} = 0$ on the boundary. This is a restatement of the fact that $\epsilon(\mathbf{r})$ possesses the symmetry and periodicity of the lattice, and that the total amount of charge described by $\nabla^2\epsilon = -4\pi l_B \Delta\rho$ in one cell, including the inner region, is zero.

6.2.7 System at equilibrium with a salt reservoir

The formalism for the new linearisation scheme was developed in the previous two sections for a salt-free system for simplicity. Here we adapt the equations to apply to a system that is open with respect to a salt reservoir containing positive and negative microions. Salt is particularly important in the regime of interest here, since a higher concentration of microions enhances screening causing a reduction of the screening length λ_D. In practice, an open system is simpler to handle than the finite salt or zero salt case since the depletion of the total amount of salt complicates solution of the PB equations, due to the additional inter-dependence between the Lagrange multiplier μ and the mean field potential Φ. As discussed in Chapter 5, for a system in contact with a salt-reservoir this Lagrange multiplier is replaced by the chemical potential of ions in the bath μ_b which is constant with respect to changes in the system. An additional complication that is avoided in the salt bath system is the divergence of either μ or Φ as the system becomes infinite, as discussed at the end of section 6.2.3.

The salt bath can be thought of an ideal gas containing a uniform density n_b of positive and negative microions. The total density of microions in the charge neutral salt bath will be $2n_b$. The chemical potential of positive and negative microions in the reservoir is fixed at $\mu_b = \ln n_b \lambda^3$ (if the masses of the two species are assumed to be the same, they share the same de Broglie wavelength λ). As the volume per macroion in the system V_W becomes large, the density of both positive and negative microions far away from any macroions tends to n_b, which is the density of both species inside the bath. The zero of the electrostatic potential Φ will be chosen to tend to zero at the W-S cell boundary as the volume per macroion V_W becomes large or $\eta_f \to 0$.

Differential equation approach

The linearisation follows the same principle as for the salt-free case. The mean field potential is linearised in $\epsilon(\mathbf{r})$ about the superposition of isolated potentials. The isolated system with a macroion centred at the origin satisfies the differential equation

$$\nabla^2 \Phi_1^{(0)} = 8\pi n_b l_B \sinh \Phi_1^{(0)}(\mathbf{r}) - 4\pi l_B n_1(\mathbf{r}) \tag{6.47}$$

subject to the same boundary conditions as for the salt free case (6.17) and (6.18).

We introduce shorthand notation for the superposition of potentials

$$S(\mathbf{r}) = \sum_n \Phi_n^{(0)}(\mathbf{r}) \tag{6.48}$$

$\Phi = S + \epsilon$ is substituted into the PB equation

$$\nabla^2 S + \nabla^2 \epsilon = 8\pi l_B n_b \sinh(S(\mathbf{r}) + \epsilon(\mathbf{r})) - 4\pi l_B n_F(\mathbf{r}) \tag{6.49}$$

where $n_b = \exp(\mu_b)/\lambda^3$, and μ_b is the chemical potential of positive and negative microions in the salt bath. If the spacing between macroions is large, the W-S cells become large, and the deviation from $S(\mathbf{r})$ will be small. Linearising the PB equation in ϵ gives

$$\nabla^2 S + \nabla^2 \epsilon \simeq 8\pi l_B n_b \Big(\sinh S(\mathbf{r}) + \epsilon(\mathbf{r}) \cosh S(\mathbf{r}) \Big) - 4\pi l_B n_F(\mathbf{r}) \tag{6.50}$$

Which is a linear differential equation for $\epsilon(\mathbf{r})$ in terms of the functions $\Phi_n^{(0)}$.

Integral equation approach

As was the case for a salt-free system, it can be shown that this is equivalent to a linearisation about a charge density distribution $\rho^{(1)} = \rho_+^{(1)} - \rho_-^{(1)}$. For a system open with respect to a salt reservoir, this is obtained from an expansion to second order of the microion grand potential $\Omega_M(\mu_b, V, T)$ in the deviations $\Delta_\pm = \rho_\pm - \rho_\pm^{(1)}$.

$$\begin{aligned}\Omega = \sum_{i=+,-} \Bigg[& \int \rho_i^{(1)}(\mathbf{r}) \left[\ln\left(\rho_i^{(1)}(\mathbf{r})/n_b\right) - 1 \right] d\mathbf{r} + \int \ln\left(\rho_i^{(1)}(\mathbf{r})/n_b\right) \Delta_i(\mathbf{r}) d\mathbf{r} + \frac{1}{2} \int \frac{\Delta_i^2(\mathbf{r})}{\rho_i^{(1)}} d\mathbf{r} \Bigg] \\ & + \frac{1}{2} \int\int \Big(\rho^{(1)}(\mathbf{r}) + \Delta(\mathbf{r})\Big) \Big(\rho^{(1)}(\mathbf{r}') + \Delta(\mathbf{r}')\Big) G(\mathbf{r} - \mathbf{r}') d\mathbf{r}' d\mathbf{r} \\ & + \int\int \Big(\rho^{(1)}(\mathbf{r}) + \Delta(\mathbf{r})\Big) n_F(\mathbf{r}') d\mathbf{r}' d\mathbf{r} + O(\Delta_\pm/\rho_\pm^{(1)})^3\end{aligned} \tag{6.51}$$

Taking functional derivatives with respect to $\Delta_\pm$ and setting them to zero, we obtain the optimising functions

$$\Delta_\pm(\mathbf{r}) = \rho_\pm^{(1)} \left[-\ln\left(\rho_\pm^{(1)}/n_b\right) \mp \int \Big(\rho^{(1)}(\mathbf{r}') + \Delta(\mathbf{r}')\Big) G(\mathbf{r} - \mathbf{r}') d\mathbf{r}' \mp \Phi_F(\mathbf{r}) \pm \mu_{el} \right] \tag{6.52}$$

These equations are coupled together through the charge density $\Delta = \Delta_+ - \Delta_-$. Substituting the quantities $\rho = \rho^{(1)} + \Delta = \rho_s + \Delta\rho$, we get the equation

$$\rho_s + \Delta\rho = \rho^{(1)} - \left(\rho_+^{(1)} + \rho_-^{(1)}\right) \left[\int \Delta\rho(\mathbf{r}') G(\mathbf{r} - \mathbf{r}') d\mathbf{r}' - \mu_{el} \right] \tag{6.53}$$

or

$$\rho_s + \Delta\rho = \rho^{(1)} - \left(\rho_+^{(1)} + \rho_-^{(1)}\right) (\epsilon(\mathbf{r}) - \mu_{el}) \tag{6.54}$$

which is the same as the microionic portion of (6.50) when μ_{el} is absorbed into $\epsilon(\mathbf{r})$.

6.2.8 Constant contribution to the reference potential

To improve the linearisation scheme, the reference potential $S(\mathbf{r})$ is altered to $S(\mathbf{r}) - \mu_{el}^{(1)}$, by the introduction of a constant $\mu_{el}^{(1)}$, making $\epsilon(\mathbf{r}) = \Phi(\mathbf{r}) - S(\mathbf{r}) + \mu_{el}^{(1)}$. This constant is chosen in an attempt to eliminate constant contributions to $\epsilon(\mathbf{r})$, making the linearisation more effective. This will be particularly important for colloidal suspensions at higher density, when the mean field potential

is relatively flat and a large constant correction to $S(\mathbf{r})$ will be required. The constant $\mu_{el}^{(1)}$ is chosen to satisfy

$$\int 2n_b \sinh(S(\mathbf{r}) - \mu_{el}^{(1)}) d\mathbf{r} = Z \tag{6.55}$$

In other words, this makes the reference charge density $\rho^{(1)}(\mathbf{r})$ contain the full amount of microionic charge. This has the consequence that $\epsilon(\mathbf{r})$ satisfies

$$\int \epsilon(\mathbf{r}) \cosh(S(\mathbf{r}) - \mu_{el}^{(1)}) d\mathbf{r} = 0 \tag{6.56}$$

The boundary conditions on $\epsilon(\mathbf{r})$, which are related to the charge neutrality condition, are unaffected by the introduction of this constant.

In the next two chapters the new linearisation approach outlined here will be applied to two systems and compared to results obtained from the traditional linearisation schemes. In Chapter 7 the PB equation is solved for the one-dimensional problem of charged plates in an electrolyte and in Chapter 8 it is solved for arrays of spherical colloidal particles.

Chapter 7

The planar geometry: charged parallel plates

7.1 One-dimensional colloids

A simplified model for colloidal suspensions arises when the colloidal 'particles' take the form of charged plates. Arrays or stacks of charged plates aligned in parallel have been used as models for various clays and gels [42, 97], and Poisson-Boltzmann theory has been used to attempt to explain the stability and swelling behaviour of these materials. It has been argued [98, 99, 100, 101, 102] that the electrostatic component of the effective interaction between such plates, calculated within mean field theory, gives rise to an effective attraction between the plates that reproduces the behaviour of these systems under experimental conditions. There has been significant controversy surrounding these theories [103, 104, 105, 106].

The effective interaction between stacks of charged plates depends on the delicate balance between the forces acting on the plates from the inner region in between the plates and from the outer region on either side of the stack of plates. In this chapter a system consisting of two parallel, like-charged plates is used as a test system for the new linearisation scheme for the Poisson-Boltzmann equation proposed in the last chapter. Only microions residing in the inner region between the plates will be considered, with a view to finding out how well the new linearisation scheme can reproduce results obtained from solution of the nonlinear PB equation.

The planar geometry is particularly convenient because if the parallel plates possess a uniform surface charge, and are sufficiently large so that edge effects can be neglected, there is translational symmetry of the electrostatic field due to the plates in the planar direction. If the mean field microionic charge distribution possess this symmetry, then variation of the electrostatic field occurs only in the perpendicular direction, which reduces the problem to a one-dimensional one. If the plates are orientated in the $y-z$ direction, then variation of the electrostatic potential occurs only in the x-direction.

There are some peculiarities of electrostatics in the one-dimensional planar geometry. An arbitrary fixed distribution of charge that possesses the appropriate symmetry is described by $\rho(\mathbf{r}) = \rho(x)$, where $\rho(x)dx$ is the amount of charge per unit area in a slab of thickness dx oriented in the $y-z$ plane located at x. The potential due to this charge distribution $\Phi(x)$ satisfies the one-dimensional Poisson equation

$$\frac{d^2\Phi(x)}{dx^2} = -l_B\rho(x) \tag{7.1}$$

where l_B is the Bjerrum length $l_b = e^2/(\epsilon k_B T)$. Note that in this chapter the definition of l_B is different by a factor of 4π for convenience. With $\epsilon = 76\epsilon_0$ and $T \sim 300K$ this corresponds to about

9.2nm. The Green's function for the potential at x due to a slab containing one charge per unit area located at x' is

$$G(x - x') = -l_B \frac{1}{2}|x - x'|/A_0 \tag{7.2}$$

where A_0 is one unit area. Unlike the familiar 3-dimensional geometry, the interaction potential due to a slab of charge does not fall off with distance but diverges linearly. The field due to a slab of charge on a test slab (containing one unit of charge per unit area) remains constant with distance, and the force on the test slab does not diminish as it moves further away. This behaviour is a consequence of the assumption that the slabs have sufficiently large dimensions compared with any lateral distances in the system so that edge effects can be neglected. The Green's function (7.2) is only valid in the finite domain in which the planar slab size is sufficiently large so that edge effects may be neglected and the slabs appear infinite.

Screening is the only mechanism by which the field due to a slab of charge can be diminished. Because the fields do not fall off with distance in this geometry, screening is also extremely effective. If we consider a slab possessing a surface charge $+\sigma$ per unit area, and an adjacent one of the opposite sign $-\sigma$, then the field on either side of these slabs will be zero. In other words the screening is 100% effective and there is no 'dipole' field due these two slabs. The planar geometry does not permit dipole or any higher order multipole fields, so there is no mechanism for the interaction between charge neutral regions.

7.1.1 Importance of non-mean field effects neglected in this treatment

Guildbrand *et. al.* performed extensive Monte-Carlo simulations [107, 42] of the two-plate system in the 1980s. The system simulated in their work makes use of the primitive model approximation for the solvent, but goes beyond the treatment outlined here in two important respects. First of all the finite size of the microions was included in their treatment, and it was shown that at small plate separations and high microion concentrations the hard-sphere correlations between the microions play an important role in the effective interaction between the plates. The second important result from their simulations, is that the mean field approximation for the electrostatic microion-microion interactions breaks down for the case when the microions have high valency i.e. $|z| > 1$ and when the plates are highly charged. This has the dramatic effect of reversing the sign of the force between the plates, causing attractions between like charged plates.

As mentioned in Section 7.1, within the symmetry of the planar geometry there is no means of interaction between two charge neutral regions. The mean field treatment always places the same number of microions in the left and right halves of the system S_L and S_R. Therefore, there is no direct interaction between the two halves within the mean field treatment. In reality instantaneous electrical fields go from S_L to S_R since charge will move between the two sectors, and at any given instant there may be more charge on one side than the other. It is only the average, mean field distribution that is equal in both sectors. Jonsson and Wennerstrom [76] have proposed this as the mechanism for the attractions observed in the simulations.

A different approach taken by Lau and Pincus [32, 108, 77] is to say that in reality there will be instantaneous fluctuations that break the planar symmetry. For a system of highly charged plates, they consider a thin layer near each plate containing the surface charge of the plates together with 'condensed' microions. The layers belonging to the two plates then undergo correlated plasmon fluctuations in the plane, giving rise to an effective attractive interaction between the plates.

Despite the peculiarities and the failure of the mean field approximation, the planar geometry serves as a good testing-ground for colloidal mean field theories because the nonlinear Poisson-Boltzmann equation can be solved without too much difficulty. Here we will investigate how the ideas of the new linearisation scheme for dilute colloidal suspensions proposed in Chapter 6 may be

put into practise for a simple test model in the planar geometry consisting of two identical like-charged parallel plates.

7.2 Two charged parallel plates

7.2.1 A simple model system

The model system consists of two uniformly charged parallel plates oriented in $y-z$ planes, both with the same surface charge density of $\sigma < 0$ electron charges per unit area. We choose the coordinate system so that the central plane in between the plates is at $x = 0$, with the plates located at $x = \pm D/2$. As with colloidal suspensions, the plates are immersed in an electrolytic solution of microions dissolved in a polar solvent. For now we only consider the inner region between the plates and ignore the outer regions. The plates are sufficiently large so that edge effects can be neglected. The mean field microion distribution is assumed to have the same symmetry as the field due to the charged plates, so that variation of ρ and Φ occurs only in the x-direction. Since this symmetry prescribes that any patch of area in the $y-z$ plane for a given x is equivalent to any other, the main system parameters are quantified per unit area in the $y-z$ plane.

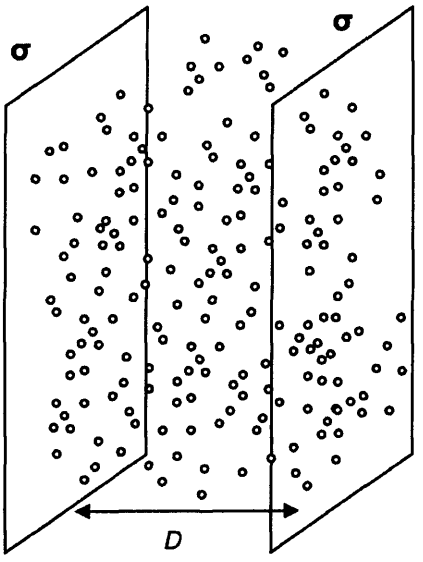

Figure 7.1: Schematic of the two-plate system after Lau [32]

The microions are taken to be univalent, and for simplicity counterions and microions arising from the dissolution of salt are assumed to be equivalent. The system may either contain a fixed amount of salt, or be in contact with a salt reservoir at fixed chemical potential. If there are N_s dissolved salt particles per unit area in the system (either as a fixed quantity or through contact with the salt bath), then there will be $N_- = N_s$ negative, and $N_+ = N_s + 2|\sigma|$ positive microions per unit area to conserve charge neutrality.

7.2.2 Adiabatic potential and force between the plates

The aim here is to obtain an adiabatic potential for the parallel plates as a function of plate separation $V^{\text{eff}}(D)$, by integrating over the microionic positions and momenta for a fixed plate separation D. It was shown in Chapter 5 that for a closed system (containing a fixed number of microions), the effective potential consists of the interaction between the fixed macroions V_{FF} and the Helmholtz free free energy of the microions F_M for a given configuration of the macroions.

In the planar geometry the plate-microion interaction energy V_{MF} contributes to the effective potential, but there is no relevant plate-plate contribution V_{FF}. This is because the field due to the two plates cancels out exactly in the inner region for all D, so V_{FF} is just a constant that is independent of D. The effective potential consists only of the Helmholtz free energy of the microions in between the plates $F_M(D, N_\pm, T)$, which contains the plate-microion interaction energy V_{MF}, the microion-microion interaction energy V_{MM} as well as a contribution from microion entropy.

$$V^{\text{eff}}(D) = F_M(D, N_\pm, T) \tag{7.3}$$

The mean field functional for $F_M(D, N_\pm, T)$ is

$$\begin{aligned} F_M(D, N_\pm, T) = &\sum_{i=\pm} \int \rho_i(x) \left(\ln \left(\rho_i(x) \lambda^3 \right) - 1 \right) dx + \frac{1}{2} \int \rho(x) \rho(x') G(x - x') dx' dx \\ &+ \int \rho(x) n_F(x') G(x - x') dx' dx \end{aligned} \tag{7.4}$$

where the charge density is defined by $\rho = \rho_+ - \rho_-$, λ is the thermal de Broglie wavelength of the microions (which are all taken to have the same mass), and F_M is in units of $k_B T$ per unit area. The first term is the kinetic term containing the kinetic energy and the entropy of the microions, the second term is the mean microion-microion interaction energy, and the third term is the mean plate-microion interaction energy. For a system that is open with respect to salt particles, the adiabatic potential is given by the grand potential of the microions $\Omega_M(D, \mu_b, T)$, which is related to F_M through the Legendre transform

$$\Omega_M(D, \mu_b, T) = F_M(D, N_\pm, T) - \mu_b N_+ - \mu_b N_- \tag{7.5}$$

where μ_b is the chemical potential of microions in the salt bath, and $N_\pm$ are the mean number of microions of each species when the system is at equilibrium with the salt bath. If the salt particles are considered to be ideal gas particles in the salt bath, then the chemical potential is related to the density of particles of each species in the reservoir n_b through $\mu_b = \ln n_b \lambda^3$.

The pressure, which is the force per unit area acting on the plates, is given by the derivative of the appropriate free energy with respect to D

$$P = -\left. \frac{\partial F_M}{\partial D} \right|_{N_s, D} \qquad \text{and} \qquad P = -\left. \frac{\partial \Omega_M}{\partial D} \right|_{\mu_b, D} \tag{7.6}$$

for a closed and open system respectively. In the planar geometry, the boundary density theorem (BDT) discussed in Chapter 5 has the result that the derivative of the free energy with respect to plate separation D is related to the total mean field density of microions in the mid-plane between the two plates. The result, which is the same for open and closed systems, is that the pressure is given by the density of microions at $x = 0$

$$P = \rho_+(0) + \rho_-(0) \tag{7.7}$$

in units of $k_B T$ per unit volume.

7.2.3 Poisson-Boltzmann equation

With the charged plates located at $x = \pm D/2$, the fixed charge distribution is represented using two delta functions as

$$n_F(x) = \sigma \delta(x + D/2) + \sigma \delta(x - D/2) \tag{7.8}$$

The general Poisson-Boltzmann equation for this system may be written as

$$\frac{d^2\Phi(x)}{dx^2} = 2l_B n_0 \sinh\left(\Phi(x) - \mu_{el}\right) - l_B n_F(x) \tag{7.9}$$

where $n_0 = \exp(\mu)/\lambda^3$ is the normalisation constant that regulates the amount of salt in the system, and μ_{el} ensures charge neutrality. As discussed before, n_0 and μ take different forms depending on whether the system is open or closed with respect to microions. The electroneutrality Lagrange multiplier μ_{el} is related to the choice of zero for the potential $\Phi(x)$. If the choice is made that mid-plane potential $\Phi(0) \to 0$ as $D \to \infty$, then $\mu_{el} = 0$.

Boundary conditions

As with the 3-dimensional geometry the symmetry and charge neutrality imposed on the mean field charge distribution dictate boundary conditions on $\Phi(x)$. The solution is assumed to be symmetrical about $x = 0$, so that the mean field distribution of microions places $-\sigma$ microions per unit area in the left half of the system S_L with the same number in right half of the system S_R. This symmetry is a consequence of the mean field approximation in which microion-microion correlations are neglected, as well as microion-macroion correlations between the two halves of the system. This symmetry, which simultaneously imposes charge neutrality on both halves of the system gives the boundary condition at $x = 0$

$$\left.\frac{d\Phi}{dx}\right|_{x=0} = 0 \tag{7.10}$$

The second boundary condition relates the gradient of the potential at the surfaces to the surface charge density. The overall charge neutrality condition for the system is

$$\int \left(\rho_+(x) - \rho_-(x) + n_F(x)\right) dx = 0 \tag{7.11}$$

where the total charge distribution is related to $\Phi(x)$ through $\nabla^2\Phi = -l_B(\rho_+ - \rho_- + n_F)$. Applying Gauss's theorem tells us that the field (which is the derivative $d\Phi/dx$) just outside the system on either side of the plates at $x = \pm(D/2 + \delta)$ where δ is a small distance, must be zero. By integrating over two Gaussian surfaces that just enclose the charge on the plates and none of the microionic charge i.e. $x = -D/2 - \delta \to -D/2 + \delta$ and $x = D/2 - \delta \to D/2 + \delta$, where $\delta \to 0$ is an infinitesimal quantity, we get boundary conditions at $x = \pm D/2$ that relate the field at either plate to the surface charge density

$$\left.\frac{d\Phi}{dx}\right|_{\pm D/2} = \pm l_B \sigma \tag{7.12}$$

The three equations in (7.10) and (7.12) make up two boundary conditions, since the two in (7.12) imply (7.10) by symmetry, or equivalently (7.10) with one of the equations in (7.12) implies the second one. The boundary conditions (7.12) account for the fixed charge distribution on the surface of the plates, and allow us to solve the PB equation in the inner region $x = -D/2 + \delta$ to $D/2 - \delta$, in which there is no macroion charge $n_F(x) = 0$.

System in contact with salt bath

For a system in contact with a salt bath, the Poisson-Boltzmann equation for the inner region (excluding the plates) is

$$\frac{d^2\Phi(x)}{dx^2} = \kappa^2 \sinh\Phi(x) \tag{7.13}$$

where $\kappa^2 = 2l_B n_0$. In this situation, the constant n_0 in (7.9) takes the form $n_b = \exp(\mu_b)/\lambda^3$ where n_b and μ_b are the density and chemical potential of positive and negative microions in the salt reservoir.

We have taken the charge-neutrality Lagrange multiplier to be $\mu_{el} = 0$, which corresponds to the choice that

$$\Phi(0) \to 0 \quad \text{as} \quad D \to \infty \tag{7.14}$$

When the plate separation becomes large, the mid-plane region tends to charge neutrality. Instead of having an excess of positive microions to neutralise the charge on the plates, the density of positive and negative microions at $x = 0$ tend towards equality as the plates move further apart. In terms of the microion charge density, this implies

$$\rho(0) = -2l_B n_b \sinh\left(\Phi(0) - \mu_{el}\right) \to 0 \qquad \text{or} \qquad \Phi(0) \to \mu_{el} \tag{7.15}$$

In this limit, both the positive and negative ion densities in the mid-plane region $\rho_{\pm}(0)$ tend towards n_b, the density of ions in the salt bath.

The nonlinear PB equation (7.13) for the optimising mean field potential $\Phi(x)$ may be solved subject to the boundary conditions above, in terms of elliptic functions. The details of this solution can be found in reference [101]. Taking account of the symmetry about $x = 0$ imposed by the boundary condition (7.10), the form of the potential is

$$\Phi(x) = 2\ln\left[\sqrt{k}\ \mathrm{sn}\left(\frac{\kappa x}{2\sqrt{k}} + K(k), k\right)\right] \tag{7.16}$$

the parameter k, which appears as the modulus of the elliptic functions, is defined as the exponential of the potential at the mid-plane $k = \exp\Phi(0)$. This parameter is a measure of the plate separation and tends to unity as D gets large. The function $\mathrm{sn}(a, k)$ is Jacobi's elliptic function defined as $\sin(\mathrm{am}(a, k))$ where the Jacobi Amplitude $\mathrm{am}(a, k)$ is the inverse of an elliptical integral of the first kind $F[\phi, k]$

$$\mathrm{am}\left(F[\phi, k], k\right) = \phi \tag{7.17}$$

where

$$F[\phi, k] = \int_0^{\phi} \frac{d\theta}{\sqrt{1 - k^2\sin^2(\theta)}} \tag{7.18}$$

The function $K(k) = F(\pi/2, k)$ is a complete elliptic integral of the first kind.

Given this form of $\Phi(x)$, which is symmetrical about $x = 0$, the second boundary condition (either one of the two equations in (7.12)) needs to be imposed to ensure representation of the correct amount of surface charge on the plates. Taking the derivative of $\Phi(x)$ with respect to x at $x = +D/2$, the second boundary condition becomes

$$\frac{1}{\sqrt{k}} \frac{\mathrm{cn}\left(\frac{\kappa D/2}{2\sqrt{k}} + K(k), k\right) \mathrm{dn}\left(\frac{\kappa D/2}{2\sqrt{k}} + K(k), k\right)}{\mathrm{sn}\left(\frac{\kappa D/2}{2\sqrt{k}} + K(k), k\right)} = \frac{l_B \sigma}{\kappa} \tag{7.19}$$

where $\mathrm{cn}(a, k) = \cos(\mathrm{am}(a, k))$ and $\mathrm{dn}(a, k) = \sqrt{1 - k^2\sin^2(\mathrm{am}(a, k))}$. For a given set of κ, D, σ, this equation needs to be solved to find the value of $k = \exp\Phi(0)$ for which the potential $\Phi(x)$ satisfies the boundary condition (7.12).

Equation (7.19) has to be solved numerically, however we point out some qualitative features here. The higher the surface charge density on the plates σ, the more negative $\Phi(0)$ will be, and therefore the smaller k. As $\kappa D \to \infty$, k tends to a maximum value of unity, corresponding to $\Phi(0) = 0$. A key feature of solutions to the nonlinear PB equation is that k also has a minimum possible value. To understand this, we note that the solution for $\Phi(x)$ contains a sinusoidal function $\mathrm{sn}(a, k) = \sin(\mathrm{am}(a, k))$. The maximum of the potential $\Phi(x)$ occurs at $x = 0$, when the argument of the sin function is $\mathrm{am}(K(k)) = \pi/2$. For a physically reasonable solution we do not expect the

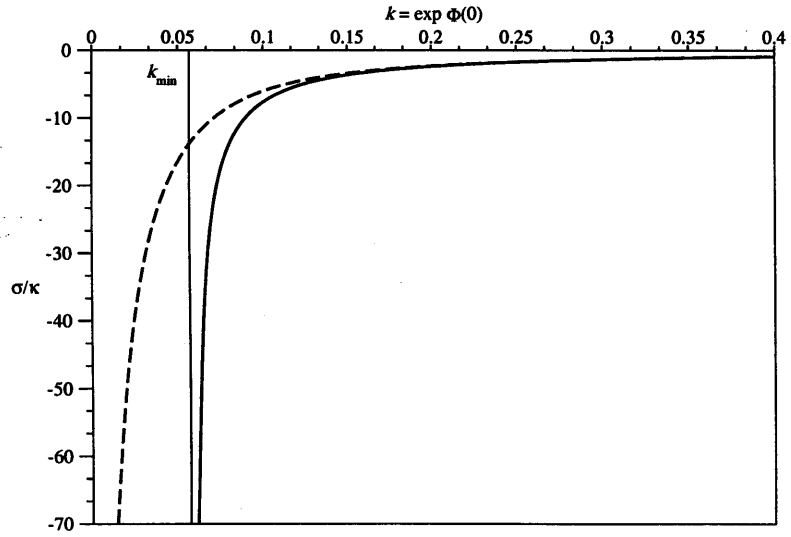

Figure 7.2: σ/κ in units of l_B^{-1} against k for two plates separated by $\kappa D = 1.5$. The full curve is for an exact solution of the PB equation, the dotted curve corresponds to a traditional linearisation about the average of the potential $\langle\Phi\rangle$ discussed in Section 7.3.

argument of sin to exceed π when x reaches $x = D/2$. Since $\mathrm{am}(2K(k), k) = \pi$, this imposes a constraint on k, D and κ

$$\frac{\kappa D/2}{2\sqrt{k}} < K(k) \tag{7.20}$$

so the smallest permissible value k_{min} satisfies

$$\sqrt{k_{min}}\, K(k_{min}) = \frac{\kappa D}{4} \tag{7.21}$$

When $k = k_{min}$, the denominator in (7.19) is zero, corresponding to an infinite surface charge density σ or an infinite Debye screening length $\lambda_D = 1/\kappa$. For a given plate separation κD, the solution saturates as the charge on the plates becomes very large. For highly charged plates k can be approximated by k_{min}.

This feature of the nonlinear solution is absent in the traditional linearisation approximation, and is what motivates the so-called 'renormalisation' approaches, whereby a colloidal particle carrying surface charge σ is represented as a renormalised particle carrying a smaller effective charge σ^*. The renormalisation approach is an attempt to introduce features of nonlinearity into the linearised solution. From Figure 7.2 it can be seen that a traditional linearisation (which will be discussed in Section 7.3) for a system of two plates carrying charge density σ generally has the same value of $\Phi(0)$ as a nonlinear solution with significantly higher charge density. With the exception of some treatments that go beyond the primitive model (PM) approximations [109], there has been little progress in developing a theory that prescribes a systematic way of choosing σ^* that allows a traditionally linearised solution to reproduce nonlinear results.

Figure 7.3 shows the grand potential Ω and pressure P against plate separation in screening lengths κD for various ratios of $|\sigma|/\kappa$. The force between the plates is always repulsive, and for a given κD is higher for larger values of $|\sigma|/\kappa$. In both cases the infinite plate separation limit Ω_∞ and P_∞ have been subtracted, so that zero corresponds to the grand potential and pressure when the plates are far apart. The solutions can be seen to saturate for large $|\sigma|/\kappa$ as expected from Figure 7.2.

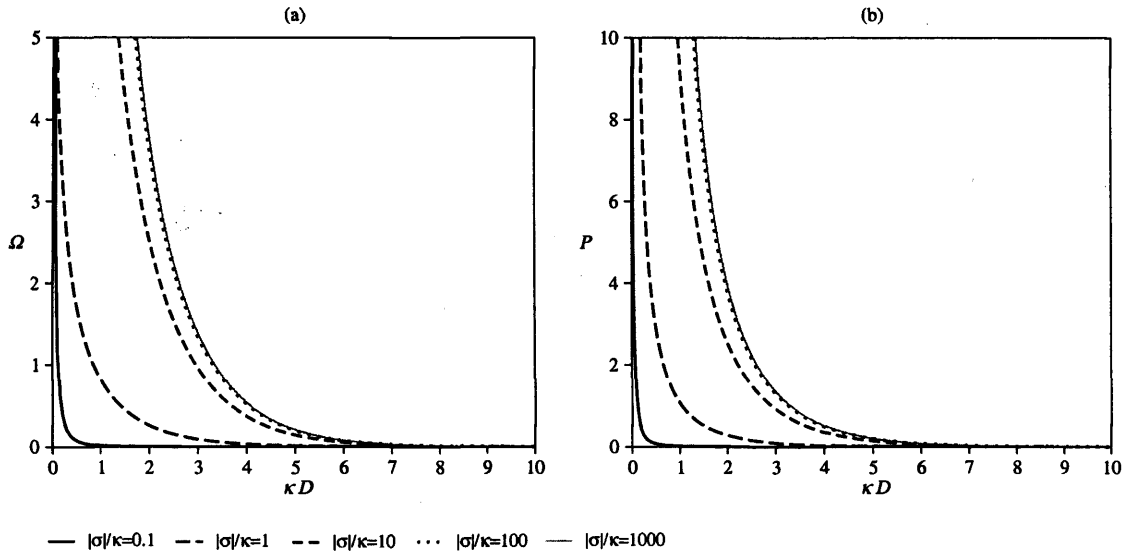

Figure 7.3: (a) Ω (in $k_BTl_b^{-3}$) vs. κD evaluated using exact solutions to the PB equation for various $|\sigma|/\kappa$ and (b) the corresponding pressure P (in $k_BTl_b^{-3}$) vs κD. Note that zero in these plots corresponds to the $D \to \infty$ limit, where the pressure is $P_\infty = 2n_B$, the pressure in the salt bath.

Closed system containing a fixed amount of salt

For a closed system containing a fixed number N_s of positive and negative salt ions per unit area, the parameter $n_0 = \exp(\mu)/\lambda^3$ takes a more complicated form than for an open system. The number of negative ions is $N_- = N_s$ and by charge neutrality the number of positive ions is $N_+ = N_s + 2|\sigma|$, where both N_s and σ are now fixed quantities for all D. The fixed-salt condition can be expressed in terms of an integral of the total microion density distribution $\rho_+(x) + \rho_-(x) = 2n_0 \cosh \Phi(x)$

$$2N_s + 2|\sigma| = \int_{-D/2}^{D/2} 2n_0 \cosh \Phi(x) dx \tag{7.22}$$

If N_s is constant, then $2N_s + 2|\sigma|$ is fixed for all D, which requires

$$n_0 = \frac{N_s + |\sigma|}{\int_{-D/2}^{D/2} \cosh \Phi(x) dx} \tag{7.23}$$

This form of n_0 converts the non-linear PB equation (7.9) into an integro-differential equation.

Solving the PB equation with this form of n_0 self-consistently is difficult, due to the complex interdependence between Φ and n_0. The solution for the fixed n_b treated above can be used in an iterative numerical procedure to solve the integro-differential Poisson-Boltzmann equation for a system containing a fixed amount of salt. This involves choosing a value n_b, finding a solution $\Phi(x)$ of the form (7.16) through numerical solution of the boundary-condition equation (7.19), and then integrating the density profiles to get n_0 from (7.23). This value of n_0 is then used as the n_b for the next iteration. The procedure is converged when the n_b put into $\Phi(x)$ and the n_0 calculated from it are the same to within numerical error. This procedure was found to converge relatively quickly requiring a few dozen iterations to converge . For the remainder of the chapter we will deal with the open system at constant chemical potential for simplicity.

7.3 Traditional linearisation schemes

7.3.1 Linearisation about a constant potential

The concept of the traditional linearisation schemes in the application of Poisson-Boltzmann theory is to linearise the mean field potential Φ about a constant value. The original Debye-Hückel treatment is a linearisation in deviations about $\Phi = 0$ (or value of the potential far away from any macroions given by μ_{el}), however subsequent treatments [86, 96, 87, 82] have suggested that the average of the potential throughout the system $\langle\Phi\rangle$ may provide a better linearisation point, especially when the separation between colloidal particles (or in this case plates) is small.

If the deviations of the mean field potential from a constant value, say C are small, then the PB equation may be linearised in the deviations $\Delta\Phi = \Phi - C$ giving the linear differential equation

$$\nabla^2\Delta\Phi \simeq \kappa^2 \sinh(C) + \kappa^2 \cosh(C)\Delta\Phi \tag{7.24}$$

which may be written as

$$\nabla^2\Delta\Phi \simeq A + B\Delta\Phi \tag{7.25}$$

The boundary conditions on $\Phi(x)$ are dictated by charge neutrality and symmetry, and since in this approximation $\Phi(x) = C + \Delta\Phi(x)$ the boundary conditions on $\Delta\Phi$ are

$$\left.\frac{d\Delta\Phi}{dx}\right|_{x=0} = 0 \quad \text{and} \quad \left.\frac{d\Delta\Phi}{dx}\right|_{x=\pm D/2} = \pm l_B\sigma \tag{7.26}$$

The general solution to (7.25) subject to boundary conditions (7.26) is

$$\Delta\Phi(x) = \frac{\sigma l_B \cosh(\sqrt{B}x)}{\sqrt{B}\sinh(\sqrt{B}D/2)} - \frac{A}{B} \tag{7.27}$$

where $A/B = \tanh C$ and $B = \kappa^2 \cosh C$.

Debye-Hückel Linearisation

When the constant potential is taken to be zero $C = 0$, then $A = 0$ and $B = \kappa^2$ so the solution becomes

$$\Phi_{DH}(x) = \frac{\sigma l_B \cosh(\kappa x)}{\kappa \sinh(\kappa d/2)} \tag{7.28}$$

It has been shown [86, 96] that the traditional linearisations are consistent with quadratic expansions of the free energy about deviations in the density distributions of the microions about constant values. It follows that the pressure P, which is the derivative of the free energy (the Helmholtz free energy F for a closed system and the grand potential Ω for an open system) with respect to D, consistent with this expansion, is also expanded to second order in these density deviations. For the D-H linearisation, where $C = 0$, the quadratic expansion of the pressure gives

$$P = 2n_B\left(1 + \frac{1}{2}\Delta\Phi^2(0)\right) = 2n_B\left(1 + \frac{1}{2}\left(\frac{\sigma l_B}{\kappa \sinh(\kappa D/2)}\right)^2\right) \tag{7.29}$$

Linearisation about the Donnan potential

An alternative scheme mentioned above involves linearisation of PB equation in deviations from the average of the mean field potential $\langle\Phi\rangle$. This quantity determines the chemical equilibrium between the salt bath and the system, known as Donnan equilibrium, so $\langle\Phi\rangle$ is referred to as the Donnan potential. In this treatment the constant c is taken to be the Donnan potential, so the mean field

potential is written as $\Phi = \langle\Phi\rangle + \Delta\Phi$ where $\langle\Phi\rangle$ is defined as

$$\langle\Phi\rangle = \frac{1}{D}\int \Phi(x)dx \tag{7.30}$$

The integral runs from $x = -D/2$ to $x = +D/2$. It follows that the integral of the deviation from the mean potential is zero

$$\int \Delta\Phi(x)dx = 0 \tag{7.31}$$

This has the consequence that if the linearised microionic charge density

$$\rho = -2n_b\left(\sinh\langle\Phi\rangle + \Delta\Phi\cosh\langle\Phi\rangle\right) \tag{7.32}$$

is integrated over the system volume (from $x = -D/2$ to $x = +D/2$), only the first term contributes. The charge neutrality requires the total microionic charge to equal -2σ

$$\int \rho(x)dx = -2\sigma \tag{7.33}$$

This provides a relation between the mean potential $\langle\Phi\rangle$ and the mean microionic charge density in the system $-2\sigma/D$,

$$2n_b\sinh\langle\Phi\rangle = \frac{2\sigma}{D} \tag{7.34}$$

In this scheme, the solution to the linearised PB equation $\Delta\Phi$ given in Equation (7.27), has parameters $A = \kappa^2\sinh\langle\Phi\rangle$ and $B = \kappa^2\cosh\langle\Phi\rangle$. Substituting the relation for $\langle\Phi\rangle$ in (7.34) into these expressions gives

$$A = \frac{2\sigma l_B}{D} \tag{7.35}$$

and

$$B = \kappa^2\sqrt{1 + \left(\frac{2\sigma l_B}{\kappa^2 D}\right)^2} \tag{7.36}$$

The linearised solution then takes the form

$$\Phi_{\text{Donn}} = \sinh^{-1}\left(\frac{2\sigma l_B}{\kappa^2 D}\right) + \frac{\sigma l_B\cosh(\sqrt{B}x)}{\sqrt{B}\sinh(\sqrt{B}D/2)} - \frac{2\sigma l_B}{DB} \tag{7.37}$$

From these expressions it can be seen that $\Delta\Phi$ in this scheme approaches that in the D-H linearisation in the limit of $D \to \infty$, since $\langle\Phi\rangle \to 0$, $A \to 0$ and $B \to \kappa^2$.

The pressure is given by a quadratic expansion of the total microion density at $x = 0$ about $2n_B\cosh\langle\Phi\rangle$, which is given by

$$P = 2n_b\left(1 + \frac{1}{2}\Delta\Phi^2(0)\right)\cosh\langle\Phi\rangle + 2n_b\Delta\Phi(0)\sinh\langle\Phi\rangle \tag{7.38}$$

7.3.2 Failure of traditional linearisation schemes

The traditional linearisation schemes generally fail when deviations from the constant $\Delta\Phi = \Phi - C$ are too large to justify the expansion. The consequence is that the traditionally linearised mean field potentials $\Phi(x)$ have a significantly higher amplitude than the exact solution to the nonlinear PB equation. Screening in the nonlinear system is generally more effective, and occurs over shorter distances than in the linearised case. Figure 7.6 is a comparison between mean field potentials obtained from the two traditional linearisation schemes (D-H, and linearisation about the Donnan potential) with the exact nonlinear solution Φ for $|\sigma|/\kappa = 2$ and $|\sigma|/\kappa = 10$ for several plate separations κD.

It can be seen that the linearisations work better for the smaller of the two ratios $|\sigma|/\kappa$. For small

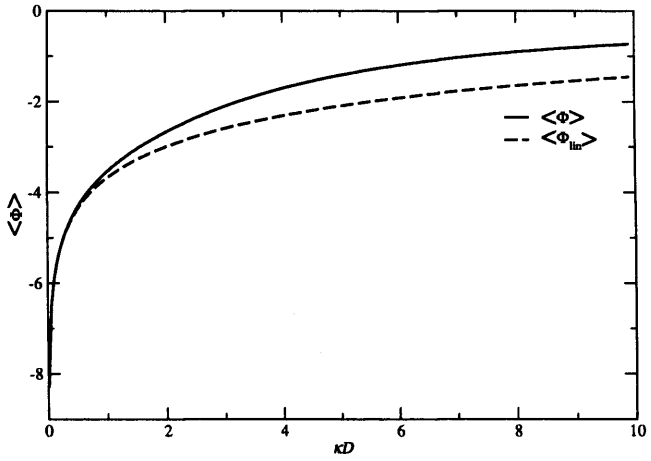

Figure 7.4: Comparison between the exact and linearised average of the mean field potential $\langle\Phi\rangle$ that forms the reference potential in Φ_{Donn}. The ratio $|\sigma|/\kappa$ has been taken to be 10.

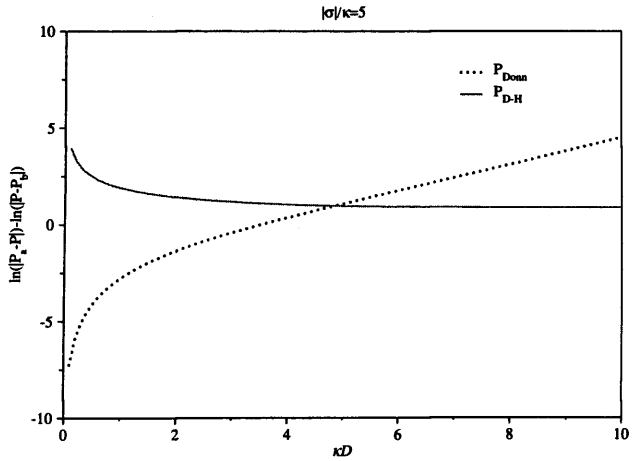

Figure 7.5: Logarithm of the relative error in pressure, for the two traditional linearisation schemes. The formula used is error=$\ln|P_a - P| - \ln(P - P_\infty)$, where P_a is the pressure obtained from the approximate scheme, P is the pressure obtained from the nonlinear PB equation, and $P_\infty = 2n_b$ is the pressure as the plates move infinitely far apart.

separations κD, linearisation about the Donnan potential is effective. This is because when $\kappa D < 1$ the mean field potential Φ is quite homogeneous since the distances are too short for significant screening to take place. In this regime the average $\langle\Phi\rangle$ is significantly smaller than zero, which is why the D-H linearisation breaks down for small κD. Figure 7.6 shows that despite appearing to reproduce the general shape of Φ better than the D-H linearisation, the linearisation about the Donnan potential does worse at estimating the mid-plane potential $\Phi(0)$ for large κD. For large κD the potential near the mid-plane is close to zero, so the deviation $\Delta\Phi$ for the D-H linearisation is small. In the Φ_{Donn} linearisation, the error due to failure of the linearisation approximation is spread throughout the system, and is reflected in the estimate of $\langle\Phi\rangle$ (see figure 7.4).

This shortcoming in the linearisation about the Donnan potential, leads to a dramatic failure in the calculation of the pressure P between the plates at large plate separations κD. Figure 7.5 shows the logarithm of the relative error in pressure P calculated from the two traditional linearisation schemes for $|\sigma|/\kappa = 5$ as a function of plate separation. Whereas the D-H linearisation fails at small plate separations and becomes better with increasing κD, the linearisation about the Donnan potential gives an increasingly bad estimate of the pressure at large plate separations.

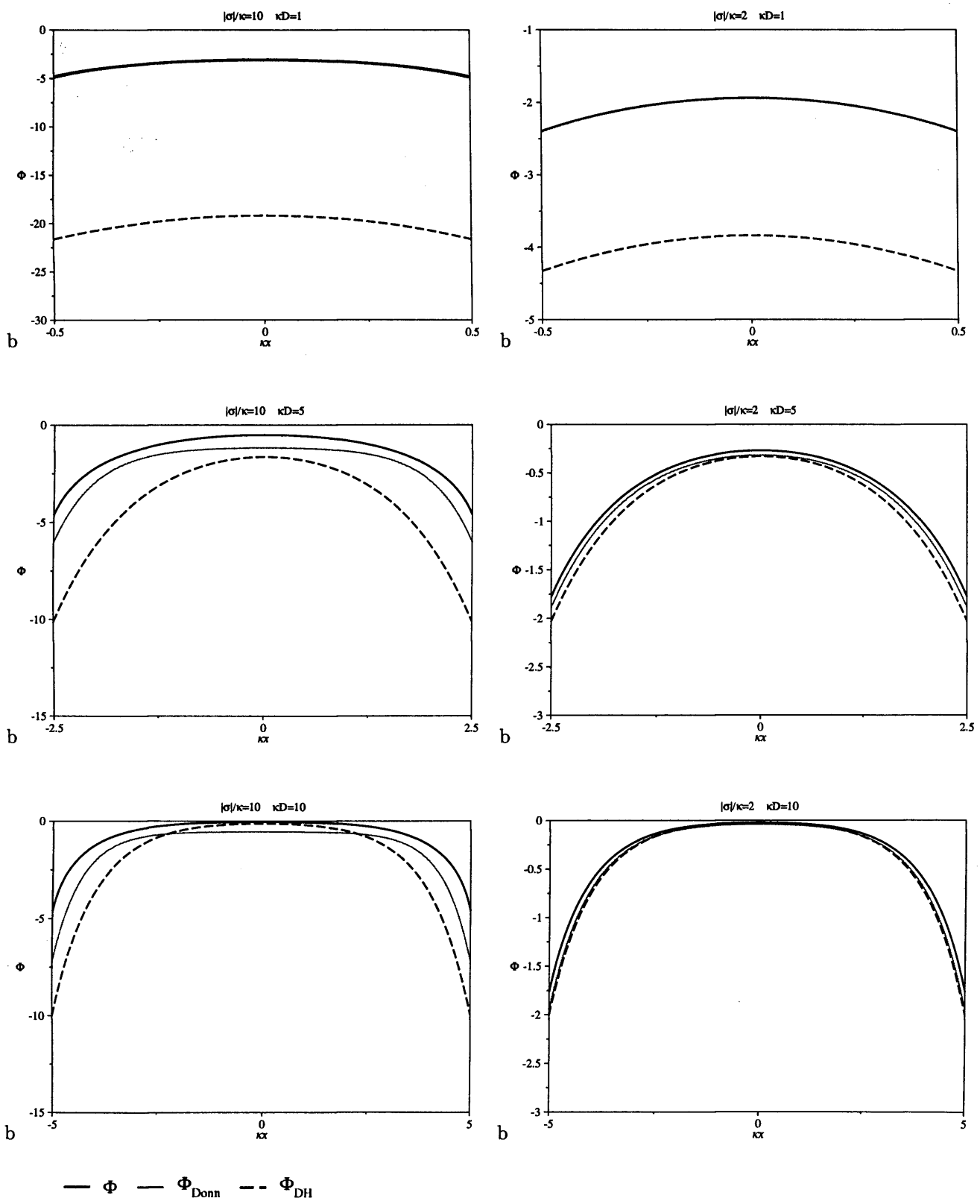

Figure 7.6: Comparisons between solutions to the PB equation obtained from the two traditional linearisation schemes Φ_{DH} and Φ_{Donn} with exact solutions of the nonlinear PB equation. The Φ_{Donn} curves are not visible in the plots for small plate separations $\kappa D = 1$ as they are very close to the exact potential in this limit.

7.4 The isolated charged plate: Guoy-Chapman theory

The isolated system consists of a single charged plate in electrolyte containing counterions. This system is one of the earliest applications of the mean field Poisson-Boltzmann approach and was developed by Guoy in 1910 and independently by Chapman in 1913 [42]. This system can be thought of as the limit of the two-plate system when $D \to \infty$. The left and right hand plates would then be effectively isolated, with solutions extending over semi-infinite half spaces $x > -D/2$ and $x < +D/2$.

As before, a system is considered in which the electrolyte contains salt ions, and which is open with respect to a salt reservoir containing positive and negative microions at chemical potential μ_b. Each isolated plate has a negative surface charge density σ. For later convenience we will look at two isolated plates, one located at $x = -D/2$ with the charged surface at $x = -D/2+\delta$ and the associated microions residing in the semi-infinite $x > -D/2$ region, and a second located at $x = +D/2$ with the charged surface at $x = D/2-\delta$ with microions in the $x < D/2$ region. The two solutions are denoted $\Phi_L^{(0)}$ and $\Phi_R^{(0)}$ respectively.

The PB equation for the microions in this situation is the same as that in (7.13) but with a different set of boundary conditions. The boundary conditions on the two solutions $\Phi_{L,R}^{(0)}$ at the plate surfaces are

$$\left.\frac{d\Phi_L^{(0)}}{dx}\right|_{-D/2} = -l_B\sigma \quad \text{and} \quad \left.\frac{d\Phi_R^{(0)}}{dx}\right|_{+D/2} = l_B\sigma \tag{7.39}$$

The second boundary condition on the isolated solutions $\Phi_{L,R}^{(0)}$ is that the derivatives vanish at points infinitely far from the plates

$$\left.\frac{d\Phi_L^{(0)}}{dx}\right|_{x\to+\infty} = 0 \quad \text{and} \quad \left.\frac{d\Phi_R^{(0)}}{dx}\right|_{x\to-\infty} = 0 \tag{7.40}$$

The solutions for $\Phi_L^{(0)}$ and $\Phi_R^{(0)}$ can be expressed in terms of elementary functions, and are given by [99]

$$\Phi_{L,R}^{(0)}(x) = 2\log\left[\frac{1+\exp\left(-\kappa\left(\pm x + D/2\right)\right)A}{1-\exp\left(-\kappa\left(\pm x + D/2\right)\right)A}\right] \tag{7.41}$$

where

$$A = \tanh\left[\frac{1}{2}\sinh^{-1}\left(\frac{l_B\sigma}{2\kappa}\right)\right] \tag{7.42}$$

From the hyperbolic tangent in (7.42) it follows that the isolated-plate solution shares the feature of the two-plate solution in that it saturates as the surface charge density σ becomes large.

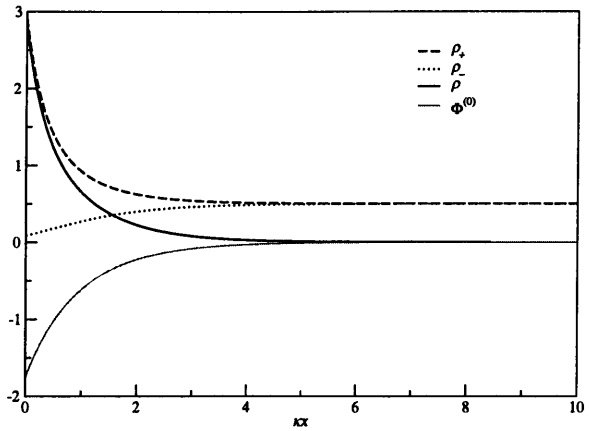

Figure 7.7: Guoy-Chapman solution to the PB equation for an isolated plate located at $x = 0$ with negative surface charge density $\sigma = -2$. The salt bath density is $n_B l_b^3 = 0.5$ and inverse screening length $\kappa = 1$. Shown are the density distribution of positive microions ρ_+, negative microions ρ_-, and the charge density $\rho = \rho_+ - \rho_-$ in units of l_b^{-3}, as well as the electrostatic mean field potential $\Phi^{(0)}$ in k_BT. Note that $\rho_\pm$ tend to $n_b = 0.5$ as D gets large.

7.5 Application of the new linearisation scheme for large plate separations

7.5.1 Charge neutral sectors

In the two-plate system, the charge neutral regions or sectors consist of the left and right half of the space in between the plates. The symmetry imposed on the solution to the PB equation in Section 7.2.3 was that it must have mirror symmetry about the $x = 0$ plane. The sectors are defined by the spaces S_L where $-D/2 \leq x \leq 0$ and S_R where $0 \leq x \leq D/2$ [1]. $S_{L,R}$ take the roles of the charge neutral sectors or cells referred to in Chapters 5 and 6.

As discussed in Section 7.1, in the planar geometry there are no dipole or higher multi-pole fields, so at the mean field level there is no electrostatic field from S_L in S_R and vice versa. The effect of the mean field electrostatic interactions between the two sectors is to confine the microions and create two finite, symmetrical, charge neutral halves of the system. At the mean field level there is no difference between a system consisting of two charged plates located at $x = \pm D/2$, and a single charged plate located at either $x = \pm D/2$ together with a charge neutral wall at $x = 0$ [42]. These systems would both share the boundary condition (7.10) at $x = 0$ and each satisfy one of the boundary conditions (7.12) at $x = \pm D/2$ but not the other.

Exact solutions to the PB equation within each sector $\Phi_{L,R}(x)$ will differ from their isolated counterparts $\Phi^{(0)}_{L,R}(x)$ in that the corresponding charge distributions are nonzero only within the finite sectors $S_{L,R}$ rather than extending infinitely.

7.5.2 Linearisation of the Poisson-Boltzmann equation

As the plate separation D becomes large, the solutions to the PB equation for the two-plate system $\Phi_{L,R}(x)$ will start to resemble $\Phi^{(0)}_{L,R}(x)$. In this regime, the linearisation scheme outlined in Chapter 6 can be applied.

As before, the solution to the PB equation for the total electrostatic mean field potential is expressed as

$$\Phi = \Phi^{(0)}_L + \Phi^{(0)}_R - \mu^{(1)}_{el} + \epsilon \tag{7.43}$$

Substituting this $\Phi(x)$ into the Poisson-Boltzmann equation for the inner region (7.13) and linearising in the deviations $\epsilon(x)$ gives a linear differential equation for $\epsilon(x)$

$$\nabla^2\Phi^{(0)}_L + \nabla^2\Phi^{(0)}_R + \nabla^2\epsilon(x) = \kappa^2 \sinh\left(\Phi^{(0)}_L + \Phi^{(0)}_R - \mu^{(1)}_{el}\right) + \epsilon(x)\kappa^2 \cosh\left(\Phi^{(0)}_L + \Phi^{(0)}_R - \mu^{(1)}_{el}\right) \tag{7.44}$$

Since $\Phi^{(0)}_{L,R}(x)$ satisfy PB equations for the isolated plate situations, we can substitute the charge distributions $\nabla^2\Phi^{(0)}_{L,R} = -l_B\rho^{(0)}_{L,R} = \kappa^2 \sinh\Phi^{(0)}_{L,R}$ to give

$$\begin{aligned}\nabla^2\epsilon(x) =& \kappa^2 \sinh\left(\Phi^{(0)}_L + \Phi^{(0)}_R - \mu^{(1)}_{el}\right) + \epsilon(x)\kappa^2 \cosh\left(\Phi^{(0)}_L + \Phi^{(0)}_R - \mu^{(1)}_{el}\right) \\ & -\kappa^2 \sinh\Phi^{(0)}_L - \kappa^2 \sinh\Phi^{(0)}_R\end{aligned} \tag{7.45}$$

This type of linearisation corresponds to an expansion of the microionic density distributions about

$$\rho^{(1)}_{\pm}(x) = n_b \exp\left[\mp\left(\Phi^{(0)}_L(x) + \Phi^{(0)}_R(x) - \mu^{(1)}_{el}\right)\right] \tag{7.46}$$

The constant $\mu^{(1)}_{el}$ is intended to make the linearisation more effective by accounting for a constant component in the difference between the $\Phi(x)$ and the superposition $\Phi^{(0)}_L + \Phi^{(0)}_R$. To achieve this, $\mu^{(1)}_{el}$

[1] These regions include an infinitesimal region beyond the left and right plates so that the surface charge on the plates represented delta functions is picked up by the integrals i.e. S_L where $-D/2-\delta \leq x \leq 0$ and S_R where $0 \leq x \leq D/2+\delta$

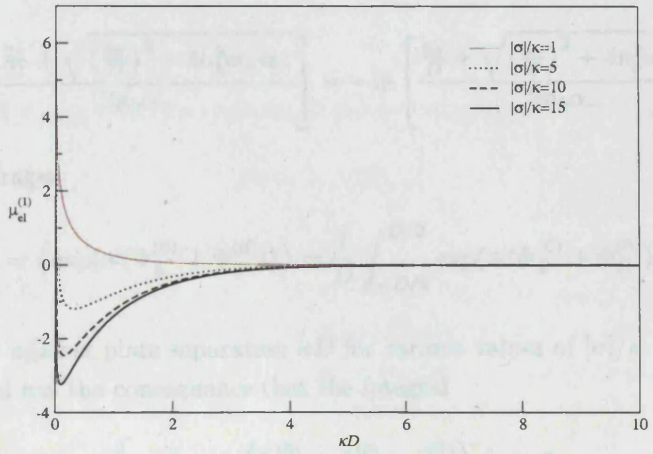

Figure 7.8: The constant contribution $\mu_{ei}^{(1)}$ to the reference potential against plate separation κD for $|\sigma|/\kappa = 1, 5, 10, 15\, l_B^{-1}$.

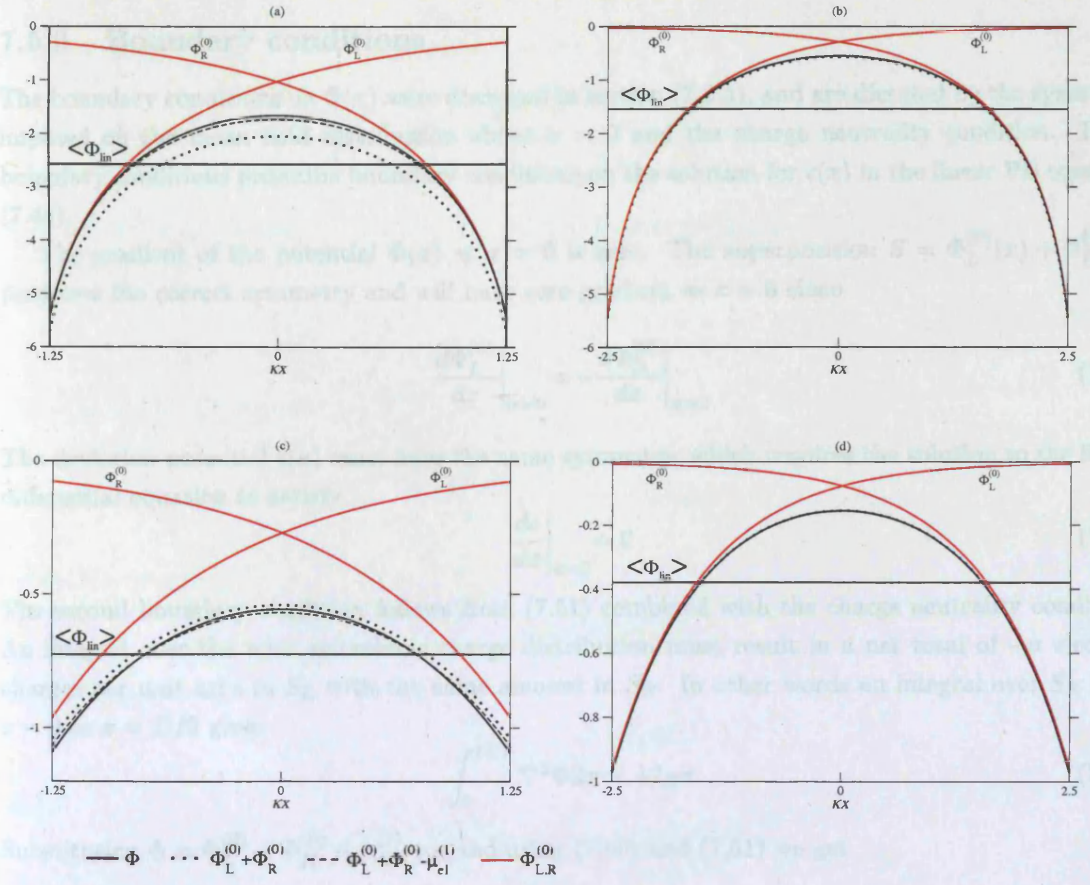

Figure 7.9: Construction of the reference potential for the new linearisation scheme: this plot shows the exact Φ, the isolated potentials $\Phi_{L,R}^{(0)}$, the superposition $\Phi_L^{(0)} + \Phi_R^{(0)}$ and the shifted superposition $\Phi_L^{(0)} + \Phi_R^{(0)} - \mu_{el}^{(1)}$ which acts as the reference potential in the new linearisation scheme. The horizontal line is $\langle \Phi_{\text{lin}} \rangle$, the constant about which the PB is linearised in the traditional Donnan linearisation scheme discussed in Section 7.3. The energy scale is in units of $k_B T$. The parameters are (a) $|\sigma| l_B/\kappa = 15$, $\kappa D = 2.5$ (b) $|\sigma| l_B/\kappa = 15$, $\kappa D = 5$ (c) $|\sigma| l_B/\kappa = 1$, $\kappa D = 2.5$ (d) $|\sigma| l_B/\kappa = 1$, $\kappa D = 5$. The superposition and shifted superposition are barely visible in (b) and (d) due to their close vicinity to the exact curve.

is chosen so that an integral of the reference charge density $\rho^{(1)}(x)$ over the system (from $x = -D/2$ to $D/2$) provides the total amount of microionic charge -2σ. This corresponds to

$$\mu_{el}^{(1)} = \ln\left[\frac{-\frac{2\sigma}{D} + \sqrt{\left(\frac{2\sigma}{D}\right)^2 + 4n_b^2\alpha_+\alpha_-}}{2n_b\alpha_+}\right] = -\ln\left[\frac{\frac{2\sigma}{D} + \sqrt{\left(\frac{2\sigma}{D}\right)^2 + 4n_b^2\alpha_+\alpha_-}}{2n_b\alpha_-}\right] \tag{7.47}$$

where $\alpha_\pm$ are the averages

$$\alpha_\pm = \left\langle \exp(\mp(\Phi_L^{(0)} + \Phi_R^{(0)})) \right\rangle = \frac{1}{D}\int_{-D/2}^{D/2} \exp(\mp(\Phi_L^{(0)} + \Phi_R^{(0)}))dx \tag{7.48}$$

Figure 7.8 shows $\mu_{el}^{(1)}$ against plate separation κD for various values of $|\sigma|/\kappa$. The choice of $\mu_{el}^{(1)}$ in the reference potential has the consequence that the integral

$$\int \epsilon(x)\cosh\left(\Phi_L^{(0)} + \Phi_R^{(0)} - \mu_{el}^{(1)}\right)dx = 0 \tag{7.49}$$

Figure 7.9 shows how the reference potential is constructed from $\Phi_L^{(0)}$, $\Phi_R^{(0)}$ and $\mu_{el}^{(1)}$. Exact solutions of the mean field potential Φ are shown for comparison. For the larger plate separation $\kappa D = 5$ the difference between $\Phi_L^{(0)} + \Phi_R^{(0)}$ and Φ is barely visible, and the contribution of $\mu_{el}^{(1)}$ is insignificant.

7.5.3 Boundary conditions

The boundary conditions on $\Phi(x)$ were discussed in section (7.2.3), and are dictated by the symmetry imposed on the mean field distribution about $x = 0$ and the charge neutrality condition. These boundary conditions prescribe boundary conditions on the solution for $\epsilon(x)$ in the linear PB equation (7.44).

The gradient of the potential $\Phi(x)$ at $x = 0$ is zero. The superposition $S = \Phi_L^{(0)}(x) + \Phi_R^{(0)}(x)$ possesses the correct symmetry and will have zero gradient at $x = 0$ since

$$\left.\frac{d\Phi_L^{(0)}}{dx}\right|_{x=0} = -\left.\frac{d\Phi_R^{(0)}}{dx}\right|_{x=0} \tag{7.50}$$

The deviation potential $\epsilon(x)$ must have the same symmetry, which requires the solution to the linear differential equation to satisfy

$$\left.\frac{d\epsilon}{dx}\right|_{x=0} = 0 \tag{7.51}$$

The second boundary condition follows from (7.51) combined with the charge neutrality condition. An integral over the total microionic charge distribution must result in a net total of $-\sigma$ electron charges per unit area in S_L with the same amount in S_R. In other words an integral over S_R from $x = 0$ to $x = D/2$ gives

$$\int_0^{D/2} \nabla^2\Phi dx = +l_B\sigma \tag{7.52}$$

Substituting $\Phi = \Phi_L^{(0)} + \Phi_R^{(0)} - \mu_{el}^{(1)} + \epsilon$ and using (7.50) and (7.51) we get

$$\left.\frac{d\Phi_L^{(0)}}{dx}\right|_{x=D/2} + \left.\frac{d\Phi_R^{(0)}}{dx}\right|_{x=D/2} + \left.\frac{d\epsilon}{dx}\right|_{x=D/2} = l_B\sigma \tag{7.53}$$

Since the isolated solution $\Phi_R^{(0)}$ satisfies the correct boundary condition at the right-hand plate

$$\left.\frac{d\Phi_R^{(0)}}{dx}\right|_{x=D/2} = l_B\sigma \tag{7.54}$$

the condition for charge neutrality requires

$$\left.\frac{d\epsilon}{dx}\right|_{x=D/2} = -\left.\frac{d\Phi_L^{(0)}}{dx}\right|_{x=D/2} \tag{7.55}$$

This boundary condition relates to the amount of charge contained in $\Delta\rho$, where

$$\nabla^2\epsilon = -l_B\Delta\rho \tag{7.56}$$

The amount of charge contained in $\Delta\rho$ is the amount of charge 'cut out' from the superposition of isolated charge distributions $\rho_s = \rho_L^{(0)} + \rho_L^{(0)}$ due to the fact that the two-plate system is finite. This is analogous to $Q_o = -Q_i$, the charge due to the superposition ρ_s inside a spherical colloidal particle, discussed in Chapter 6. The solution to the PB equation for an isolated plate located at $x = -D/2$ gives the isolated distribution of microions $\rho_L^{(0)}(x)$ extending to $x \to \infty$. Over the infinite interval $x > -D/2$ this contains sufficient excess charge to neutralise the plate $-\sigma$

$$\int_{-D/2}^{\infty} \rho_L^{(0)}(x)dx = -\sigma \tag{7.57}$$

but over the finite interval

$$\int_{-D/2}^{D/2} \rho_L^{(0)}(x)dx = -\sigma - Q_o \tag{7.58}$$

in terms of derivatives

$$\left.\frac{d\Phi_L^{(0)}}{dx}\right|_{x=D/2} - \left.\frac{d\Phi_L^{(0)}}{dx}\right|_{x=-D/2} = -l_B\left(-\sigma - Q_o\right) \tag{7.59}$$

Since the isolated solution $\Phi_L^{(0)}$ satisfies the correct boundary condition at $x = -D/2$

$$\left.\frac{d\Phi_L^{(0)}}{dx}\right|_{x=D/2} = l_B Q_o \tag{7.60}$$

and equivalently for the solution $\Phi_R^{(0)}$

$$\left.\frac{d\Phi_R^{(0)}}{dx}\right|_{x=-D/2} = -l_B Q_o \tag{7.61}$$

so that we require

$$\int_{-D/2}^{D/2} \Delta\rho(x)dx = 2Q_o \tag{7.62}$$

and therefore

$$\left.\frac{d\epsilon}{dx}\right|_{x=\pm D/2} = \mp l_B Q_o \tag{7.63}$$

where

$$l_B Q_o = \left.\frac{d\Phi_L^{(0)}}{dx}\right|_{x=D/2} = -\frac{4\kappa A\exp(\kappa D)}{\exp(2\kappa D) - A^2} \tag{7.64}$$

and A was given in (7.42). Figure 7.10 shows $Q_o/|\sigma|$ against κD for various $|\sigma|/\kappa$. Clearly Q_0 diminishes to zero as the plate separation becomes large. It can also be seen that for a given κD, a lower fraction $Q_o/|\sigma|$ of the microion charge is 'cut out' from the isolated solution $\rho_L^{(0)}$ for higher $|\sigma|/\kappa$ indicating that the microions are comparatively closer to the plates for higher values of $|\sigma|/\kappa$.

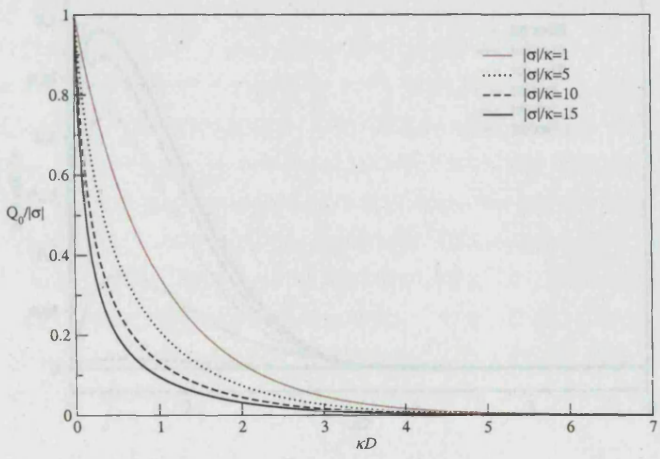

Figure 7.10: Ratio of the amount of charge Q_0 represented by the deviation potential ϵ and the charge on the plates σ, as a function of plate separation κD, for a variety of ratios of $|\sigma|/\kappa = 1, 5, 10, 15\, l_B^{-1}$.

7.5.4 Properties of the deviation potential

Figure 7.11 shows typical solutions $\epsilon(x)$ obtained from numerical integration of the linearised PB equation (7.45) for a variety of plate separations κD with the ratio $|\sigma|/\kappa = 15$. Exact evaluations of the deviation potential $\Phi - (\Phi_L^{(0)} + \Phi_R^{(0)} - \mu_{el}^{(1)})$ are also plotted on the same graph. The small differences between these solutions and exact evaluations reveal that the linearisation is successful for a range of κD. Figure 7.12 shows the 'amplitude' $\epsilon(0) - \epsilon(D/2)$ for several $|\sigma|/\kappa$. It can be seen that even for large $|\sigma|/\kappa$ this quantity is relatively small, which is what makes this linearisation scheme successful.

For small plate separations $\kappa D << 1$ the size of the deviation potential ϵ is generally small. In this regime, the mean field potential Φ, as well as the superposition $\Phi_L^{(0)} + \Phi_R^{(0)}$, are relatively flat or constant between $x = -D/2$ and $D/2$. The constant $\mu_{el}^{(1)}$ ensures that the reference potential $\Phi_L^{(0)} + \Phi_R^{(0)} - \mu_{el}^{(1)}$, which will be nearly flat in this regime, is at the correct level making ϵ small. The amplitude of the deviation ϵ then increases to a maximum near $\kappa D \sim 1$, and then begins to fall as κD gets large.

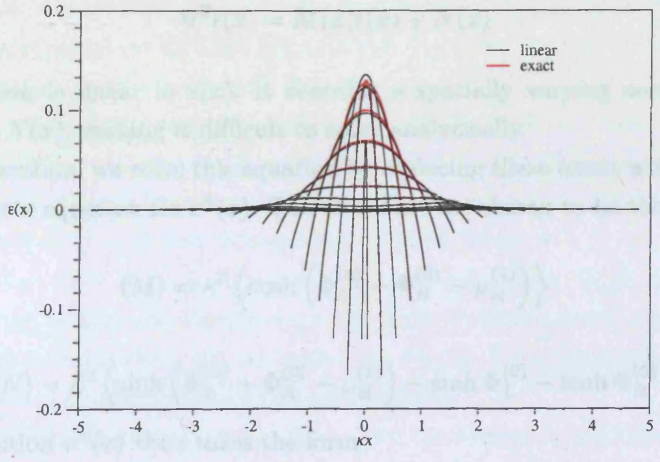

Figure 7.11: The deviation potential $\epsilon = \Phi - (\Phi_L^{(0)} + \Phi_R^{(0)} - \mu_{el}^{(1)})$ for 19 different plate separations κD ranging between 0.1 and 9.6 and with $|\sigma|/\kappa = 15$. Exact solutions to the nonlinear equation are in red, and numerical solutions to the linearised PB equation (7.44) are in black. The small difference means that the curves are nearly completely overlapping with the exception of some intermediate κD.

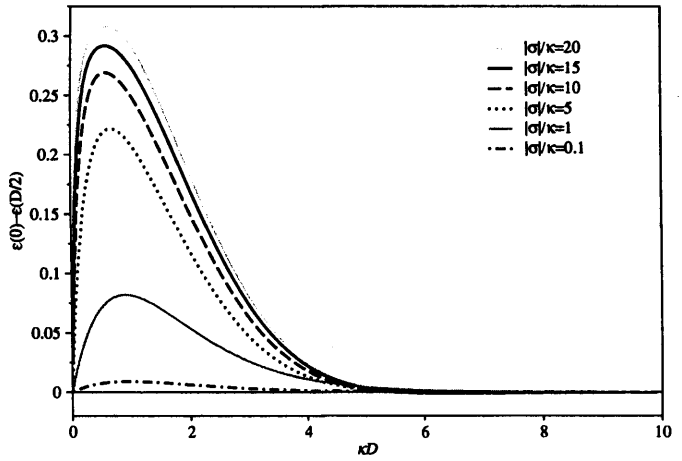

Figure 7.12: Amplitude of the deviation potential $\epsilon(0) - \epsilon(D/2)$ as a function of κD for various $|\sigma|/\kappa$.

7.5.5 Linearised grand potential and pressure

Once the linearised PB equation (7.45) has been solved to obtain the linearised deviation potential $\epsilon(x)$, this is used to estimate the pressure between the plates P.

The pressure is the derivative of the grand potential Ω with respect to D. In this linearisation scheme, the grand potential has been expanded to second order in density deviations $\Delta_\pm = \rho_\pm - \rho_\pm^{(1)}$. Using the BDT, an expression for the pressure consistent with this expansion is obtained, which corresponds to a second order expansion of the density of microions at $x = 0$

$$P = 2n_b \cosh\left(\Phi_L^{(0)}(0) + \Phi_R^{(0)}(0) - \mu_{el}^{(1)}\right)\left(1 + \frac{1}{2}\epsilon^2(0)\right) + 2n_b \sinh\left(\Phi_L^{(0)}(0) + \Phi_R^{(0)}(0) - \mu_{el}^{(1)}\right)\epsilon(0) \tag{7.65}$$

As $D \to \infty$ the pressure tends towards $P_\infty = 2n_b$, which is the pressure in the salt reservoir.

7.5.6 Approximation to the linearised equation

In shorthand notation, the linearised PB equation (7.45) is re-written as

$$\nabla^2\epsilon(x) = M(x)\epsilon(x) + N(x) \tag{7.66}$$

Although this equation is linear in $\epsilon(x)$, it contains a spatially varying coefficient $M(x)$ and an inhomogeneous term $N(x)$, making it difficult to solve analytically.

As a first approximation, we solve this equation by replacing these terms with constants, resulting in a simple approximate equation for $\epsilon^A(x)$. The constants are chosen to be the average values of the functions

$$\langle M\rangle = \kappa^2\left\langle \cosh\left(\Phi_L^{(0)} + \Phi_R^{(0)} - \mu_{el}^{(1)}\right)\right\rangle \tag{7.67}$$

and

$$\langle N\rangle = \kappa^2\left\langle \sinh\left(\Phi_L^{(0)} + \Phi_R^{(0)} - \mu_{el}^{(1)}\right) - \sinh\Phi_L^{(0)} - \sinh\Phi_R^{(0)}\right\rangle \tag{7.68}$$

The approximate solution $\epsilon^A(x)$ then takes the form

$$\epsilon^A(x) = \frac{l_B Q_0 \cosh(\sqrt{\langle M\rangle}x)}{\sqrt{\langle M\rangle}\sinh(\sqrt{\langle M\rangle}D/2)} - \frac{\langle N\rangle}{\langle M\rangle} \tag{7.69}$$

Clearly this approach suffers a similar deficiency to the traditional linearisation scheme in that the large inhomogeneities brought about by a high surface charge σ will not be represented adequately, since the functions $M(x)$ and $N(x)$ are expected to be very inhomogeneous in the limit of large $|\sigma|$

and large κD. As D increases, $N(x)$ becomes small since the difference between the reference charge density $\rho^{(1)}$ and the superposition $\rho_L^{(0)} + \rho_R^{(0)}$ diminishes in this limit.

This new linearisation scheme has similarities with a traditional linearisation about a constant potential, but with a spatially varying inverse screening length $\sqrt{M(x)}$ and a 'source term' $N(x)$ that extends throughout the system. In the linearisation about the Donnan potential the effective screening length depends on the plate separation, but is constant throughout the system. The new linearisation scheme reproduces features of the nonlinear PB equation, in that the screening near a highly charged surface is more effective than far away from it. This allows the new scheme to reproduce the correct behaviour of the system in the $D \to \infty$ limit. The approximate treatment involving $\epsilon^A(x)$ will clearly not be as successful in doing this, but it does have the advantage of employing spatially varying reference potential that reproduces the correct $D \to \infty$ behaviour.

7.6 Comparison between estimates of pressure

In this section the various methodologies for approximating the pressure P between the plates will be compared. Figure 7.13 shows the logarithm of the relative error in pressure of the various approximate schemes discussed in this chapter

$$\text{error} = \ln \left| \frac{P_a - P}{P - P_\infty} \right| \tag{7.70}$$

where P_a is an estimate of the pressure produced from one of the approximate methods, P is the pressure obtained from exact solution of the nonlinear PB equation, and P_∞ (denoted P_b in the figure) is the pressure in the salt bath $2n_b$ which is the limit of P when $D \to \infty$.

The line denoted P_{TB} is the error in pressure from numerical solutions of the PB equation within the new linearisation scheme. The solutions obtained for $\epsilon(x)$ were used in Equation (7.65) to obtain the pressure consistent with this linearisation. The line denoted P_{ref} refers to an estimate of the pressure based on the reference potential alone i.e. when $\epsilon = 0$, and indicates to what extent the reference potential is able to reproduce the exact pressure without the need for further calculation. P_{TBcc} is the error in the pressure estimate when the approximate ansatz ϵ^A in equation (7.69) is used rather than a full solution to the linearised PB equation.

As expected, between P_{TB}, P_{ref} and P_{TBcc} the numerical solution (P_{TB}) consistently performs best. For small values of $|\sigma|/\kappa$ the approximate solution P_{TBcc} improves on the pressure estimated from the reference potential alone P_{ref}, but tends to the P_{ref} error for large κD. For larger $|\sigma|/\kappa$, the improvement through the use of ϵ^A is largely insignificant.

The traditional linearisations, denoted by P_{DH} and P_{Donn}, perform badly with the exception of the smallest values of $|\sigma|/\kappa$. At very small values of ($\kappa D < 1$), the plate separation is too small for significant screening to occur so the potential Φ is very homogeneous. In this regime the linearisation about the Donnan potential performs better than the DH linearisation, as the potential takes a significantly lower value than $\Phi = 0$. However at large κD, when $\Phi(x)$ is close to zero over a significant portion of the system, the linearisation about the Donnan potential provides poor pressure estimates. The failure in estimating $\langle\Phi\rangle$ correctly (see Figure 7.4) causes the relative error for the P_{Donn} estimate to become increasingly large as κD increases.

The cusps seen in the error curves for P_{ref},P_{TBcc} and the change in curvature of P_{TB} are a result of a change in sign of the error in the pressure estimates. This change in sign occurs because the reference potential $\Phi_L^{(0)} + \Phi_r^{(0)} - \mu_{el}^{(1)}$ contains the constant $\mu_{el}^{(1)}$. The reference potential gives an underestimate of the pressure at small κD and then an overestimate for larger plate separations κD. The superposition of isolated potentials $\Phi_L^{(0)} + \Phi_R^{(0)}$ on its own underestimates the pressure for all plate separations. The constant $\mu_{el}^{(1)}$ introduces a nonmonotonic difference between the exact and approximate pressures, but it also makes the linearisation more effective.

In summary, the new linearisation scheme was applied to a one-dimensional two-plate system. Numerical solution of the newly linearised differential equation reproduces the nonlinear solution to the PB equation accurately. An approximation to the linearised solution $\epsilon^A(x)$ performs reasonably well. It enhances the accuracy relative to an estimate based on the reference potential $\Phi_L^{(0)} + \Phi_R^{(0)} - \mu_{el}^{(1)}$ for small plate separations, and tends to the same result for large plate separations. Both of these approaches (numerical solution for ϵ and approximation by ϵ^A) reproduce the pressure more accurately than the traditional linearisation schemes over the entire volume range. The Donnan linearisation scheme fails at large plate separations, and the Debye-Hückel scheme fails for small plate separations. Both traditional linearisations perform less well for larger ratios of $|\sigma|/\kappa$.

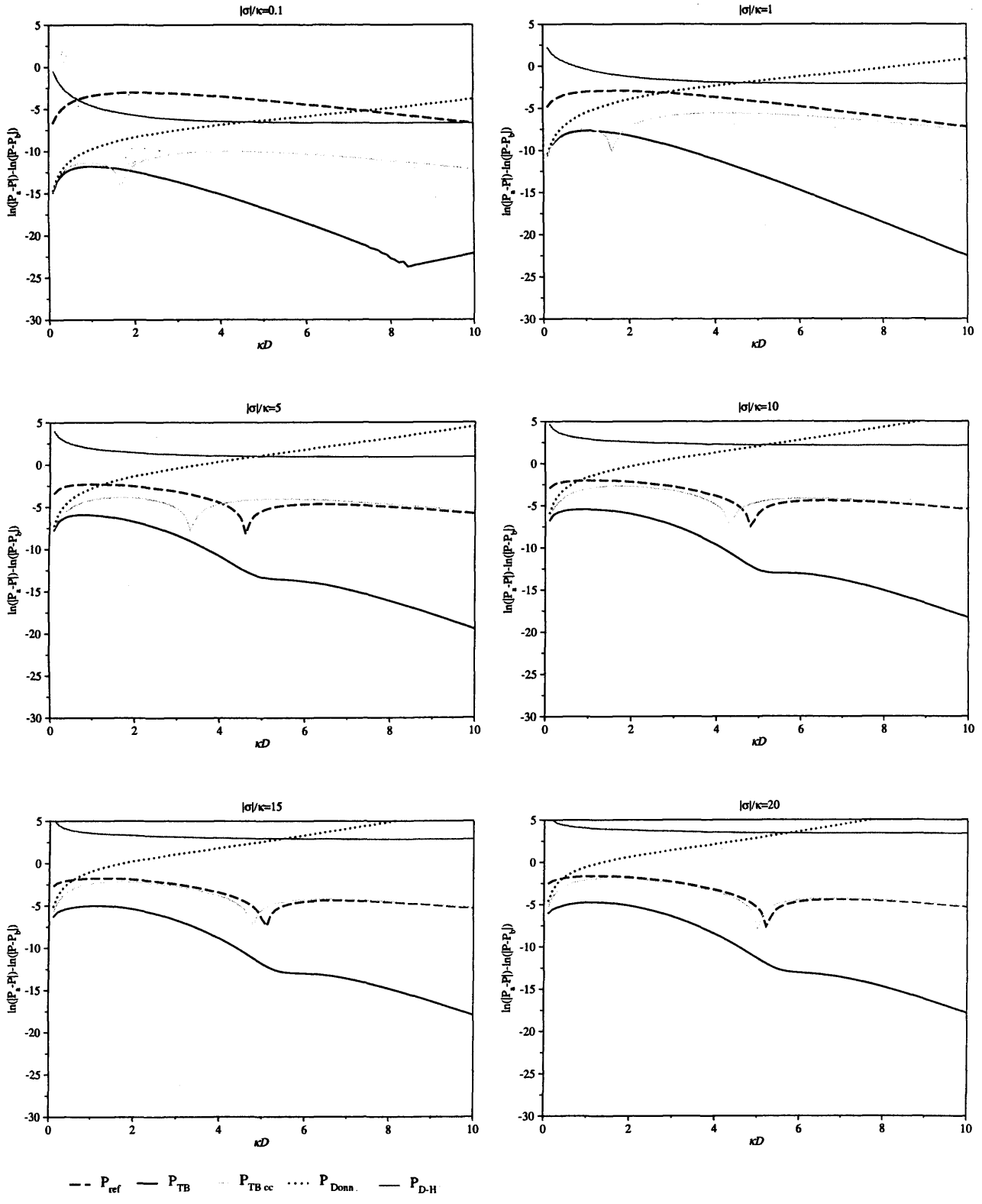

Figure 7.13: Logarithmic relative error for various approximations to the excess pressure $P - P_b$ (where $P_b = P_\infty$) against plate separation κD. The key relates each line to one approximate pressure estimation method P_a. P_{TB} refers to a numerical solution of the new linearisation scheme, P_{TBcc} the approximate solution to the new linearisation, P_{ref} is the pressure calculated using the reference potential $\Phi_L^{(0)} + \Phi_R^{(0)} - \mu_{el}^{(1)}$ alone, P_{D-H} is for the Debye-Hückel linearisation about $\Phi = 0$ and P_{Donn} is a linearisation about the Donnan potential $\langle\Phi\rangle$. The upward turn in the error for P_{TB} at $|\sigma|/\kappa = 0.1$ for large κD is a due to numerical errors as a result of the small numbers involved.

Chapter 8

Suspension of spherical particles

8.1 Introduction

In this chapter the new linearisation scheme outlined in Chapter 6 will be applied to the calculation of thermodynamic properties of colloidal suspensions in three dimensions. The system, which was described in Chapter 5, consists of a perfect lattice of identical spherical colloidal particles. The particles carry a fixed uniform surface charge, and are suspended in a polar solvent containing a low concentration of univalent microions which are taken to be in the grand ensemble. Calculations will be done on spherical W-S cells as well as simple cubic W-S cells so that comparisons can be made between them.

For comparative purposes, the same parameters as those in [87] are used. These parameters translate to macroions of radius $a = 133$ nm carrying between $Z = 100 - 3500$ electron charges corresponding to surface charge densities of $\sigma = 4.4 \times 10^{-4} - 1.6 \times 10^{-2}$ nm^{-2}. The salt bath concentration is taken to be $n_b = 3.6\mu M$ or 2.17×10^{-6}nm^{-3}. This equates to around 21 salt ions in a volume equal to the volume of one macroion $V_f = (4/3)\pi a^3$. The resulting screening length is $\lambda_D = 160$nm. As in previous calculations, the temperature is taken to be around $T = 300K$ and the relative permittivity of water $\epsilon = 76$, resulting in the Bjerrum length $l_B = 0.72$ nm.

These calculations may be seen as an investigation into the relevance of the W-S cell geometry. The W-S cell geometry determines the symmetry imposed on the mean field potential $\Phi(\mathbf{r})$ and distribution functions $\rho_{\pm}(\mathbf{r})$. By choosing the W-S cell to have the same geometry as the macroions, the spherical W-S cell achieves the considerable simplification of making the solution of the mean field equations a one-dimensional problem. Solving the mean field equations for a cubic W-S cell with a spherical macroion at its centre is significantly harder. In the PB formulation this requires the solution of a nonlinear partial differential equation.

In Section 8.2 the new linearisation technique is applied to spherical W-S cells, where comparisons are made to the exact solution of the PB equation. This system has been studied extensively in the literature, for example in references [88, 87]. In section 8.3, the method will be applied to solving the PB equations for spherical macroions in simple cubic W-S cells. Systems in which the macroions and their surrounding W-S cells have different geometries are less well studied in the literature.

Comparisons between spherical and cubic W-S cell geometries were made by Groot [110] using Monte Carlo (MC) simulations. This means that microion-microion correlations were included that are neglected within mean field theory. The spherical cell simulated by Groot also differs from the the W-S cell model in mean field theory because the boundary condition for the electrostatic field to vanish on the W-S cell boundary was not enforced (though the integral over the entire boundary will have been zero due to charge neutrality). This means that the spherical cell simulated by Groot did not correctly account for interactions between W-S cells beyond the confinement effect. The cubic cell

simulated by Groot included these interactions through the use of periodic boundary conditions, and the Ewald summation technique for the evaluation of the long-range electrostatic interactions. These simulations over-represented correlations between neighbouring cells by making all of the microionic configurations in the entire lattice identical for every MC configuration. The simulations also have the disadvantage of only being able to handle low-valency macroions (with a maximum charge of $Z \sim 500$) due to the computational expense of increasing the number of degrees of freedom.

8.2 Spherical Wigner-Seitz cell

8.2.1 Poisson-Boltzmann Equation

In the spherical W-S cell approximation, the Poisson-Boltzmann equation reduces to an ordinary differential equation. In the microionic region the PB equation is

$$\frac{d^2\Phi}{dr^2} + \frac{2}{r}\frac{d\Phi}{dr} = \kappa^2 \sinh \Phi(r) \tag{8.1}$$

with boundary conditions

$$\left.\frac{d\Phi}{dr}\right|_{r=a} = -4\pi l_B \sigma \qquad \text{and} \qquad \left.\frac{d\Phi}{dr}\right|_{r=R} = 0 \tag{8.2}$$

where σ is surface charge density of the macroion, and R is the W-S cell radius for a system with a volume fraction $\phi = a^3/R^3$.

8.2.2 Exact numerical solution

Equation (8.1) is a nonlinear ordinary differential equation. The two boundary conditions (8.2) at $r = a$ and $r = R$ make this a two-point boundary value problem [95]. Solutions are obtained by iteratively solving an initial value problem with the gradient specified at $r = a$ as in (8.2) and a guess for the value of the surface potential $\Phi(a) = M$. The correct value of M will result in a solution $\Phi(r)$ that satisfies the second boundary condition in (8.2), which requires gradient at $r = R$ to vanish.

Since the macroionic charge has been taken to be negative $Z < 0$, the microionic charge density within the W-S cell will generally be positive $\rho > 0$, becoming smaller towards the boundary of the cell. As the volume of the W-S cell increases, the microionic charge density at the W-S cell boundary $\rho(R)$ tends to zero. The mean field electrostatic potential Φ satisfying the PB equation (8.1) and its second derivative $\nabla^2\Phi$ will be negative within the W-S cell, whilst the first derivative is greater than or equal to zero. As $R \to \infty$ the potential at the W-S cell boundary $\Phi(R)$ tends to zero, which is a consequence of our choice that the constant $\mu_{el} = 0$.

Values of the surface potential M above a critical value lead to solutions for which Φ diverges to $+\infty$ for large r. Values below this critical value lead to potentials for which $\Phi(r)$ diverges to $-\infty$ as r increases, but with $\Phi(r)$ passing through a maximum at which the derivative $d\Phi/dr$ is zero. The critical value of M is the surface potential for an isolated macroion in an infinitely large W-S cell, and corresponds to the surface potential for the isolated solution $\Phi^{(0)}(a)$. Values of M lower than this give solutions for finite W-S cells. The radius at which Φ is a maximum corresponds to the W-S cell radius R. Smaller (more negative) values of M give rise to smaller cell radii R.

To obtain numerical solutions to the nonlinear PB equation our strategy is to sweep through different values of M from a minimum value up to the maximum $M = \Phi^{(0)}(a)$. For each of these values, the initial value problem is solved numerically. From these solutions the radius $r = R$ for which $d\Phi/dr = 0$ is obtained, which is the W-S cell radius the solution corresponds to. This method avoids the iterations necessary to find solutions for R specified a priori, and provides solutions for a

range of R.

8.2.3 The isolated macroion

As the volume fraction goes to zero, the W-S cell volume and radius tend to infinity, and $\Phi(\mathbf{r})$ tends towards the solution for an isolated macroion $\Phi^{(0)}$. As long as the surface charge density σ on the spherical macroion is uniform, the solution for an isolated macroion is expected to be spherically symmetric, and can be regarded as the limit of the solution for a spherical W-S cell with infinite volume. Solutions to the nonlinear PB equation for isolated macroions are required because they are used to construct the reference potential about which the PB equation is linearised in the new linearisation scheme proposed in Chapter 6, for both the spherical and non-spherical W-S cell geometries.

To obtain the solution to the nonlinear PB equation for an isolated macroion, iterative solution of the initial value problem described above is employed to find the critical value $M = \Phi^{(0)}(a)$. A solution with this value of the surface potential and the gradient at $r = a$ specified as in (8.1) is the solution of the PB equation for an isolated macroion $\Phi^{(0)}(r)$.

The numerical solution is obtained up to a large radius R_0, where the potential is very close to zero. Beyond this point, a linearised ansatz can be used to give $\Phi^{(0)}(r)$ at arbitrarily large radii. A sphere with the large radius R_0, will contain most of the microionic charge required to neutralise the charge Z carried by the macroion. This sphere is then like a very slightly charged large particle with radius R_0. The amount of charge contained in the sphere Z^* is obtained from the gradient of the numerical solution at R_0

$$\left.\frac{d\Phi^{(0)}}{dr}\right|_{r=R_0} = -l_B\frac{Z^*}{R_0^2} \tag{8.3}$$

The radius R_0 has been chosen to be sufficiently large so that Z^* is very small, and $\Phi^{(0)}(R_0)$ is close to zero. This allows the use of the Debye-Hückel solution for radii beyond R_0

$$\Phi^{(0)}_{r>R_0}(r) = -\frac{l_B Z^* \exp\left(-\kappa(r-R_0)\right)}{(1+\kappa R_0)r} \tag{8.4}$$

8.2.4 New linearisation scheme

In Chapter 6 a new linearisation scheme for the PB equation was introduced for a lattice of colloidal particles. The Poisson-Boltzmann equation was linearised about a reference potential consisting of the superposition of potentials $S(\mathbf{r})$ given by

$$S(\mathbf{r}) = \sum_n \Phi_n^{(0)} \tag{8.5}$$

where the $\Phi_n^{(0)}$ are (spherically symmetric) solutions to the PB equation for an isolated macroion carrying surface charge density σ, centred at the nth lattice site. The reference potential (8.5) has the property that the normal derivative of S on the surface of the corresponding W-S cell boundary vanishes.

The analogue to this reference potential in the spherically symmetric geometry is obtained by taking

$$S(r) = \Phi^{(0)}(r) + \Phi^{(0)}(2R - r) \tag{8.6}$$

where the first term is the isolated solution centred within the W-S cell, and $\Phi^{(0)}(2R-r)$ takes the place of the superposition of the isolated solutions centred at all of the other cells in an infinite lattice. The superposition (8.6) satisfies one of the boundary conditions in (8.2), namely that the gradient at $r = R$ vanishes. The gradient of S at $r = a$ is different from the required gradient which

is a consequence of the difference between the amount of microionic charge contained in the correct solution Φ and in the reference potential S.

$$\left.\frac{dS}{dr}\right|_{r=a} = -4\pi l_B \sigma + Q_i \qquad \text{where} \qquad Q_i = -\left.\frac{d\Phi^{(0)}}{dr}\right|_{r=2R-a} \tag{8.7}$$

As described in Chapter 6, a constant $\mu_{el}^{(1)}$ is subtracted from S to make the reference potential more effective. This constant has the property of making the reference charge density $\rho^{(1)}$ satisfy

$$\int_{Wo} 2n_b \sinh(S(\mathbf{r}) - \mu_{el}^{(1)}) d\mathbf{r} = Z \tag{8.8}$$

where the integral is over the outer region of the W-S cell.

To proceed with the linearisation, the right hand side of equation (8.1) is expanded to first order in the deviations $\epsilon = \Phi - S + \mu_{el}^{(1)}$

$$\frac{d^2\Phi}{dr^2} + \frac{2}{r}\frac{d\Phi}{dr} \simeq \kappa^2 \sinh(S(r) - \mu_{el}^{(1)}) + \left(\Phi(r) - S(r) + \mu_{el}^{(1)}\right) \kappa^2 \cosh(S(r) - \mu_{el}^{(1)}) \tag{8.9}$$

where $\Phi(r)$ satisfies the boundary conditions (8.2). This linear ordinary differential equation in terms of $\Phi(r)$ can be solved numerically using standard methods without much difficulty. The numerical solution for the isolated macroion $\Phi^{(0)}(r)$ is used as input for the construction of $S(r) - \mu_{el}^{(1)}$ before solving for the linearised potential $\Phi(r)$.

8.2.5 Traditional linearisations

In the traditional linearisation schemes the PB equation (8.1) is solved by linearising Φ in deviations $\Delta\Phi$ from a constant potential. In the Debye-Hückel (D-H) linearisation scheme, the potential is expanded about $\Phi = 0$. This is the limit of Φ far away from the macroion in the low density limit if the constant μ_{el} has been set to zero. In an alternative scheme Φ is linearised about the mean of the potential (or the Donnan potential) $\langle\Phi\rangle$. von Grünberg *et. al.* [87] showed that while the linearisation about the Donnan potential performs better at high packing fractions ϕ, it leads to spurious negative compressibilities for low ϕ when the charge on the macroions is large.

The D-H linearisation proceeds by expanding the right hand side of (8.1) to first order in Φ

$$\nabla^2\Phi \simeq \kappa^2\Phi \tag{8.10}$$

This equation is solved subject to the boundary conditions (8.2), giving the solution

$$\Phi_{DH}(r) = -4\pi l_B Z a^2 \left[A\frac{\exp(-\kappa r)}{r} + B\frac{\exp(+\kappa r)}{r}\right] \tag{8.11}$$

where

$$A = \exp(\kappa(a+2R))(\kappa R - 1)\Gamma \qquad \text{and} \qquad B = \exp(\kappa a)(\kappa R + 1)\Gamma \tag{8.12}$$

and

$$\Gamma = \frac{1}{(\kappa a + 1)(\kappa R - 1)\exp(2\kappa R) - (\kappa a - 1)(\kappa R + 1)\exp(2\kappa a)} \tag{8.13}$$

The linearisation about the Donnan potential $\langle\Phi\rangle$ is obtained by expanding (8.1) in the deviations $\Delta\Phi = \Phi - \langle\Phi\rangle$

$$\nabla^2\Delta\Phi \simeq \kappa^2 \sinh\langle\Phi\rangle + \Delta\Phi\kappa^2 \cosh\langle\Phi\rangle \tag{8.14}$$

By introducing a new effective screening length $\bar{\kappa}^2 = \kappa^2 \cosh\langle\Phi\rangle$, this equation is rewritten as

$$\nabla^2 \Delta\Phi \simeq \bar{\kappa}^2 \tanh\langle\Phi\rangle + \bar{\kappa}^2 \Delta\Phi \tag{8.15}$$

Since $\langle\Phi\rangle$ is a constant, $\Delta\Phi$ must satisfy the same boundary conditions as Φ given in (8.2). The solution is given by

$$\Phi_{\text{Donn}}(r) = \langle\Phi\rangle - \tanh\langle\Phi\rangle - 4\pi l_B Z a^2 \left[\bar{A}\frac{\exp(-\bar{\kappa}r)}{r} + \bar{B}\frac{\exp(+\bar{\kappa}r)}{r}\right] \tag{8.16}$$

where $\bar{A}$ and $\bar{B}$ are the same as A and B but with κ replaced by $\bar{\kappa}$.

8.2.6 Pressure and compressibility comparisons

Figure 8.1 shows comparisons between various calculations of the excess pressure and its derivative as a function of packing fraction ϕ. Within the mean-field theory applied here, the pressure is given by the boundary density theorem discussed in Chapter 5. This relates the pressure to the total microion density at the W-S cell boundary $P = \rho_+(R) + \rho_-(R)$. The pressure of microions in the salt bath is $P_b = 2n_b$, and a dimensionless excess pressure can be defined as $P/2n_b - 1$.

The derivative of the pressure with respect to ϕ is related to the isothermal compressibility χ through $\partial P/\partial\phi = (\eta_f \chi)^{-1}$, where

$$\chi^{-1} = \eta_f \frac{\partial P}{\partial \eta_f} \tag{8.17}$$

η_f is the macroion density.

Estimates based on the Debye-Hückel linearisation and the new linearisation scheme described in Section 8.2.4 are compared to results from exact numerical solutions to the nonlinear PB equation in Figure 8.1 . The Donnan linearisation was omitted since von Grüenberg [87] pointed out that this gives spurious results for low packing fractions. Also shown for comparison is the pressure calculated using the reference potential $S - \mu_{el}^{(1)}$ alone.

What can be seen is the failure of the D-H linearisation, with the exception of the low density and low surface charge regime. The new linearisation scheme succeeds in following the exact solutions closely for the range of parameters shown here. Even for the largest volume fraction $\phi = 0.6$ corresponding to a W-S cell radius of $R = 1.2a$, deviations from the exact pressure and compressibility are negligibly small. It can also be seen that the deviation potential $\epsilon = \Phi - S + \mu_{el}^{(1)}$ makes an important contribution to the pressure calculations, especially for higher ϕ and for large $|Z|$ when the pressure calculated using the reference potential $S - \mu_{el}^{(1)}$ deviates significantly from the exact potential.

8.2.7 Salt content

None of the results in Figure 8.1 display a negative compressibility, indicating that for the parameters used, phases with a homogeneous density remain stable. This feature will persist for the fixed salt problem as well. However, the P-V diagram is expected to be qualitatively different for this case. For the calculations shown here (at fixed chemical potential μ_b) the number of salt particles N_s in the system varies with volume. Figure 8.2 shows the ratio of salt particles to macroion charge $N_s/|Z|$ as a function of volume for the three cases studied in Section 8.2.6.

Solution of the exact nonlinear PB equation for the fixed salt problem is difficult due to the interdependence between n_0 and Φ. Numerically this requires a doubly iterative routine to find solutions for a given cell radius R and quantity of salt particles N_s. For each volume, this requires finding the value of the Lagrange multiplier μ for which the number of particles is N_s. Using the new linearisation scheme, this can be done more efficiently as only one set of iterations is required to ensure the correct number of salt particles. Using the linearised equation, we have implemented a

scheme whereby for a given value of $n_0 = \lambda^{-3}\exp(\mu)$, the correct cell radius R was obtained to ensure the correct quantity of salt in the system. The initial results however, did not display qualitatively different behaviour to the results in Section 8.2.6. Further studies are planned to investigate the fixed-salt scenario in more detail.

8.3 Simple cubic Wigner-Seitz cell

8.3.1 Geometry and symmetry

To extend the new linearisation method to a non-spherical geometry, it will be applied here to the calculation of pressure versus packing fraction for a simple cubic lattice (SC) of macroions. The simple cubic lattice (described in 5.5.2) has a geometry with a high degree of symmetry, and as such is not too dissimilar from the spherical geometry. It should also be pointed out that colloidal crystals tend to form close packed structures rather than a SC geometry. Nevertheless, the SC lattice is used here for simplicity.

With lattice spacing D, the system consists of macroions centred at sites described by the position vectors $\mathbf{R}_{lmn} = l\mathbf{r_1} + m\mathbf{r_2} + n\mathbf{r_3}$, where $\mathbf{r_1}, \mathbf{r_2}, \mathbf{r_3}$ are lattice vectors of length D which we take to point in the $\hat{\mathbf{i}}, \hat{\mathbf{j}}$ and $\hat{\mathbf{k}}$ directions respectively, and l, m, n are integers. The W-S cell is a cube with sides of length D containing a single macroion at its centre. As discussed in 5.5.2, the mean field potential $\Phi(\mathbf{r})$ and distribution of microions $\rho_{\pm}(\mathbf{r})$ in this geometry possess the full symmetry of the octahedral group O, which contains 48 symmetry operations.

8.3.2 Poisson-Boltzmann equation

In this geometry it is convenient to use Cartesian coordinates. The PB equation in the microionic region may be written as

$$\frac{\partial^2\Phi}{\partial x^2} + \frac{\partial^2\Phi}{\partial y^2} + \frac{\partial^2\Phi}{\partial z^2} = \kappa^2 \sinh\Phi(\mathbf{r}) \tag{8.18}$$

Since the microions are not able to penetrate the macroions, the inner region must satisfy

$$\nabla^2\Phi = 0 \quad \text{for} \quad r < a \tag{8.19}$$

The periodicity and charge neutrality conditions prescribe that the electric field vanishes at the W-S cell boundary, so

$$\nabla\Phi \cdot \mathbf{n} = 0 \tag{8.20}$$

at the W-S cell boundaries, where $\mathbf{n}$ is a vector perpendicular to the W-S cell boundary (this equation is given in expanded form in equations 5.55-5.57).

8.3.3 New linearisation scheme

The new linearisation scheme was introduced in Chapter 6. The first step is to construct the superposition of potentials $S(\mathbf{r})$ for isolated macroions positioned at the lattice sites $\mathbf{R}_{lmn}$.

$$S(\mathbf{r}) = \sum_{l,m,n} \Phi^{(0)}(|\mathbf{r} - \mathbf{R}_{lmn}|) \tag{8.21}$$

where $\Phi^{(0)}$ is the spherically symmetric solution for an isolated macroion centred at the origin.

As before, in order to make the linearisation more effective a constant $\mu_{el}^{(1)}$ is obtained which satisfies equation (8.8). The reference potential then consists of $S(\mathbf{r}) - \mu_{el}^{(1)}$. The PB equation (8.18)

is linearised about this to give an equation for the deviation potential $\epsilon = \Phi - S + \mu_{el}^{(1)}$

$$\frac{\partial^2 \epsilon}{\partial x^2} + \frac{\partial^2 \epsilon}{\partial y^2} + \frac{\partial^2 \epsilon}{\partial z^2} \simeq P(\mathbf{r})\epsilon(\mathbf{r}) + F(\mathbf{r}) \tag{8.22}$$

where the functions $P(\mathbf{r})$ and $F(\mathbf{r})$ are defined as

$$P(\mathbf{r}) = \kappa^2 \cosh(S(\mathbf{r}) - \mu_{el}^{(1)}) \tag{8.23}$$

and

$$F(\mathbf{r}) = \kappa^2 \sinh(S(\mathbf{r}) - \mu_{el}^{(1)}) - \sum_{\substack{l,m,n \neq \\ 0,0,0}} \kappa^2 \sinh \Phi^{(0)}(|\mathbf{r} - \mathbf{R}_{lmn}|) \tag{8.24}$$

[1] Equation (8.22) is a linear partial differential equation for $\epsilon(\mathbf{r})$, and takes the place of the nonlinear PB equation when the proposed linearisation approximation is valid, which occurs for large κD.

For the inner region $r < a$, Φ satisfies the Laplace equation in (8.19), so $\epsilon(\mathbf{r})$ must satisfy

$$\nabla^2 \epsilon = - \sum_{\substack{l,m,n \neq \\ 0,0,0}} \kappa^2 \sinh \Phi_{lmn}^{(0)} \tag{8.25}$$

It will be convenient to extend the definitions of $P(\mathbf{r})$ and $F(\mathbf{r})$, so that Equation (8.22) becomes (8.25) in the inner region. This means that when $r < a$, $P = 0$ and F is given by the right hand side of (8.25).

In Chapter 6 it was also found that the boundary condition on $\epsilon(\mathbf{r})$ at the W-S cell boundary is that the normal derivative vanishes

$$\nabla \epsilon \cdot \mathbf{n} = 0 \tag{8.26}$$

where $\mathbf{n}$ is a vector perpendicular to the boundary.

8.3.4 Method of solution

In the model employed here, the macroions are assumed to reside at the sites of a perfect, infinite lattice. The mean field equations are assumed to give rise to a potential $\Phi(\mathbf{r})$ and distribution of microions $\rho_{\pm}(\mathbf{r})$ that possess the periodicity and symmetry of this lattice. The function $\epsilon(\mathbf{r})$ must have both of these properties in common with $\Phi(\mathbf{r})$ and $\rho_{\pm}(\mathbf{r})$.

The periodicity motivates searching for a solution to (8.22) in Fourier space. Expanding $\epsilon(\mathbf{r})$ in a Fourier series, ensures that it possesses the periodicity required. The symmetries that must be satisfied by $\epsilon(\mathbf{r})$ require certain terms in the Fourier series to have the same Fourier coefficient. A Fourier series may be constructed by employing a set of basis functions $E_{lmn}(\mathbf{r})$ in which such terms have been grouped together

$$\begin{aligned} E_{lmn}(\mathbf{r}) = & \cos[\frac{2\pi}{D}lx] \cos[\frac{2\pi}{D}my] \cos[\frac{2\pi}{D}nz] + \\ & \cos[\frac{2\pi}{D}nx] \cos[\frac{2\pi}{D}ly] \cos[\frac{2\pi}{D}mz] + \\ & \cos[\frac{2\pi}{D}mx] \cos[\frac{2\pi}{D}ny] \cos[\frac{2\pi}{D}lz] + \\ & \cos[\frac{2\pi}{D}lx] \cos[\frac{2\pi}{D}ny] \cos[\frac{2\pi}{D}mz] + \\ & \cos[\frac{2\pi}{D}nx] \cos[\frac{2\pi}{D}my] \cos[\frac{2\pi}{D}lz] + \\ & \cos[\frac{2\pi}{D}mx] \cos[\frac{2\pi}{D}ly] \cos[\frac{2\pi}{D}nz] \end{aligned} \tag{8.27}$$

[1] Note that $F(\mathbf{r})$ and $P(\mathbf{r})$ are the names given to these functions in this context, and they do not denote free energy or pressure.

These functions are invariant under all 48 point group symmetry operations belonging to the octahedral group O. They also possess the correct periodicity, making each W-S cell invariant under translations by lattice vectors $\mathbf{R}_{lmn}$. The boundary condition (8.26) is implicitly satisfied by the functions E_{lmn}. It is also clear that this basis is orthogonal so that

$$\int_W E_{lmn}(\mathbf{r})E_{l'm'n'}(\mathbf{r})d\mathbf{r} \propto \delta_{ll'}\delta_{mm'}\delta_{nn'} \tag{8.28}$$

where δ_{ij} is the Kronecker Delta. The constant of proportionality varies for different combinations of lmn.

The solution to the linearised differential equation (8.22) is expanded in this basis

$$\epsilon(\mathbf{r}) = \sum_{l\geq m\geq n\geq 0} A_{lmn}E_{lmn}(\mathbf{r}) \tag{8.29}$$

where the summation runs only over the irreducible volume of reciprocal space defined by $l \geq m \geq n \geq 0$, reflecting the built-in symmetry of the E_{lmn} functions. A solution $\epsilon(\mathbf{r})$ to the linearised differential equation must now be found in terms of the coefficients A_{lmn}. This is done by substituting (8.29) into the differential equation (8.22), which gives

$$-\sum_{l\geq m\geq n\geq 0} \left(\mathbf{k}_{lmn}^2 + P(\mathbf{r})\right) A_{lmn}E_{lmn}(\mathbf{r}) = F(\mathbf{r}) \tag{8.30}$$

where the reciprocal vector is defined as $\mathbf{k}_{lmn} = (2\pi/D)(l, m, n)$.

To proceed, the W-S cell volume is discretised into a set of evenly spaced points denoted by $\mathbf{r}_{ijk}$ where the indices i, j, k determine the position of the points in the x, y, z directions respectively. It can be shown that the functions $E_{lmn}(\mathbf{r})$ are orthogonal over discrete points evenly spaced over the periodicity interval (the W-S cell), so that a relation analogous to the integral relation (8.28) is valid for a sum over the discrete points [2]

$$\sum_{ijk} E_{lmn}(\mathbf{r}_{ijk})E_{l'm'n'}(\mathbf{r}_{ijk}) \propto \delta_{ll'}\delta_{mm'}\delta_{nn'} \tag{8.31}$$

This property allows equation (8.30) to be converted into a set of linearly independent simultaneous equations for the unknown coefficients A_{lmn}

$$-\sum_{l\geq m\geq n\geq 0} \left(\mathbf{k}_{lmn}^2 + P(\mathbf{r}_{ijk})\right) A_{lmn}E_{lmn}(\mathbf{r}_{ijk}) = F(\mathbf{r}_{ijk}) \tag{8.32}$$

A new indexing system is introduced in which one integer i is assigned to each of the discrete points in real space $\mathbf{r}_{ijk}$ and one integer j is assigned to each point in reciprocal space $\mathbf{k}_{lmn}$. Equation (8.32) is then written as

$$-\sum_j \left(\mathbf{k}_j^2 + P(\mathbf{r}_i)\right) A_j E_j(\mathbf{r}_i) = F(\mathbf{r}_i) \tag{8.33}$$

or in more compact form

$$-\sum_j \left(\mathbf{k}_j^2 + P_i\right) A_j E_{ij} = F_i \tag{8.34}$$

If the number of evenly spaced points in real space is taken to equal the number of points for which coefficients are sought in reciprocal space N_{pt}, then a non-trivial solution for the A_{lmn} can be found. In fact, to get the correct number of independent equations, the N_{pt} real-space points $\mathbf{r}_{ijk}$ must lie

[2] The phenomenon of Aliasing may occur in a discrete Fourier series [111, 112], whereby higher frequency terms emulate lower frequencies. This means that arguments such as l, l' in the Kronecker Deltas of (8.31) should be replaced by $l, l' \pm 2qN_{pts}$ where q is an integer.

within an irreducible volume of the W-S cell such as $x \geq y \geq z \geq 0$. Defining the matrix M as $M_{ij} = -\left(\mathbf{k}_j^2 + P_i\right) E_{ij}$, (8.34) may be written as the matrix equation

$$M \cdot A = F \tag{8.35}$$

where A and F are column vectors with components A_j and F_i as in (8.34). A solution to the simultaneous equations provides the Fourier coefficients A_{lmn}, and is obtained by numerically inverting M to give

$$A = M^{-1} \cdot F \tag{8.36}$$

A solution $\epsilon(\mathbf{r})$, together with the superposition of potentials $S(\mathbf{r})$ is plotted in Figure 8.3 for packing fraction $\phi = 0.1$ and the same system parameters as used in the case of spherical W-S cells.

Convergence

For this approach to be effective, the series for $\epsilon(\mathbf{r})$ given in (8.29) must converge after a finite number of terms. If the index l runs from 0 to N_{pt}, then there will be $N_T = (N_{pt}+1)(N_{pt}+2)(N_{pt}+3)/6$ terms in the series, corresponding to the number of reciprocal lattice vectors $\mathbf{k}_{lmn}$ for which $l \geq m \geq n \geq 0$. Obtaining a solution $\epsilon(\mathbf{r})$ is numerically challenging, since the number of points N_T increases rapidly with N_{pt}, which in turn increases the size of the matrix M which has dimensions $N_T \times N_T$. This puts a limit on the computational feasibility of the approach.

The main obstacle to convergence comes from the discontinuity at the spherical boundary $r = a$, where the equation for $\epsilon(\mathbf{r})$ changes. The spherical boundary is incommensurate with the cubic grid on which the points $\mathbf{r}_{ijk}$ are defined, and a sufficient number of points must be taken to accurately resolve the curved boundary. This difficulty is an inherent feature of any treatment for which the macroionic and W-S cell geometries are different.

For our purposes, convergence is defined by the requirement that the pressure P changes negligibly when the number of points N_{pt} is increased. For the parameters used in this study, it was found that N_{pt} between 15 and 20 was sufficient to achieve convergence.

8.3.5 Comparisons between pressure in the spherical and cubic geometries

In Section 5.6.5, the Boundary Density theorem was extended to the cubic geometry with the result that the pressure P is given by

$$P = \langle \rho_+ + \rho_- \rangle_{surf} \tag{8.37}$$

where the average is over the W-S cell boundary or surface. Plugging solutions $\epsilon(\mathbf{r})$ into this equation, and keeping terms up to second order in $\epsilon(\mathbf{r})$, the pressure P corresponding to the linearised PB equation is obtained. Figures 8.4-8.6 show the dimensionless excess pressure against packing fraction calculated in this way, for three different values of Z. Also shown on these plots is the pressure for spherical W-S cells of the same packing fraction, obtained from solutions to the nonlinear Poisson-Boltzmann equation. It can be seen that for low packing fractions, pressures from the spherical and cubic W-S cells are very similar. Deviations occur at higher packing fractions, especially for the more highly charged spheres with $Z = -1000$ and $Z = -3500$. It is not entirely clear whether these deviations arise from failure of the linearisation approximation employed in obtaining $\epsilon(\mathbf{r})$ for the cubic W-S cells, or if they represent a genuine difference between the spherical and cubic W-S cells. Using the new linearisation scheme, it was shown in Figure 8.1 that for the case of spherical W-S cells the linearisation approximation holds up to very high packing fractions, even for the most highly charged colloidal particles $Z = -3500$. This does not necessarily mean that the linearisation scheme works over the same range of parameters for cubic W-S cells. To illustrate this, Figure 8.7 shows $\epsilon(\mathbf{r})$ and the full potential $\Phi(\mathbf{r})$ for cubic and spherical W-S cells at two different packing fractions. The

potentials are plotted against distance from the centre of the cell r, and in the cubic case they are plotted for various directions denoted by Miller indices in brackets. It can be seen that for a given packing fraction, the deviation potential in the cubic geometry has larger values in certain directions than in the spherically symmetric geometry. This indicates that the linearisation is likely to start breaking down at lower packing fractions for cubic W-S cells than spherical ones.

8.4 Summary

In this chapter the new linearisation technique was applied to a system consisting of identical, spherical colloidal particles carrying a high amount of surface charge, arranged in a lattice. This method enabled efficient solution of the PB equation for cubic as well as spherical W-S cell geometries. In the spherical case, comparison with exact solutions to the nonlinear PB equation revealed that the method is reliable even at high packing fractions. A comparison between the spherical and cubic W-S cells was made by examining curves of pressure against packing fraction for the two cases. This revealed that the mean field thermodynamic behaviour in the two geometries is very similar. At high packing fractions the two approaches appear to differ for the most highly charged macroions. It is not clear whether this is a result of the linearisation approximation in the cubic case. Further studies will be required to resolve this question.

In both the spherical and cubic W-S cell geometries, the compressibility remained positive for the parameters used. This is consistent with the findings of von Grünberg, van Roij and Klein [87] that for the case of open systems, the nonlinear PB equation does not lead to instability of homogeneous phases. Although the behaviour will be qualitatively different due to the effect of salt density on the screening behaviour, the stability with respect to phase separation is expected to persist for a closed system containing a fixed amount of salt. The increased efficiency of the new linearisation technique means that it can be applied to the fixed salt case without too much computational difficulty. The increased range of validity as compared with the traditional linearisation schemes makes this approach more reliable, especially for systems with highly charged macroions.

For the spherical W-S cells, the extent to which the reference potential alone could reproduce the P-V characteristics was also investigated. Under certain conditions, this approach may be advantageous as it requires minimal further calculations beyond solution of the PB equation for an isolated macroion. This approach may be useful in situations where the traditional linearisations fail and obtaining an exact solution is unfeasible or difficult. One potential application of this approach is for the calculation of properties of disordered dilute suspensions of highly charged macroions, for which an exact or even a linearised solution to the PB equations is difficult to obtain. The superposition of isolated mean field potentials will automatically possess some of the features expected from solutions to the PB equation.

Another potential application of this approach is the calculation of 3-body interactions in charged colloidal suspensions. Löwen and Allahyarov [85] showed within the framework of a traditional linearisation scheme (about a constant microion density) that for a triangular arrangement of macroions, triplet interactions make a cohesive contribution to the effective potential between macroions. In their theory, triplet interactions occur as a correction to the free energy expansion, when cubic terms in the inhomogeneous microion distribution functions are included. This correction is calculated using the density distribution obtained from the quadratic expansion i.e. from the linearised theory. The cohesive effect of the 3-body interactions was shown to be stronger for more highly charged macroions. The drawback of the theory is that the linearised solutions, from which the correction is calculated, are not accurate for highly charged macroions. Several years later, van Roij *et. al.* [114] used finite element methods to calculate 3-body potentials from solutions to the nonlinear PB equation. These calculations confirmed that 3-body interactions are attractive, and become more cohesive for larger

Z and longer screening lengths.

Recent work by van Roij *et. al.* [113] involving simulations that included the 3-body potential obtained by van Roij *et. al.* previously [114], has highlighted the effect of 3-body interactions on the phase diagram of charged colloidal suspensions. Chatterji *et. al.* [115] have also performed simulations recently in which 3-body interactions were investigated by explicit simulation of the microions.

The expansion method proposed in Chapter 6 could be useful in developing an expansion similar to that of Löwen and Allahyarov, but which is applicable to larger Z, for which the triplet interactions are more cohesive. The 3-body interactions are essentially a result of enhanced screening of two macroions in the vicinity of a third macroion. The approach proposed in Chapter 6 has the essential ingredients required to reproduce this effect.

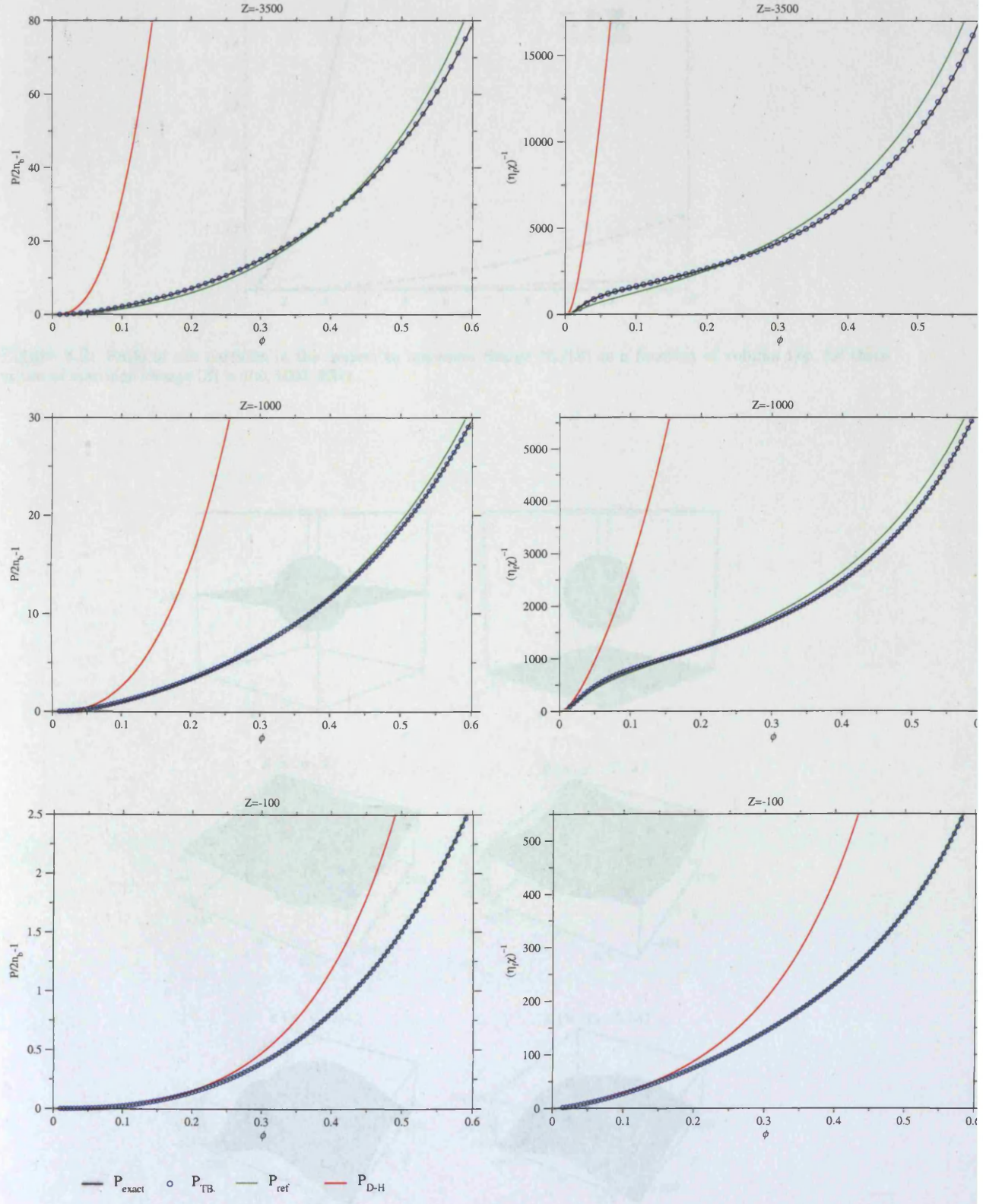

Figure 8.1: Dimensionless excess pressure and compressibility: comparison between various approximations and exact numerical solutions to the nonlinear Poisson-Boltzmann equation for a spherical W-S cell. Plots on the left display excess pressure $P/2n_b - 1$ vs. packing fraction ϕ, and plots on the right show the derivative of the pressure, which gives $(\eta_f \chi)^{-1}$ where $\eta_f = \phi/(4\pi a^3/3)$ is the macroion density, and χ is the isothermal compressibility. The three rows of graphs are for macroion charge $Z = -3500, -1000, -100$ respectively. The macroion radius is $a = 133$ nm and the salt reservoir density is $3.6\mu M$.

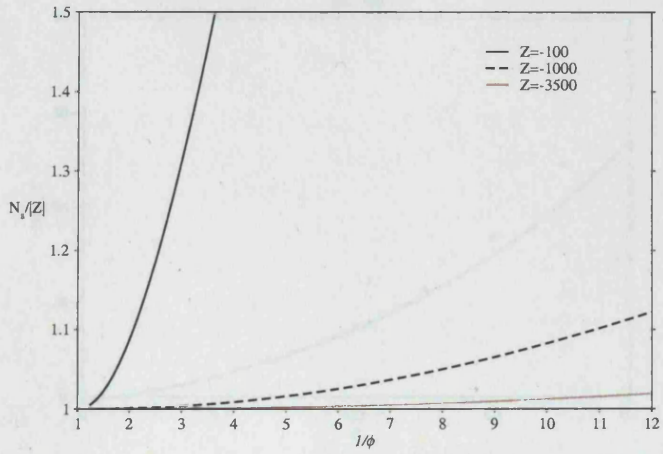

Figure 8.2: Ratio of salt particles in the system to macroion charge $N_s/|Z|$ as a function of volume $1/\phi$, for three values of macroion charge $|Z| = 100, 1000, 3500$.

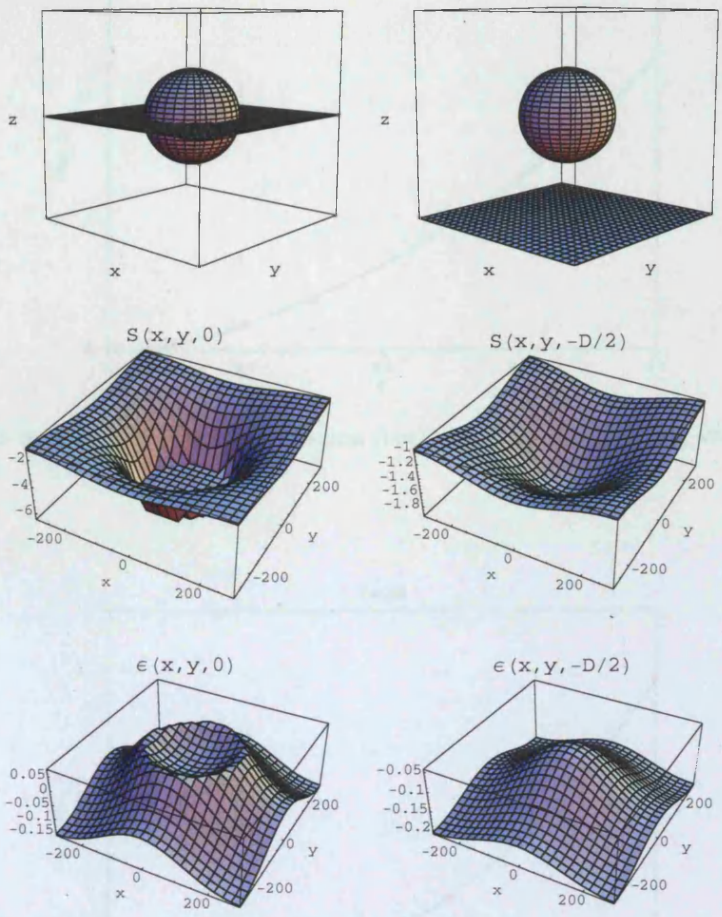

Figure 8.3: Cross-sectional plots in the $x-y$ plane of the potentials $S(\mathbf{r})$ (top row) and $\epsilon(\mathbf{r})$ (bottom row) for $z = 0$ (left column) and $z = -D/2$ (right column). The parameters used here were $Z = -3500$, $a = 133nm$, with packing fraction $\phi = 0.1$ and W-S cell cube length $D = 461.9nm$. The spatial dimensions are in nm and the energy axis is in units of k_BT. The diagrams on the topmost row illustrate the geometry of the system and show the planes for which the potentials are plotted in the two columns.

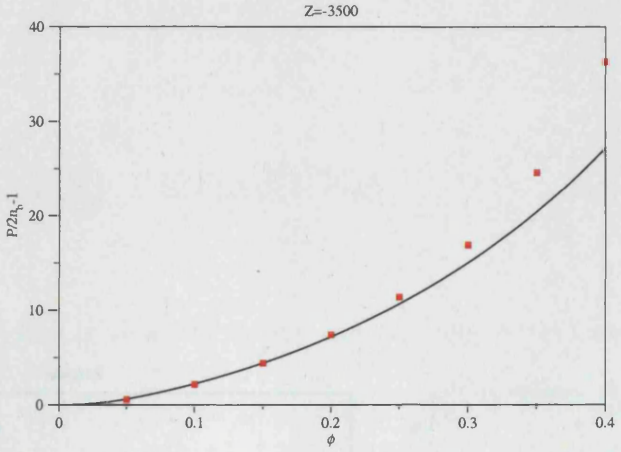

Figure 8.4: Pressure vs. packing fraction for a spherical (line) and simple cubic (points) W-S cell. The macroion valency is $Z = -3500$.

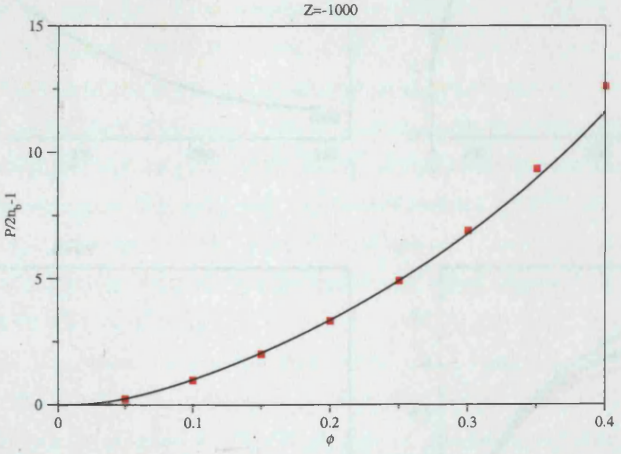

Figure 8.5: Pressure vs. packing fraction for a spherical (line) and simple cubic (points) W-S cell. The macroion valency is $Z = -1000$

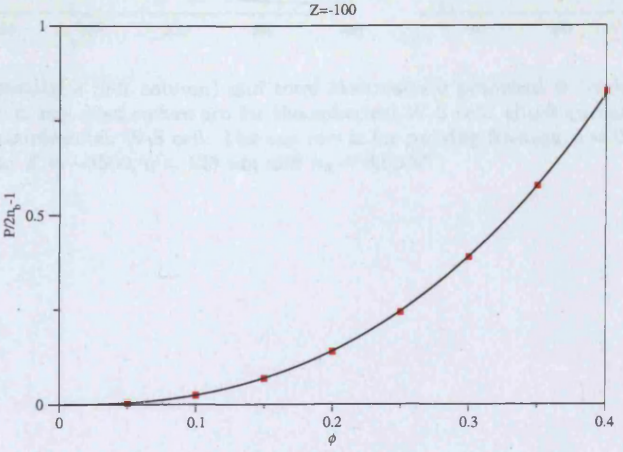

Figure 8.6: Pressure vs. packing fraction for a spherical (line) and simple cubic (points) W-S cell. The macroion valency is $Z = -100$

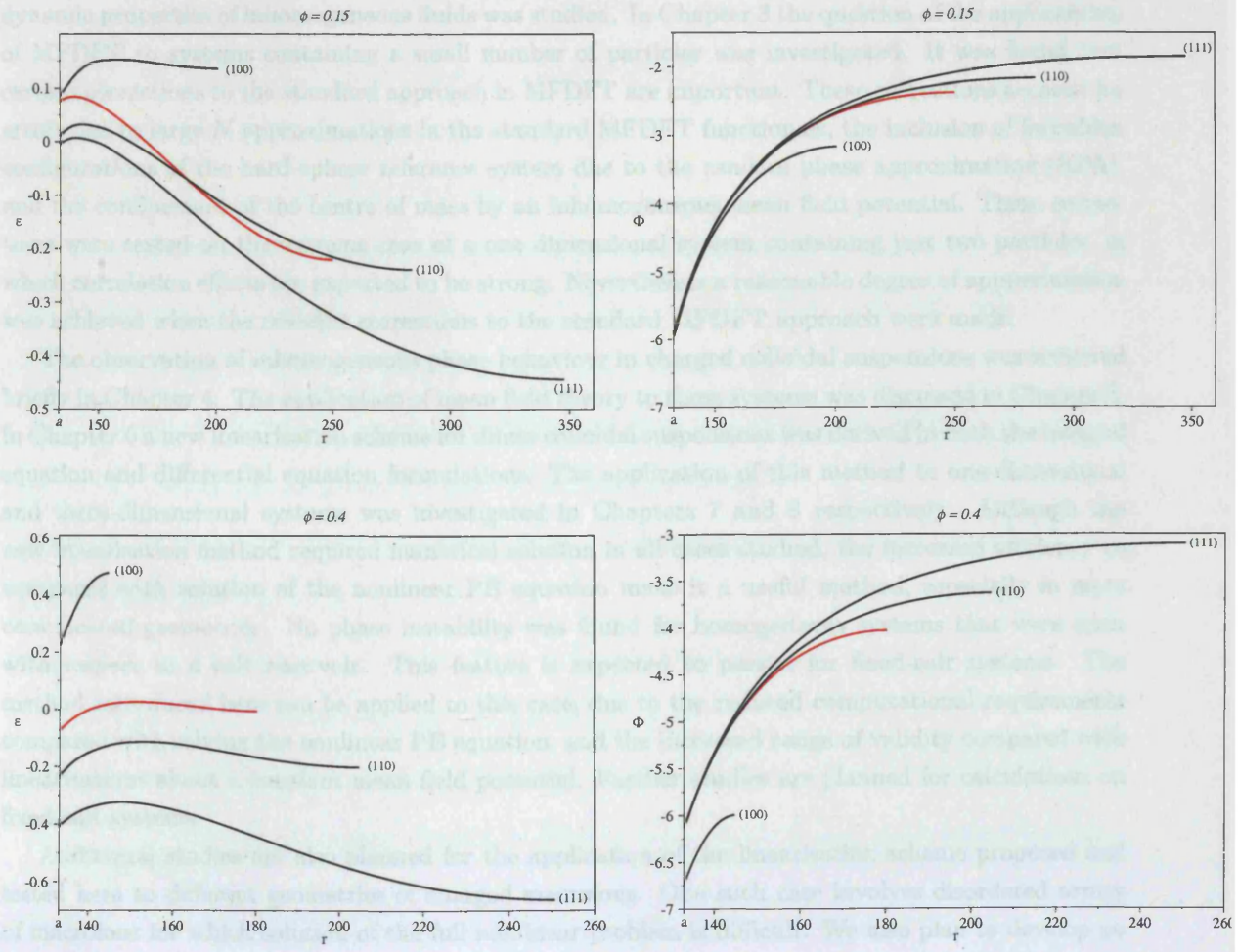

Figure 8.7: Deviation potential ϵ (left column) and total electrostatic potential Φ (right column) against distance from the centre of the cell r in nm. Red curves are for the spherical W-S cell. Black curves are for different directions (shown in brackets) in the simple cubic W-S cell. The top row is for packing fraction $\phi = 0.15$ and the bottom row for $\phi = 0.4$. System parameters: $Z = -3500$, $a = 133$ nm and $n_b = 3.6\mu M$.

Concluding remarks

In this thesis, the application of mean field density functional theory to the description of the thermodynamic properties of inhomogeneous fluids was studied. In Chapter 3 the question of the applicability of MFDFT to systems containing a small number of particles was investigated. It was found that certain corrections to the standard approach in MFDFT are important. These corrections account for errors due to large N approximations in the standard MFDFT functionals, the inclusion of forbidden configurations of the hard-sphere reference system due to the random phase approximation (RPA), and the confinement of the centre of mass by an inhomogeneous mean field potential. These corrections were tested on the extreme case of a one dimensional system containing just two particles, in which correlation effects are expected to be strong. Nevertheless a reasonable degree of approximation was achieved when the relevant corrections to the standard MFDFT approach were made.

The observation of inhomogeneous phase behaviour in charged colloidal suspensions was reviewed briefly in Chapter 4. The application of mean field theory to these systems was discussed in Chapter 5. In Chapter 6 a new linearisation scheme for dilute colloidal suspensions was derived in both the integral equation and differential equation formulations. The application of this method to one-dimensional and three-dimensional systems was investigated in Chapters 7 and 8 respectively. Although the new linearisation method required numerical solution in all cases studied, the increased efficiency as compared with solution of the nonlinear PB equation make it a useful method, especially in more complicated geometries. No phase instability was found for homogeneous systems that were open with respect to a salt reservoir. This feature is expected to persist for fixed-salt systems. The method introduced here can be applied to this case, due to the reduced computational requirements compared with solving the nonlinear PB equation, and the increased range of validity compared with linearisations about a constant mean field potential. Further studies are planned for calculations on fixed-salt systems.

Additional studies are also planned for the application of the linearisation scheme proposed and tested here to different geometries of charged macroions. One such case involves disordered arrays of macroions for which solution of the full nonlinear problem is difficult. We also plan to develop an expansion based on the technique laid out in Chapter 6, to obtain expressions for the effective 3-body interactions between colloidal particles (as discussed at the end of Section 8.4) in terms of numerical solutions of the nonlinear PB equation for isolated macroions.

Bibliography

[1] P. G. Debenedetti, *Metastable Liquids- concepts and principles* (Princeton University Press, Princeton, NJ, 1996).

[2] B.Cowan, *Topics in Statistical Mechanics* (Imperial College Press, London, 2005).

[3] H. Yoshida *et al.*, Langmuir **15**, 2684 (1999).

[4] M. Schmidt *et al.*, Phys. Rev. Lett. **86**, 1191 (2001).

[5] T. Hill, *Thermodynamics of Small Systems* (Dover, London, 1994), Vol. I and II.

[6] D. Reguera, R. K. Bowles, Y. Djikaev, and H. Reiss, J. Chem. Phys. **118**, 340 (2003).

[7] G. Koper and H. Reiss, J. Phys. Chem. **100**, 422 (1996).

[8] K. Huang, *Statistical Mechanics* (John Wiley and Sons, Inc., New York, 1963).

[9] D. W. Oxtoby and R. Evans, J. Chem. Phys. **89**, 7521 (1988).

[10] R. A. L. Jones, *Soft Condensed Matter* (Oxford University Press, New York, 2002).

[11] R. Evans, Mol. Phys. **42**, 1169 (1981).

[12] J.-S. Li and G. Wilemski, J. Chem. Phys. **118**, 2845 (2003).

[13] M. Knott and I. J. Ford, Phys. Rev. E. **65**, 61401 (2002).

[14] P. B. Warren, Phys. Rev. E **73**, 11411 (2006).

[15] V. I. Kalikmanov, *Statistical Physics of Fluids - Basic concepts and applications* (Springer, Berlin, 2001).

[16] P. Hohenberg and W. Kohn, Phys. Rev. **136**, B864 (1964).

[17] R. Evans, Adv. Phys. **28**, 143 (1979).

[18] W. A. Curtin and N. W. Ashcroft, Phys. Rev. Lett. **56**, 2775 (1986).

[19] V. Talanquer and D. W. Oxtoby, J. Chem. Phys. **109**, 223 (1998).

[20] V. Talanquer and D. W. Oxtoby, J. Chem. Phys. **113**, 7013 (2000).

[21] P. Teixeira and M. Telo da Gamma, J. Phys. Cond. Matt **3**, 111 (1991).

[22] R. van Roij and J. Hansen, Phys. Rev. Lett. **79**, 3082 (1997).

[23] V. Talanquer and D. W. Oxtoby, J. Chem. Phys. **100**, 5190 (1994).

[24] J. J. Binney, N. J. Dowrick, A. J. Fisher, and M. E. J. Newman, *Theory of Critical Phenomena- an introduction to the renormalization group* (Oxford University Press, Oxford, 1992).

[25] J. Langer, Ann. Phys. **54**, 258 (1969).

[26] J. Langer and L. Turski, Phys. Rev. A **8**, 3230 (1973).

[27] D. Reguerra and H. Reiss, J. Chem. Phys. **120**, 2558 (2004).

[28] J. C. Barrett, J. Chem. Phys. **107**, 7989 (1997).

[29] R. D. Coalson and A. Duncan, J. Chem. Phys. **97**, 5653 (1992).

[30] R. Netz and H. Orland, Eur. Phys. J. E **1**, 203 (2000).

[31] A. Moreira and R. Netz, Europhys. Lett. **52**, 705 (2000).

[32] A. Lau, Ph.D. thesis, University of California, Santa Barbara, 2000.

[33] D. J. Lee, M. M. T. da Gama, and K. E. Gubbins, J. Chem. Phys. **85**, 490 (1986).

[34] A. Laaksonen, V. Talanquer, and D. W. Oxtoby, Ann. Rev. Phys. Chem. **46**, 489 (1995).

[35] J. C. Barrett, J. Chem. Phys. **111**, 5938 (1999).

[36] S. Khakshouri and I. Ford, J. Chem. Phys. **121**, 5081 (2004).

[37] J. K. Percus, J. Chem. Phys. **75**, 1316 (1981).

[38] J. K. Percus, J. Stat. Phys. **28**, 67 (1982).

[39] J. Frenkel, *Kinetic Theory of Liquids* (Oxford Clarendon Press, Oxford, 1946).

[40] H. Reiss, J. L. Katz, and E. R. Cohen, J. Chem. Phys. **48**, 5553 (1968).

[41] F. M. Kuni and A. I. Rusanov, Physics Letters **29 A**, 337 (1969).

[42] D. F. Evans and H. Wennerstrom, *The Colloidal Domain: where physics, chemistry, biology and technology meet* (VCH Publishers, New York, 1994).

[43] A. Larsen and D. G. Grier, Nature **385**, 230 (1997).

[44] E. J. W. Verwey and J. G. Overbeek, *Theory of the Stability of Lyophobic Colloids* (Elsevier, New York, 1948).

[45] D. A. MacQuarrie, *Statistical Mechanics* (University Science Books, Sausalito,CA, 2000).

[46] J.-M. Victor and J.-P. Hansen, J. Chem. Soc., Faraday Trans. **81**, 43 (1985).

[47] M. Knott, Ph.D. thesis, UCL, 2001.

[48] D. G. Grier and C. A. Murray, J. Chem. Phys. **100**, 9088 (1994).

[49] K.-Q. Zhang and X. Liu, Nature **429**, 739 (2004).

[50] B. V. R. Tata, M. Rajalakshmi, and A. K. Arora, Phys. Rev. Lett. **69**, 3778 (1992).

[51] N. Ise *et al.*, J. Am. Chem. Soc **101**, 5836 (1979).

[52] M. D. Narendra and C. Zukoski, Phys. Rev. E. **66**, 51602 (2002).

[53] T. Alfrey Jr., E. Bradford, J. Vanderhoff, and G. Oster, J. Opt. Soc. Am. **44**, 603 (1954).

[54] S. Hachisu and Y. Kobayashi, J. Coll. Interface Sci. **46**, 470 (1974).

[55] Y. Monovoukas and A.P.Gast, J. Coll. Interface Sci. **128**, 533 (1989).

[56] K. Kremer, M. Robbins, and G. Grest, Phys. Rev. Lett **57**, 2694 (1986).

[57] M. Robbins, K. Kremer, and G. Grest, J. Chem. Phys. **88**, 3286 (1988).

[58] W. Hoover and F. Ree, J. Chem. Phys. **49**, 3609 (1966).

[59] N. Ise *et al.*, J. Chem. Phys. **78**, 536 (1983).

[60] A. Arora, B. Tata, A. Sood, and R. Kesavamoorthy, Phys. Rev. Lett. **60**, 2438 (1988).

[61] S. Sosho *et al.*, Langmuir **9**, 394 (1993).

[62] B. V. R. Tata, E. Yamahara, P. Rajamani, and N. Ise, Phys. Rev. Lett. **78**, 31 (1997).

[63] N. Ise, T. Konishi, and B. Tata, Langmuir **15**, 4176 (1999).

[64] T. Palberg and M. Würth, Phys. Rev. Lett **72**, 786 (1994).

[65] H. Matsuoka, T. Harada, and H. Yamaoka, Langmuir **10**, 4423 (1994).

[66] J. Yamanaka *et al.*, Langmuir **15**, 4198 (1999).

[67] H.-J. Butt, K. Graf, and M. Kappl, *Physics and Chemistry of Interfaces* (Wiley-VCH, Weinheim, 2006).

[68] R. van Roij, M. Dijkstra, and J. Hansen, Phys. Rev. E. **59**, 2010 (1999).

[69] C. Howard, H. Thomson, J. Wasse, and N. Skipper, J. Am. Chem. Soc. **126**, 13228 (2004).

[70] L. Belloni, J. Phys.: Cond. Matt **12**, R549 (2000).

[71] B.W.Ninham and V. Parsegian, J. Theor. Biol. **31**, 405 (1971).

[72] S. H. Behrens and M. Borkovec, Phys. Rev. E. **60**, 7040 (1999).

[73] P. Linse and V. Lobaskin, Phys. Rev. Lett. **83**, 4208 (1999).

[74] P. Linse and V. Lobaskin, J. Chem. Phys. **112**, 3917 (2000).

[75] F. Oosawa, Biopolymers **6**, 134 (1968).

[76] B. Jonsson and H. Wennerstrom, in *Electrostatic Effects in Soft Matter and Biophysics* (NATO Science Series, Amsterdam, 2000).

[77] A. Lau and P. Pincus, Phys. Rev. E **66**, 41501 (2002).

[78] Y. Levin, Rep. Prog. Phys. **65**, 1577 (2002).

[79] E. Canessa, M. J. Grimson, and M. Silbert, Mol. Phys. **64**, 1195 (1988).

[80] I. Sogami and N. Ise, J. Chem. Phys. **81**, 6320 (1984).

[81] J. T. G. Overbeek, J. Chem. Phys. **87**, 4406 (1987).

[82] M. Knott and I. J. Ford, Phys. Rev. E. **63**, 31403 (2001).

[83] P. B. Warren, J. Chem. Phys. **112**, 4683 (2000).

[84] M. Dijkstra and R. van Roij, J. Phys.: Cond. Matt. **10**, 1219 (1998).

[85] H. Löwen and E. Allahyarov, J. Phys.: Cond. Matt **10**, 4147 (1998).

[86] M. Tamashiro and H. Schiessel, J. Chem. Phys. **119**, 1855 (2003).

[87] H. H. von Grünberg, R. van Roij, and G. Klein, Europhys. Lett. **55**, 580 (2001).

[88] S. Alexander *et al.*, J. Chem. Phys. **80**, 5776 (1983).

[89] A. Diehl, M. Barbosa, and Y. Levin, Europhys. Lett. **53**, 86 (2001).

[90] F.-R. Chang, N. Skipper, and G. Sposito, Langmuir **14**, 1201 (1998).

[91] H. Wennerstrom, B. Jonsson, and P. Linse, J. Chem. Phys. **76**, 4665 (1982).

[92] C. Kittel, *Introduction to Solid State Physics* (John Wiley and Sons, New York, 1953).

[93] S. J. Joshua, *Symmetry Principles and Magnetic Symmetry in Solid State Physics* (IOP Publishing Ltd, New York, 1991).

[94] J. D. Jackson, *Classical Electrodynamics* (John Wiley and Sons, Inc., New York, 1999).

[95] W. Press, S. Teukolsky, W. Vetterling, and B. Flannery, *Numerical Recipes in Fortran 77- The Art of Scientific Computing* (Cambridge University Press, Cambridge, 1986).

[96] M. Tamashiro and H. Schiessel, Phy. Rev. E **68**, 66106 (2003).

[97] M. Smalley, Mol. Phys. **71**, 1251 (1990).

[98] I. Sogami, T. Shinohara, and M. Smalley, Mol. Phys. **74**, 599 (1991).

[99] I. Sogami, T. Shinohara, and M. Smalley, Mol. Phys. **76**, 1 (1992).

[100] M. Smalley, Langmuir **10**, 2884 (1994).

[101] T. Shinohara, M. Smalley, and I. Sogami, Mol. Phys. **101**, 1883 (2003).

[102] I. Sogami and T. Shinohara, Coll. and Surf. A **190**, 25 (2001).

[103] R. Ettelaie, Langmuir **9**, 1888 (1993).

[104] S. Levine and D. Hall, Langmuir **8**, 1090 (1992).

[105] D. Hall, Langmuir **12**, 4305 (1996).

[106] D. Hall, Langmuir **12**, 4308 (1996).

[107] L. Guldbrand, B. Jonsson, H. Wennerstrom, and P. Linse, J. Phys. Chem. **80**, 2221 (1984).

[108] A. Lau and P. Pincus, Phys. Rev. Lett. **84**, 4116 (2000).

[109] W. Hsin, T.-Y. Wang, Y.-J. Sheng, and H.-K. Tsao., J. Chem. Phys. **121**, 5494 (2004).

[110] R. D. Groot, J. Chem. Phys. **95**, 9191 (1991).

[111] G. B. Arfken and H. Weber, *Mathematical Methods for Physicists* (Harcourt Academic Press, San Diego, 2001).

[112] R. W. Hamming, *Numerical methods for scientists and engineers* (Dover, London, 1986).

[113] A.-P. Hynninen, M. Dijkstra, and R. van Roij, J. Phys.: Cond. Matt **15**, S3549 (2003).

[114] C. Russ, H. von Grunberg, M. Dijkstra, and R. van Roij, Phys. Rev. E **66**, 11402 (2002).

[115] T. Kreer, J. Horbach, and A. Chatterji, Phys. Rev. E **74**, 21401 (2006).